Biochemical Characterization and Optimization of RNA Aptamers Bound to Hoechst Dye Derivatives

by

Natasha Evans

A thesis

presented to the University of Waterloo

in fulfillment of the

thesis requirement for the degree of

Master of Science

in

Chemistry

Waterloo, Ontario, Canada, 2023

© Natasha Evans 2023

Author's Declaration

This thesis consists of material all of which I authored or co-authored: see Statement of Contributions included in the thesis. This is a true copy of the thesis, including any required final revisions, as accepted by my examiners.

I understand that my thesis may be electronically available to the public.

Statement of Contributions

All experimental work in Chapter 2 was performed and analyzed by the candidate.

In Chapter 3, the ITC control experiments (**Figures 5.2** and **5.3**); the ITC experiments for replicates 1 and 2 of the Original, UUCG Tetraloop, GAAA Tetraloop and Elongated Duplex RNA aptamers with tBu (PEG) Hoechst dye (**Figures 3.4A, C, D, E** and **5.4A, C, D, E**); the ITC experiment for replicate 1 of the Original RNA aptamer with biotinylated tBu (PEG) Hoechst (**Figure 3.6**) and the ITC experiments for replicates 1 and 2 the Original RNA aptamer with tBu (PEG) Hoechst dye at 5, 15, 25 and 35 °C (**Figures 3.8** and **5.8**) were performed by Lindsey Shivers, however the raw data was processed and analyzed by the candidate. All other experimental work was performed and analyzed by the candidate.

Abstract

Ribonucleic acid (RNA) aptamers are single-stranded nucleic acids that are typically selected through a process known as Systematic Evolution of Ligands by EXponential Enrichment (SELEX). These oligonucleotides can bind to small target molecules, including proteins and chemical toxins, with high specificity and affinity. They can be further modified with recognition elements, such as light-up fluorophore molecules, to become aptamer-based biosensors. In the year 2008, Sando et al. selected for an RNA aptamer that is capable of specific binding to a Hoechst dye derivative with bulky tert-Butyl (tBu) groups, which prevents the non-specific binding to DNA sequences. The group performed some preliminary biochemical characterization experiments; however little information is currently known about the specific molecular interactions between the optimized Aptamer II-mini3-4 sequence and the tBu Hoechst dye. Therefore, this research project aimed to develop a complete biochemical profile of the SELEX-selected 71-nucleotide (nt) Aptamer II sequence and the optimized 29-nt Aptamer II-mini3-4 sequence. In addition, new RNA aptamer variants were developed within this research project to not only gain a deeper understanding of the aptamer's folded conformation and binding interactions with the tBu Hoechst dye, but to also optimize the aptamer system further.

In Chapter 2 fluorescence emission experiments were performed to determine if binding was present between the RNA aptamer variants and the derivative tBu Hoechst dyes. The fluorescence enhancement of each bound complex was also compared and evaluated to understand binding interactions within the aptamer systems. Moreover, fluorescence titration assays were conducted to estimate the binding affinities for between the interacting molecules.

In Chapter 3 native polyacrylamide gel (PAGE) experiments were conducted to determine the conformation of the tBu Hoechst-bound and unbound conformations of the RNA aptamer

variants. In addition, isothermal titration calorimetry (ITC) experiments were employed as an alternative method to determine the dissociation constants of the studied aptamer systems. It was also used to obtain the thermodynamic and kinetic properties of each of the tBu Hoechst-binding RNA aptamers. The information gained within this research project was intended to lay the groundwork for future work including the structure elucidation of the Aptamer II-mini3-4 RNA sequence bound with the tBu Hoechst dye through nuclear magnetic resonance (NMR) spectroscopy techniques. It was also intended to aid in optimizing the aptamer system for its development as a building block for an aptamer-based biosensor that can be used for potential commercial applications.

Acknowledgments

To begin, I would like to say thank you to my supervisor, Dr. Thorsten Dieckmann. Thank you for taking a chance on me as an undergraduate research student as well as continuing to provide the support and guidance required to help me grow as a researcher. Thank you as well to my committee members, Dr. Juewen Liu and Dr. Rui Huang for agreeing to be on my committee and your many words of wisdom. I would also like to thank NMR technician Blossom Yan. Thank you for your guidance and support as I navigated my way through graduate school.

Thank you as well to the all the past and present members of the Dieckmann research group whom I have had the pleasure of working with including Kyle Piccolo, Kyla Egerdeen, Alex Tormann, Aiden Hong, and Dina Abu Baker. I would like to acknowledge Kyle and Kyla in particular. They both played an essential role in training and mentoring me when I first started working in the Dieckmann lab. As well I would like to thank the undergraduate students whom I have worked with during my time as a graduate student. I would like to specifically mention Lindsey Shivers, who was a great help in obtaining the initial ITC data for this research project. Finally, I would like to thank my friends and family – I wouldn't be where I am today without your unconditional support.

Table of Contents

Author's Declaration……...ii

Statement of Contributions…….iii

Abstract……...iv

Acknowledgments…….……vi

List of Figures…….xi

List of Tables……....xiv

List of Abbreviations……...…xvii

Chapter 1: Literature Review……...1

1.0 Introduction……2

1.1 RNA Structure and Function…...……...……..3

1.2 Aptamers……...6

1.2.1 Aptamer Selection ……..……...10

1.2.2 Aptamer-Based Biosensors…….……...13

1.2.3 Biochemical Characterization of Aptamers…….……..16

1.3 Fluorogen-Binding RNA Aptamers and their Applications……...19

1.3.1 Malachite Green RNA Aptamer……..20

1.3.2 Spinach RNA Aptamer……...22

1.3.3 Mango RNA Aptamer…….23

1.3.4 Derivative Hoechst Dyes…….24

1.3.5 Selection of an RNA Aptamer Specific for Derivative Hoechst Dyes……...26

1.4 Research Objectives……28

Chapter 2: Characterization of Derivative Hoechst-Binding RNA Aptamers through Fluorescence Methods……...30

2.0 Introduction…..……..……...31

2.1 Materials and Methods…...…….32

2.1.1 RNA Aptamer Variants…….…….....…32

2.1.2 Derivative Hoechst Dyes……..35

2.1.3 RNA Transcription……...……37

2.1.4 RNA Purification……..38

2.1.5 Ultraviolet Absorption Spectra……..…...41

2.1.6 Determination of the Molar Extinction Coefficients by Ultraviolet Spectroscopy……..42

2.1.7 Fluorescence Emission Spectra……...…….…42

2.1.8 Fluorescence Titration Assays……..44

2.2 Results and Discussion…….……...46

2.2.1 Ultraviolet Absorption Spectra……..……...46

2.2.2 Determination of the Molar Extinction Coefficients by Ultraviolet Spectroscopy……..47

2.2.3 Fluorescence Emission Spectra of the RNA Aptamer Variants with tBu (PEG) Hoechst……48

2.2.4 Fluorescence Emission Spectra of the Original RNA aptamer with Biotinylated tBu (PEG) Hoechst……...…….…52

2.2.5 Fluorescence Titration Binding Buffer Optimization……...53

2.2.6 Fluorescence Titration of the Variant RNA Aptamers with tBu (PEG) Hoechst……...55

2.2.7 Fluorescence Titration of the Original RNA Aptamer with Biotinylated tBu (PEG) Hoechst……...…….58

2.3 Conclusion…….……..59

Chapter 3: Conformational, Thermodynamic, and Kinetic Analysis of Derivative Hoechst-Binding RNA Aptamers……...……..…61

3.0 Introduction……..……62

3.1 Material and Methods……..……63

3.1.1 RNA Aptamer Variants…….63

3.1.2 Derivative Hoechst Dyes……..64

3.1.3 RNA Transcription……64

3.1.4 RNA Purification……..64

3.1.5 Native PAGE for the Comparison of the Bound and Unbound Conformations……64

3.1.6 Native PAGE Time Experiment……...65

3.1.7 Native PAGE for the Comparison of the Unbound Conformations of the RNA Aptamer Variants……..66

3.1.8 Isothermal Titration Calorimetry of the RNA Aptamer Variants…….67

3.1.9 Isothermal Titration Calorimetry Temperature Series……..69

3.2 Results and Discussion……70

3.2.1 Native PAGE for the Comparison of the Bound and Unbound RNA Aptamer Variants……...70

3.2.2 Native PAGE Time Experiment……72

3.2.3 Native PAGE for the Comparison of the Unbound Conformations of the RNA Aptamer Variants……..74

3.2.4 Isothermal Titration Calorimetry of the RNA Aptamer Variants with tBu (PEG) Hoechst……..……..75

3.2.5 Isothermal Titration Calorimetry of the Original RNA Aptamer with Biotinylated tBu (PEG) Hoechst……85

3.2.6 Isothermal Titration Calorimetry Temperature Series of the Original RNA Aptamer with tBu (PEG) Hoechst……..88

3.3 Conclusions……..…96

Chapter 4: Summary and Future Work……..99

4.0 Summary and Future Work……100

References……..…..104

Appendix A: Supplementary Figures……...131

List of Figures

Figure 1.1 Structural components of RNA……4

Figure 1.2 Double-stranded A-form helical RNA……..6

Figure 1.3 Binding mechanisms of an RNA aptamer to its target molecule……..7

Figure 1.4 RNA degradation mechanism by the RNase enzyme……..10

Figure 1.5 General overview of the SELEX process for selecting RNA aptamers……..12

Figure 1.6 Types of fluorescent aptamer-based biosensors……...…...16

Figure 1.7 Malachite Green RNA aptamer……...21

Figure 1.8 Spinach RNA aptamer……23

Figure 1.9 Chemical structure of the TO1-Biotin fluorophore……24

Figure 1.10 An example of a Hoechst-DNA complex……..25

Figure 1.11 Sando selected RNA aptamers and their target derivative tBu Hoechst dyes……...27

Figure 1.12 Optimization of the Hoechst-binding RNA sequence……...28

Figure 2.1 Nomenclature of the RNA aptamer variants……...33

Figure 2.2 Predicted secondary structures of the variant Hoechst RNA aptamer sequences used for experimentation……....35

Figure 2.3 Comparison of the chemical structures of the tBu Hoechst dye derivatives……...36

Figure 2.4 DNA template examples……..38

Figure 2.5 Example of an intermediate UREA PAGE gel under ultraviolet shadowing using experimental data……..….39

Figure 2.6 Example chromatograms of nucleic acids purified using the FPLC system……...41

Figure 2.7 UV absorption spectra to determine the λ_{max}……47

Figure 2.8 Fluorescence emission assays of the variant RNA aptamers……..51

Figure 2.9 Fluorescence emission assay of the variant tBu Hoechst dyes……52

Figure 2.10 Binding buffer optimization through fluorescence titration assays……...54

Figure 2.11 Binding affinities of the RNA aptamer variants……57

Figure 2.12 Binding affinity of the tBu Hoechst variants……..58

Figure 3.1 Bound versus unbound conformations of the RNA aptamer variants…….72

Figure 3.2 Time experiment to monitor the conformational changes over time……...73

Figure 3.3 SYBR Safe-stained native gels for the comparison of the unbound RNA aptamer variant conformations……75

Figure 3.4 Processed ITC and equilibrium isotherm data for the RNA aptamer variants……81

Figure 3.5 Processed ETC for the RNA aptamer variants……84

Figure 3.6 Processed ITC and equilibrium isotherm data for the tBu Hoechst dye derivatives...86

Figure 3.7 Processed ETC for the tBu Hoechst dye derivatives……...88

Figure 3.8 Processed ITC and equilibrium isotherm data for the temperature series……...90

Figure 3.9 Processed ETC for the temperature series……...91

Figure 3.10 Plotted temperatures series……94

Figure 3.11 Eyring plots from the multitemperature series……..96

Figure 5.1 Dilution series to determine the molar extinction coefficient of the tBu Hoechst dye derivatives in MQW…….131

Figure 5.2 Control ITC experiments for the Original RNA aptamer and tBu (PEG) Hoechst dye……....131

Figure 5.3 Control ITC experiments for the biotinylated tBu (PEG) Hoechst dye……132

Figure 5.4 Duplicate data for the processed ITC and equilibrium isotherm data for the RNA aptamer variants……...132

Figure 5.5 Duplicate data for the processed ETC for the RNA aptamer……134

Figure 5.6 Duplicate data for the processed ITC and equilibrium isotherm data for the tBu Hoechst dye derivatives……...135

Figure 5.7 Duplicate data for the processed ETC for the tBu Hoechst dye derivatives…….136

Figure 5.8 Duplicate data for the processed ITC and equilibrium isotherm data for the temperature series……..……..137

Figure 5.9 Duplicate data for the processed ETC for the temperature series…….138

List of Tables

Table 1.1 Examples of fluorogen-binding RNA aptamers in literature and their corresponding biochemical properties……...20

Table 1.2 Summary of the biochemical properties determined by Sando et al. for the tBu Hoechst-binding RNA aptamers ……...……...……....29

Table 2.1 Variant Hoechst RNA aptamer sequences used for biochemical characterization experiments……35

Table 2.2 Recipe for a 10 mL RNA transcription mixture to produce 1-2 mM of the target RNA aptamer in a final volume of 500 µL……..……...38

Table 2.3 Percent acrylamide chosen for the UREA PAGE gels that were run for each of the variant Hoechst RNA aptamers…….40

Table 2.4 Heat-treatment of the RNA aptamers prior to experimentation to ensure proper folding……44

Table 2.5 Summary of the buffer conditions tested for the fluorescence titration experiments to optimize the binding system……..45

Table 2.6 Comparison of the experimentally determined molar extinction coefficients for the tBu Hoechst dye derivatives in water……...48

Table 2.7 Comparison of the relative I_{on}/I_{off} ratios produced by the tBu (PEG) Hoechst - variant RNA aptamer complexes……...51

Table 2.8 Comparison of the relative I_{on}/I_{off} ratios produced upon the interaction of the Original RNA with the biotinylated and non-biotinylated tBu (PEG) Hoechst dye……52

Table 2.9 Comparison of the dissociation constants produced for the complex formation of the Original RNA aptamer with tBu (PEG) Hoechst under different buffer conditions…….55

Table 2.10 Comparison of the dissociation constants obtained for the variant Hoechst RNA aptamers with tBu (PEG) Hoechst dye under low salt conditions and in the absence of Mg^{2+} ions…….57

Table 2.11 Comparison of the dissociation constants produced upon interaction of the Original RNA aptamer with the tBu Hoechst dye derivatives under low salt conditions and in the absence of Mg^{2+} ions……...58

Table 3.1 Percent acrylamide chosen for the native PAGE gels based on the number of bases present within the variant RNA aptamer sequences……..67

Table 3.2 RNA and tBu Hoechst dye sample concentrations that were prepared for the ITC experiments at 25 °C……...……...68

Table 3.3 ITC experimental and injection parameters that were used for each of the variant RNA aptamer-tBu dye systems at 25 °C……...……..68

Table 3.4 Preparation of the dye and RNA control samples titrated into 1× PBS…..…….69

Table 3.5 Comparison of the averaged data for the binding affinities and thermodynamic properties of the variant RNA aptamers with the tBu (PEG) Hoechst dye at 25 °C……..……..81

Table 3.6 Comparison of the averaged data for the kinetic properties of the RNA aptamer variants with the tBu (PEG) Hoechst dye at 25 °C……...….85

Table 3.7 Comparison of the averaged data for the binding affinities and binding enthalpies of the Original RNA aptamer with biotinylated versus non-biotinylated tBu Hoechst dye at 25 °C……...……...87

Table 3.8 Comparison of the averaged data for the kinetic properties of the Original RNA aptamer with biotinylated versus non-biotinylated tBu Hoechst dye at 25 °C……...…...88

Table 3.9 Averaged data for the binding affinities and thermodynamic properties obtained from the titration of 600 μM tBu (PEG) Hoechst into 50 μM Original RNA at different temperatures……...91

Table 3.10 Averaged data for the kinetic parameters obtained from the titration of 600 μM tBu (PEG) Hoechst into 50 μM Original RNA at different temperatures……91

Table 3.11 Thermodynamic properties calculated from the temperature dependence of ΔH and van't Hoff plots……..94

Table 3.12 Thermodynamic properties of the activation energies determined from the Eyring plots……...……96

Table 4.1 Summary of the biochemical properties determined at 25 °C for each of the tBu Hoechst-RNA aptamer systems that were studied within this research project……..101

Table 5.1 Raw data for the binding affinities and thermodynamic properties of the variant RNA aptamer with the tBu (PEG) Hoechst dye at 25 °C. ……...……..…133

Table 5.2 Raw data for the kinetic properties of the RNA aptamer variants with the tBu (PEG) Hoechst dye at 25 °C……...……135

Table 5.3 Raw data for the binding affinities and thermodynamic properties of the Original RNA aptamer with biotinylated versus non-biotinylated tBu Hoechst dye at 25 °C. ……...…...135

Table 5.4 Raw data for kinetic properties of the Original RNA aptamer with biotinylated versus non-biotinylated tBu Hoechst dye at 25 °C……...……..136

Table 5.5 Raw data for the binding affinity and thermodynamic properties obtained for the titration of 600 μM tBu (PEG) Hoechst into 50 μM Original RNA at different temperatures…138

Table 5.6 Raw data for the kinetic parameters obtained from the titration of 600 μM tBu (PEG) Hoechst into 50 μM Original RNA at different temperatures ……139

List of Abbreviations

A	Adenine
ATP	adenosine triphosphate
BB	bromophenol blue
bp	base pair
C	cytosine
cDNA	complementary DNA
ΔC_p	change in heat capacity
DEAE	diethylaminomethyl
DFBHI	3,5-difluoro-4-hydroxybenzylidene imidazolinone
DMSO	dimethyl sulfoxide
DNA	deoxyribonucleic acid
ds	double-stranded
dsRBM	double-stranded RNA-binding motif
EDTA	ethylenediamine tetraacetic acid
eGFP	enhanced green fluorescent protein
ETC	equilibrium time curve
FLAP	fluorescent light-up aptamer
FPLC	fast performance liquid chromatography
G	guanine
ΔG	Gibbs free energy
GFP	green fluorescent protein
ΔH	change in enthalpy
$\Delta^{\ddagger}H$	enthalpy of activation
ΔH_{25}	change in enthalpy at 25 °C
HBI	4-hydroxybenzlidene imidazolinone
HIV	human immunodeficiency virus
HPLC	high-performance liquid chromatography
IDT	Integrated DNA Technologies
ITC	isothermal titration calorimetry
K_a	association constant
K_d	dissociation constant
k_{off}	dissociation rate
k_{on}	association rate
MG	malachite green
mM	millimolar
mRNA	messenger RNA
MQW	Milli-Q water
MW	molecular weight
N	stoichiometry of the binding sites
nM	nanomolar
NMR	nuclear magnetic resonance
NOE	nuclear Overhauser effect
nt	nucleotide
NTP	nucleoside triphosphate

OG	OliGreen
PAGE	polyacrylamide gel electrophoresis
PBS	phosphate-buffered saline
PCR	polymerase chain reaction
PEG	polyethylene glycol
RFU	relative fluorescence units
RNA	ribonucleic acid
rRNA	ribosomal RNA
RNase	ribonuclease
ROS	reactive oxygen species
ΔS	change in entropy
$\Delta^{\ddagger}S$	entropy of activation
SAM	S-adenosylmethionine
SELEX	Systematic Evolution of Ligands by EXponential Enrichment
siRNA	small interfering RNA
SPR	surface plasmon resonance
ss	single-stranded
T	thymine
TBE	tris-borate ethylenediamine tetraacetic acid
TBS	tris-buffered saline
tBu	tert-Butyl
TMR	tetramethylrosamine
TO	thiazole orange
TO1-Biotin	thiazole orange 1-biotin
tRNA	transfer RNA
T7 RNAP	T7 RNA polymerase
$T\Delta S_{25}$	change in entropy at 25 °C
U	uracil
UV	ultraviolet
λ_{em}	emission wavelength
λ_{ex}	excitation wavelength
λ_{max}	wavelength at which the sample absorbs light maximally

Chapter 1: Literature Review

1.0 Introduction

The detection of small molecules is an integral process for many applications within commercial industries. For instance, medical diagnostic procedures often involve the identification of biological markers within the human body, such as those involved in cancer development.[1] Additionally, chemical toxin recognition can be essential for environmental conservation efforts, including the maintenance of clean bodies of water.[2–4] Antibodies are a class of biomolecules that can be used as a therapeutic agent and molecular detection tool due to their ability to bind to target antigens.[5] These molecules can be developed into drugs that are designed to combat medical conditions such as various autoimmune diseases and cancers. The production of antibodies, however, is expensive and can vary from batch to batch, hence reducing their detection accuracy.[6] The use of analytical instrumentation, such as high-performance liquid chromatography (HPLC), is another type of detection method that is commonly used by many scientific industries.[7] For example, researchers within the pharmaceutical industry can rely on HPLC instrumentation to separate and analyze enantiomers of chiral molecules during the drug manufacturing process. Unfortunately, these analytical instruments cannot be used for the real-time detection of samples at environments located outside the lab.[8] For instance, to test samples obtained from a body of water, the samples must first be transported to the lab and prepared for chemical analysis before detection can take place. The use of nucleic acid aptamer-based biosensors for small molecule detection has progressively become an appealing area of research due to their low production costs and ability to be employed at the sample source for real-time results.[8–10] Hence, these aptamer-based biosensors can potentially replace traditional recognition methods that are currently being used within commercial industries.

1.1 RNA Structure and Function

Ribonucleic acid (RNA) is a complex biomolecule that until the last few decades, was not very well understood despite its presence in the majority of living organisms.[11,12] It is well known that RNA is heavily involved in the production of proteins through the transcription of deoxyribonucleic acid (DNA) sequences into messenger RNA (mRNA), as well as through the use of transfer RNA (tRNA) and ribosomes for the assembly of the final protein products.[11] Additional types of RNA molecules were also discovered in living systems that at first glance, appeared to be somewhat random and functionless but were later found to be involved in many biological processes. For instance, the untranslated region of mRNA sequences is sensitive to temperature changes and can aid in controlling gene expression.[11,13] Moreover, small double-stranded RNA molecules, termed small interfering RNA (siRNA), target and silence foreign mRNA sequences through homology-directed recognition.[14] Studies have also revealed that some RNA molecules, known as ribozymes, are capable of adopting defined structures and performing a wide range of catalytic functions, such as bond formation and breakage.[11,15] For example, a study by Kruger et al.[15] analyzed the self-splicing action of ribosomal RNA (rRNA) in *Tetrahymena.* From the results, it was concluded that the three-dimensional structure of the rRNA molecule is linked to its catalytic function. The rRNA sequence folds into specific arrangements such that the functional groups required for catalytic activity are exposed.[16] Therefore, RNA molecules are involved in numerous roles within biological systems and the three-dimensional structures that these molecules form can have an influence on their ability to perform the desired function.

RNA molecules are composed of four different nitrogenous bases; adenine (A), uracil (U), guanine (G), and cytosine (C); which are each attached to a ribose sugar molecule and a phosphate group forming the basic block called a nucleotide (nt).[17] The molecular interactions, such as

hydrogen bonding and stacking, between the bases of the RNA phosphate backbone can lead to the formation of unique secondary and tertiary structures that contribute to the overall three-dimensional configuration of nucleic acids.[16] Some of the notable elements that can be found within secondary structures include unpaired single-stranded (ss) regions, duplexes, internal loops and bulges caused by mismatched base pairs, hairpin loops, and junctions, as depicted in **Figures 1.1a-f**.[16,18] The folded three-dimensional structures of RNA is typically stabilized by additional tertiary interactions, shown in **Figures 1.1g** and **h**. For instance, two different loop regions of an RNA molecule's secondary structure can interact to form a kissing hairpin (**Figure 1.1g**), or hydrogen bonds can form between unpaired nucleotides to produce pseudoknots within the RNA's backbone (**Figure 1.1h**).[16,19] Hence, the combination of these different nucleotide interactions allow for the various RNA molecules to take on the unique structures required to maintain their biological roles.

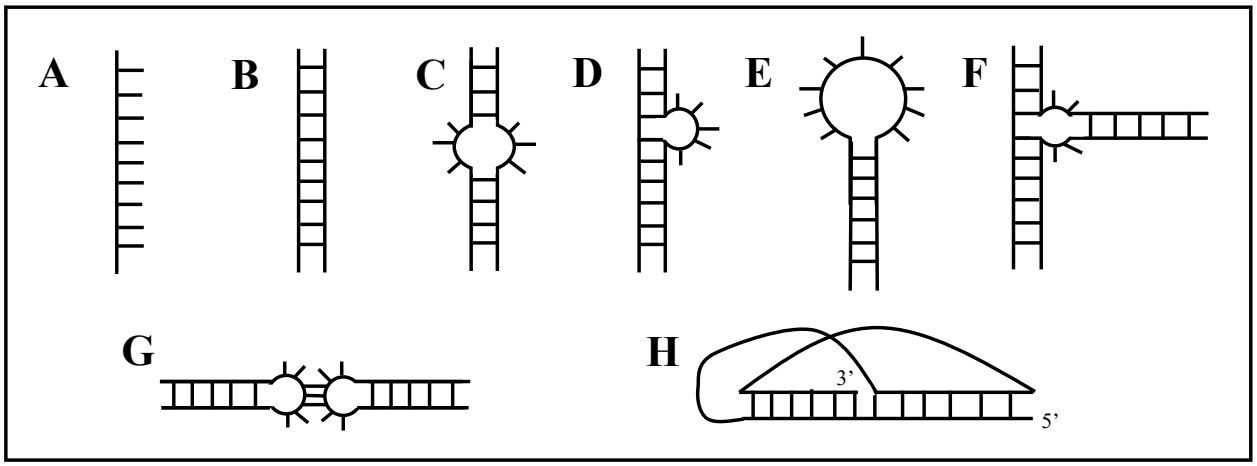


Figure 1.1: Structural components of RNA. A look into the various elements that comprise the secondary structure of nucleic acids. The phosphate backbone can arrange into **A)** single-stranded regions, **B)** duplexes, **C)** internal loops, **D)** bulges, **E)** hairpins, and **F)** junctions based on the interactions between the nucleic acid bases.[16] Some of the tertiary interactions that stabilize the overall RNA molecule include **G)** kissing hairpins and **H)** pseudoknots.[16,19] Figure 1.1 was modified from Chastain and Tincoco[16], as well as Lim and Brown[19] using PowerPoint.

Under certain physiological conditions, such as viral infections,[20,21] the nucleotide bases of an RNA molecule's backbone can interact in a way that causes it to form a double-stranded (ds) anti-parallel helix.[22,23] These RNA helices primarily exist in a right-handed A-form, as shown in **Figure 1.2**.[22,24,25] Within the A-form helical structure, the ribose molecules adopt a $C_{3'}$-endo sugar pucker conformation (**Figure 1.2A**), which in turn causes the base-pairs to have a large displacement of approximately 4 Å from the helical axis (**Figure 1.2B**).[22,24] Therefore, A-form RNA contains wide and shallow minor grooves, as well as deep and narrow major grooves, as depicted in **Figure 1.2C**.[24,25] By studying the RNA's helical structure and resulting grooves, one can gain some insight into its binding mechanisms with cellular macromolecules such as proteins.[26,27] For example, certain protein molecules contain a double-stranded-RNA-binding motif (dsRBM), which binds to the interface of A-form RNA through site-specific interactions with the minor and major grooves of the helical structure.[26,28,29] These protein-dsRNA complexes can take on several roles within cellular systems, including gene expression regulation and protecting the cell from potential pathogens.[26] Thus, these types of studies help to further understand the impact that an RNA molecule's structure may have on its intended biological function.

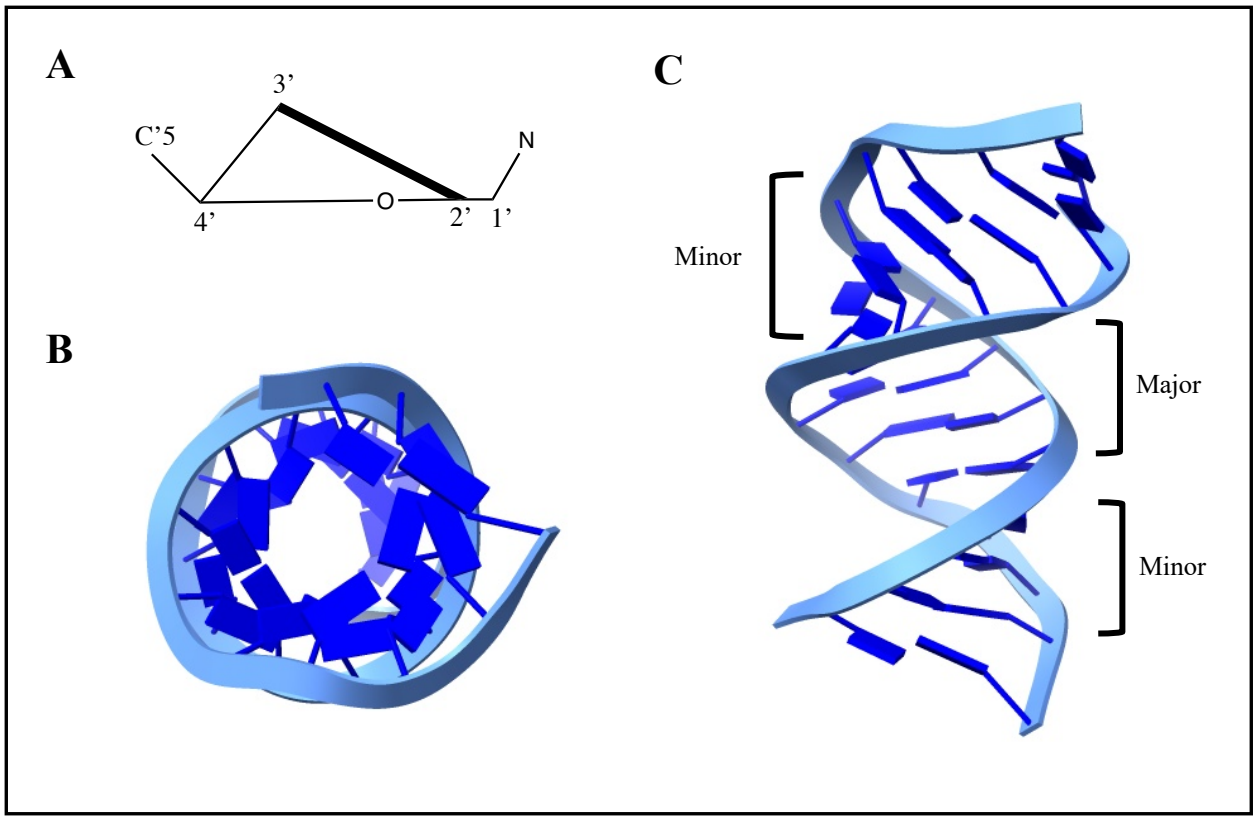


Figure 1.2: Double-stranded A-form helical RNA. The **A)** $C_{3'}$-endo sugar puckering of the ribose molecule,[24,30] as well as the **B)** top and **C)** side view of an A-form RNA helix (PBD: 1RNA)[22] to observe the base-pair displacement, as well as the major and minor grooves of the helix. Figure 1.2A was modified from Arias-Gonzalex[30] using Chemdraw and Figures 1.2B-C were modified from Saenger.[24] The molecular graphics were created using ChimeraX.[31,32]

1.2 Aptamers

RNA aptamers are single-stranded nucleic acid sequences, typically between 10-200 nucleotides in length, that are capable of specific binding to target molecules with high affinity.[6,7,33,34] They can be used to identify small ligands, such as chemical toxins or proteins. Upon interaction with a target molecule, the aptamer can undergo a process known as adaptive binding in which an unstructured aptamer sequence folds into a stable and defined three-dimensional configuration around the ligand, as depicted in **Figure 1.3A**.[35–37] Unbound RNA aptamers can also form complex three-dimensional structures with protein-like binding pockets that allow for the specific recognition of a target molecule (**Figure 1.3B**).[38,39] The idea of specific

binding between nucleic acids and macromolecules was first conceived during the 1980s when structured RNA molecules produced by adenovirus and human immunodeficiency virus (HIV) were identified.[40,41] These RNA structures were capable of specific binding to both cellular and viral proteins with high affinities.[40] Specific target-binding nucleic acid sequences were later coined "aptamers" by a research group led by Szostak in the early 1990s.[35,42] This discovery paved the way for innovative research, which focused on the development of a new type of molecular detection tool.

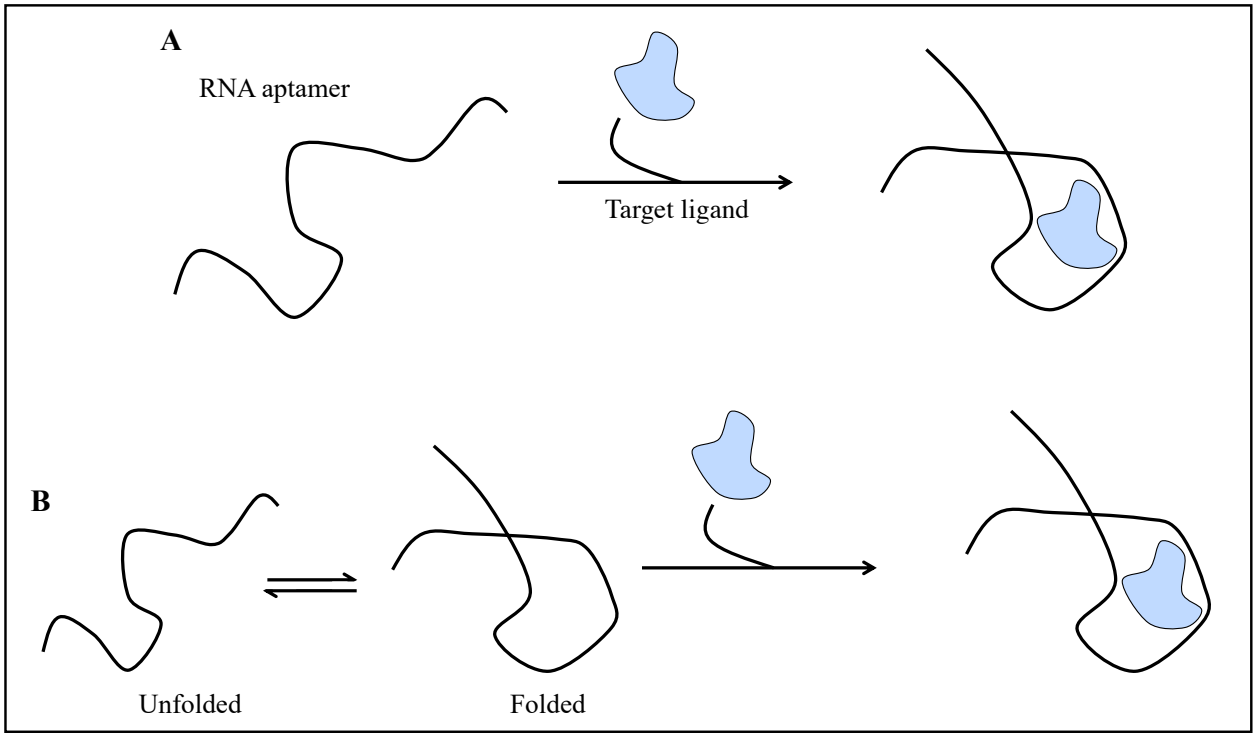


Figure 1.3: Binding mechanisms of an RNA aptamer to its target molecule. A) Adaptive binding mechanism, where the aptamer folds around the small molecule.[36] **B)** The binding of a folded RNA aptamer to its target molecule.[39] The unbound RNA aptamer is in equilibrium between the folded and unfolded state before interaction with the target ligand. Figure 1.3A was modified from Da Costa et al.[36] as well as Zhu et al.,[43] and Figure 1.3B was modified from Elskens et al.[39] using PowerPoint.

One of the most promising aspects of aptamers comes from their similarity to antibodies.[5] Not only are the functions of aptamers and antibodies similar, with comparable levels of specificity

and affinity towards the molecules of interest, but aptamers appear to offer a wide range of advantages when compared to traditional molecular recognition techniques.[6] Due to their small size, aptamers are able to overcome many of the biological obstacles faced by antibodies. For instance, aptamers can easily penetrate the membranes of solid tumors and form complexes with binding sites that are often inaccessible to large antibodies. Additionally, the chemical production of aptamers is often accompanied by high levels of accuracy and reproducibility.[6,44] This is a great improvement from antibodies, which are prone to variations between each batch produced. The resulting differences may affect the specificity and strength of binding toward the target molecule. Moreover, aptamers are selected using *in vitro* techniques and as a result can be specific for toxic and immunogenic compounds.[6] This is a great advantage over antibodies, which are produced within biological systems that may not be able to withstand these toxic compounds. Therefore, aptamer sequences serve as an alternative method for traditional molecular recognition techniques within commercial applications.

Consequently, aptamers have emerged as a promising therapeutic and detection tool that can be used in a wide range of applications within medical industries, scientific communities, and environmental conservation programs. Numerous *in vitro* studies have identified RNA aptamer sequences that can behave as therapeutic agents for viral infections and diseases through specific binding to cell surface receptors.[40] Although many of these identified RNA aptamers have great potential for drug development, there is only one aptamer that is actively being used within the medical industry.[10] After extensive clinical trials, an RNA aptamer that targets the vascular endothelial growth factor isoform 165 was approved as a medical treatment for the eye disease macular degeneration.[6,10] In addition to their role as a therapeutic agent, aptamers can be used in the lab as an imaging tool to visualize and understand specific intracellular structures and

processes.[45] For instance, fluorophore-binding RNA aptamers can be fused to mRNA sequences to monitor the transcription mechanisms of a living cell.[46] Furthermore, aptamers can be used help preserve natural resources by detecting and quantifying chemical contaminants. For example, aptamers have the potential to be used for the identification and removal of contaminants, such as mycotoxins, from drinking water sources.[9] Hence, the function of RNA aptamers is extremely versatile, which goes to highlight their significance in the scientific community.

Despite the many benefits of using aptamer sequences as a molecular detection tool, these oligonucleotides face their own set of difficulties when used *in vivo*. Although their small size promotes flexibility in movement and target binding, their function as therapeutic agents within the human body can be compromised. For instance, they are filtered through the kidneys at a much faster rate than other larger biological tools like antibodies.[6,47] Therefore, these RNA sequences must undergo additional chemical modifications to improve their working lifetime, such as the attachment of bulky chains like polyethylene glycol (PEG) or fluorophore molecules to the nucleotide backbone, which can help to resist kidney filtration.[6,47,48] Additionally, RNA aptamers have short half-lives of less than 10 minutes due to their high susceptibility to degradation by the enzyme ribonuclease (RNase).[6,49] RNase A cleaves the phosphodiester backbone of RNA molecules through a transphosphorylation and a hydrolysis reaction (**Figure 1.4**), in which histidine-12 and histidine-119 likely act as the proton acceptors and donors within the catalytic mechanism.[50–53] To resist recognition by RNases a mirror image of the aptamer, called a Spiegelmer, can be created.[48] These resulting L-RNA aptamers not only display enhanced biostability compared to natural RNA sequences but also retains the same high affinity and selectivity for the target molecules.[54–56] Published studies have revealed that Spiegelmer molecules can exhibit long half-lives of up to 40 hours when employed as drug molecules within the human

body.[55,57] Therefore, before a desired aptamer sequence can be used for commercial applications, researchers must not only have an in-depth understanding of the aptamer and its target ligand, but they must also have extensive information regarding its potential working environment. This will provide the necessary information for aptamer sequence modifications to ensure its proper function for the desired length of time.

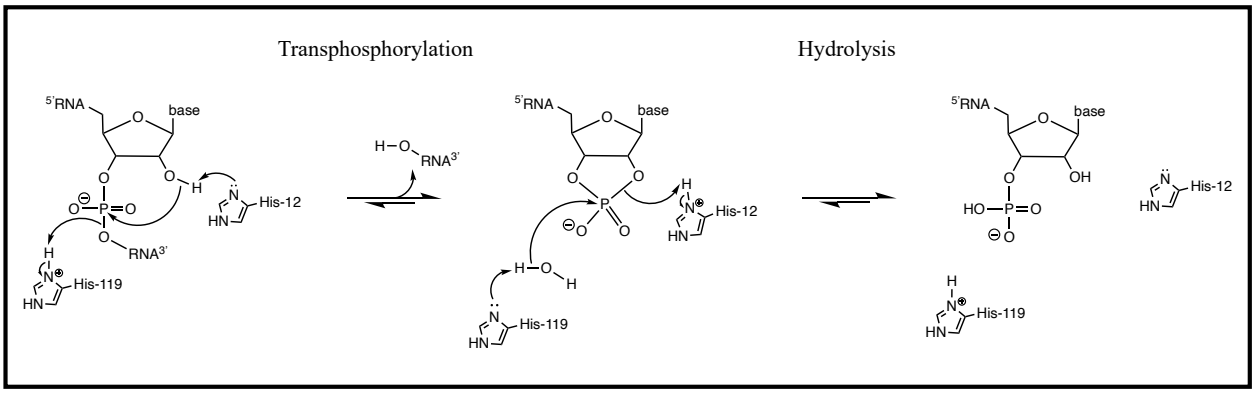


Figure 1.4: RNA degradation mechanism by the RNase enzyme. Transphosphorylation and hydrolysis reaction mechanisms of the RNA molecule, catalyzed by RNase A.[50,52] Figure 1.4 was modified from Raines[52] as well as Palmer and Bonner,[50] using Chemdraw.

1.2.1 Aptamer Selection

RNA molecules that function as aptamers have been identified in natural sources, such as those produced by viruses[40] and those encoded by eukaryotes to form riboswitches.[58] Many of the studied aptamer sequences in literature, however, have been generated through an *in vitro* selection process known as the Systematic Evolution of Ligands by EXponential Enrichment (SELEX).[59] This aptamer selection method was introduced to the scientific community during the 1990s by two separate research groups led by Gold and Szostak.[35,59,60] Within the study conducted by Tuerk and Gold,[60] SELEX was used to identify RNA sequences capable of specific binding to the enzyme T4 DNA polymerase. From the results, it was determined that not only were the isolated RNA sequences highly selective for the T4 enzyme and able to form strong binding interactions, but the

formation of the aptamer-enzyme complex alters the function of the enzyme by inhibiting its ability to replicate. Similarly, in the study conducted by Ellington and Szostak,[35] the *in vitro* selection process was used to identify RNA molecules that are capable of binding to certain types of organic dyes. During the analysis of the resulting RNA molecules, similarities were observed between short segments of two of the isolated sequences. Through additional investigations, it was concluded that these conserved sequence motifs were involved in the binding to the target dyes. Thus, these preliminary studies highlighted the promise of SELEX within the research community by showcasing its ability to identify highly selective aptamer sequences. These studies also noted the potential applications of SELEX, such as for the isolation of both single- and double-stranded DNA aptamers, and for the selection of ribozyme molecules.[35,60]

To identify highly selective RNA aptamers using the traditional SELEX method, an experiment would typically begin with a large pool of approximately 10^{15} randomized RNA fragments.[38,60–62] These RNA sequences are transcribed from ssDNA templates, each consisting of fixed 3' and 5' primer binding sites surrounding a randomized nucleotide region.[62] To briefly outline the SELEX process (**Figure 1.5)**, as described in the paper by Tuerk and Gold,[60] the pool of random RNA ligands is mixed with the target molecule, and the bound sequences are eluted out. The resulting eluted RNA molecules then undergo reverse transcription to produce complementary DNA (cDNA), which is then amplified using polymerase chain reaction (PCR). The amplified cDNA molecules are then transcribed back into RNA and used as the new pool of enriched sequences for the following round of SELEX. This process is typically repeated up to 15 times until there are only a handful of target-binding RNA sequences remaining in the selection pool.[60,62] During the later rounds of SELEX, the remaining RNA molecules are sequenced to evaluate the

sequence similarity. The binding strength between the target ligand and the isolated RNA molecules are also evaluated to identify the sequence that would be the ideal aptamer candidate.[62]

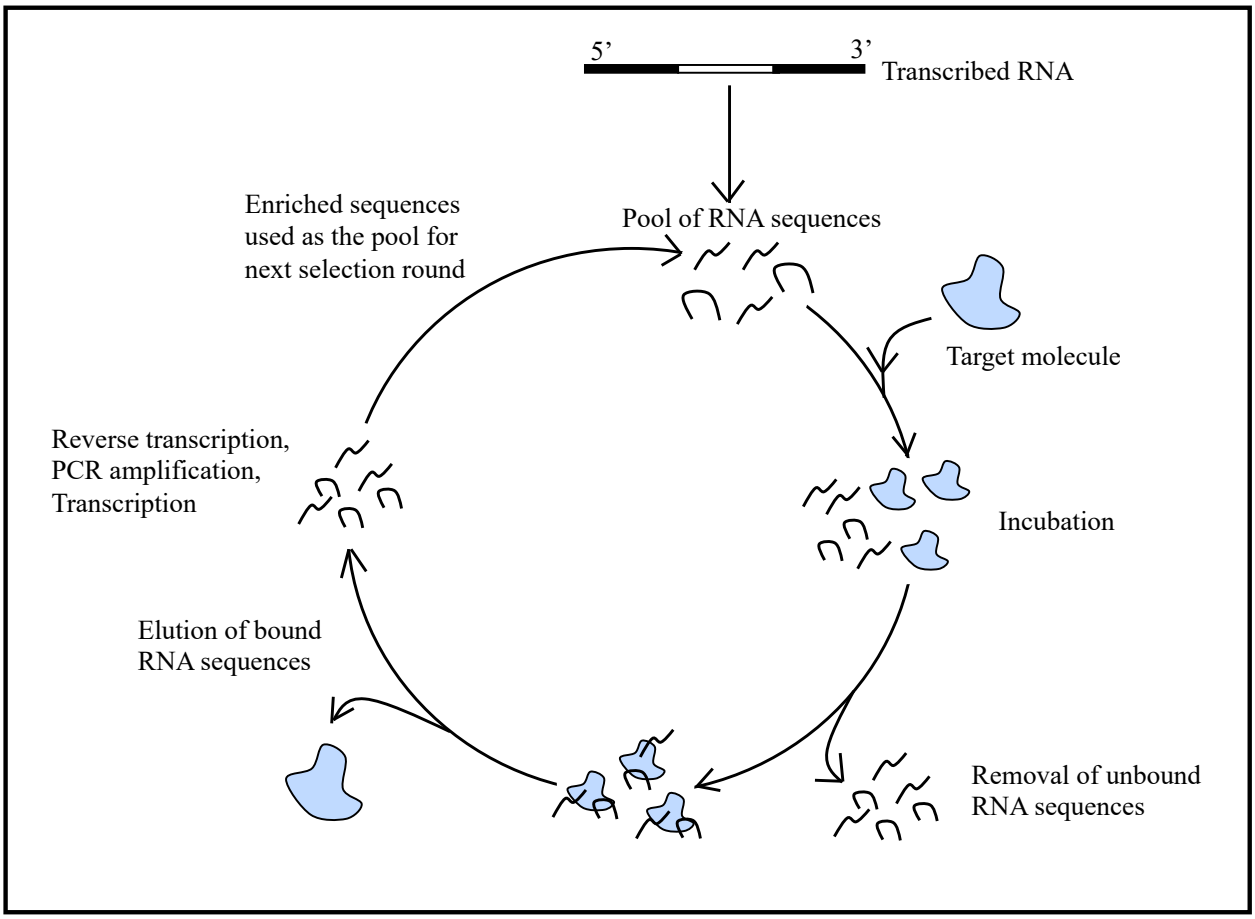


Figure 1.5: General overview of the SELEX process for selecting RNA aptamers. A large pool of randomized oligonucleotides is subjected to numerous rounds of selection and amplification.[60] The process is typically repeated up to 15 times, using both positive and negative controls to identify the RNA molecules capable of specific binding with high affinity to the target ligand.[62] Figure 1.5 was modified from Zhuo et al.[62] using PowerPoint.

Although SELEX is a relatively easy and straightforward method to produce aptamers, it is not without flaws.[63] It is possible that a target molecule may be too small, hence reducing the potential surface interactions with the folded aptamer sequence.[38] Consequently, this would make it difficult to isolate an RNA aptamer that can bind with the target ligand. A publication by Hasegawa et al.[63] also noted that it is possible for aptamers with intricate structures required for

strong binding to the target molecule to reject PCR amplification and subsequently be lost from the pool of enriched nucleotides destined for additional rounds of SELEX. Moreover, aptamers may bind to compounds with similar structural components as the target molecule, hence decreasing the accuracy of the aptamer's function.[47] To help mitigate this problem, additional rounds must be included during the latter half of the SELEX process where these analogous structures are introduced as negative targets.[62] Any oligonucleotide sequences that bind to these negative targets are then removed from the pool and excluded from future selection rounds. To further improve the selection process, researchers have also developed modified versions of the SELEX method to select aptamers under ideal conditions for both the aptamer sequence and the target molecule. For instance, high-throughput sequencing SELEX greatly shortens the aptamer selection process by identifying the enriched sequences during the earlier rounds of selection.[62,64] Additionally, *in vivo* SELEX was developed to help address the functionality of aptamer sequences when used for living systems by performing the selection process within model animals for a desired disease.[62,65] Therefore, researchers much be aware of the potential barriers that may arise when selecting for a new aptamer system, however there are many modifications that can be incorporated into the selection process to help overcome these obstacles.

1.2.2 Aptamer-Based Biosensors

Biosensor are analytical devices, typically composed of a bioreceptor and transducer, that allow for the *in vivo* visualization and quantification of target molecules.[66,67] The bioreceptor consists of a biomolecule, such as an enzyme, which acts to detect the target molecule, whereas the transducer produces a measurable signal using the energy released during the biorecognition event.[66,68] These biosensors can be used for a wide range of commercial applications. For instance,

they can be employed as glucose monitors within the medical industry[67,69] or as detectors for potential food-borne pathogens within the food industry.[67,70,71] To visualize molecular interactions *in vivo*, aptamers can be modified with recognition elements, such as light-up fluorophores, to generate a type of aptamer-based biosensor also known as an aptasensor.[46] The use of aptasensors for industrial functions is advantageous compared to other detection methods as the target ligand can be detected directly in solution without the need for additional sample treatments, such as washing or immobilization.[72] Additionally, the fluorescence intensity produced upon binding to the target can be measured and quantified to determine the ligand concentration within the sample solution. Therefore, these aptasensors are useful tools for the rapid, real-time detection of target molecules.[43]

There are a variety of approaches that can be used to generate a functional aptasensor; however, the method chosen should be based on considerations regarding the functional limitations of the aptasensor, the time required to produce the aptasensor, and the intended applications. For instance, aptamers can be fluorescently-labelled, in which a fluorophore molecule is covalently linked to the phosphate backbone of an aptamer, as shown in **Figure 1.6A**.[72,73] Upon binding to the target ligand, the aptamer folds in a way that alters the chemical environment surrounding the fluorophore.[72–74] Therefore, the aptasensor will exhibit either an increase or decrease in fluorescence intensity upon binding to the ligand. A study by Jhaveri et al.[72] used this method to conjugate fluorescent labels to the adenosine triphosphate (ATP)-binding RNA and DNA aptamers that were previously selected by the Szostak research group.[72,75,76] From the results, it was observed that not only did both the RNA and DNA aptamers retain their specificity for ATP, but they also showed that the fluorescence emission produced is proportional to the ligand concentrations present in the solution.[72] The development of fluorescently-labelled aptamers,

however, can be both time-consuming and expensive. Extensive modelling and analysis must first be conducted to ensure that the linked fluorophore molecules do not interfere with the intended function of the aptamer.[72,73]

As an alternative approach, aptasensors can also be generated through label-free methods.[73] Using this technique, the fluorescent molecules can exhibit a change in fluorescence intensity either upon the binding **(Figure 1.6B)** or displacement **(Figure 1.6C)** of a fluorophore molecule from the aptamer sequence.[43,73] A study by Xu and Lu[77] used the label-free method to develop a hybrid RNA aptamer, which is composed of the malachite green (MG) aptamer joined to the adenosine DNA aptamer, which was previously selected by Grate and Wilson[78] as well as Huizenga and Szostak,[76] respectively. In the absence of adenosine molecules, the binding of the aptamer to the MG dye is prevented by the addition of a bridging strand that remains hybridized to the fused RNA-DNA aptamer strand.[77] Upon the addition of adenosine to the solution, the adenosine aptamer folds around the ligand which displaces the bridging strand. This allows for the MG aptamer to also fold around the fluorophore in a similar mechanism to the one displayed in **Figure 1.6B**. From the results, it was noted that not only was this hybrid aptamer sequence capable of specific binding to adenosine, but the fluorescence intensity produced upon recognition was once again proportional to the ligand concentration present in the solution. Moreover, a 2008 study by Huang and Chang[79] used the adenosine-binding DNA aptamer and OliGreen (OG) dye to develop a label-free aptasensor for the detection of potassium ions. Upon interaction of the DNA aptamer with the potassium ions, the OG dye gets displaced and exhibits reduced fluorescence, similar to the mechanism outlined in **Figure 1.6C**. Thus, researchers have developed and investigated numerous methods to produce viable aptasensors. These methods can be applied to a

variety of aptamer systems and can be further modified to optimize their function as an optical biosensor.[77]

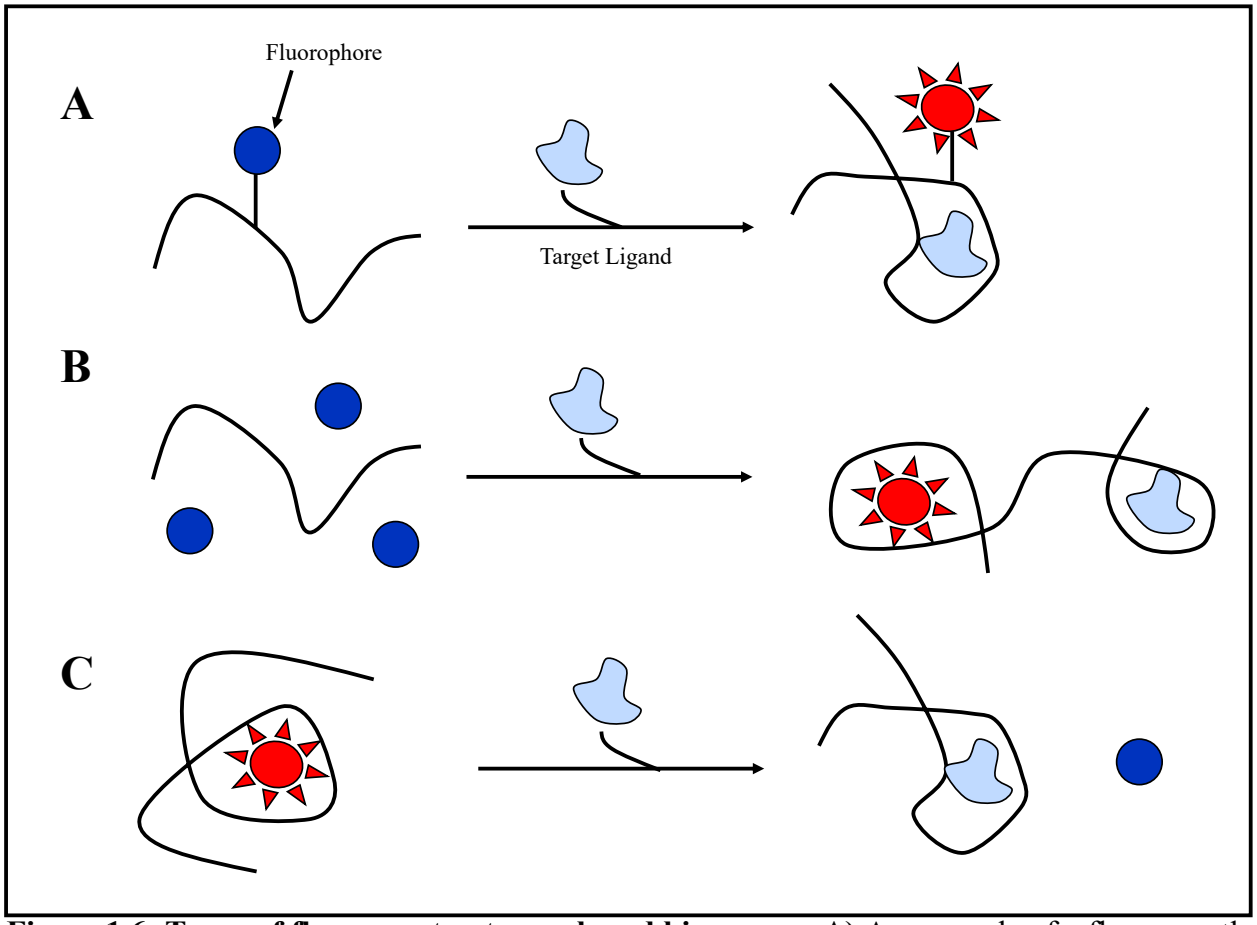


Figure 1.6: Types of fluorescent aptamer-based biosensors. A) An example of a fluorescently labelled aptamer in which there is an increase in fluorescence intensity upon the formation the aptasensor-ligand complex.[73] Examples of label-free aptamers where **B)** the fluorophore molecule undergoes an increase in fluorescence upon binding to the aptamer caused by target-induced conformational changes, and **C)** the fluorophore molecule undergoes a decrease in fluorescence upon displacement from the aptamer in the presence of the target ligand. Figure 1.6A was modified from Jhaveri et al.[72] and Musumeci et al.,[73] Figure 1.6B was modified from Xu and Lu,[77] and Figure 1.6C was modified from Huang and Chang[79] as well as Musumeci et al.[73] using PowerPoint.

1.2.3 Biochemical Characterization of Aptamers

The biochemical characterization of aptamer-ligand systems is important for understanding the potential molecular interactions and mechanisms present between the aptamer sequence and its target molecule.[80] Having a well-characterized aptamer system is essential for its potential use

in commercial applications, as it helps to ensure that the chosen aptamer can function efficiently when used for diagnostic or therapeutic purposes.[47,80] For instance, determining the binding affinity between two molecules of interest through a measure of the dissociation constant (K_d) can provide some insight as to how tightly the molecules are bound to each other.[81] Experimentally determined K_d values that fall within the nanomolar (nM) range are indicative of high binding affinities, while values that fall within the millimolar (mM) range are representative of significantly lower binding strengths between the molecules of interest.[82,83] There are many factors that may contribute to a reduced binding affinity. For instance, an aptamer's three-dimensional structure has the potential to limit interactions with the target molecule, hence reducing the binding strength.[63] Therefore, if the experimental results reveal weak binding between the aptamer and its target molecule, then modifications such as the sequence refinement or truncation of a selected aptamer can be made to help improve the binding interactions for optimal function.[39,63]

Examining the binding kinetics can also be useful for determining the rates of association (k_{on}) and dissociation (k_{off}) within an aptamer-ligand system.[84] The data obtained for the binding kinetics can reflect the binding affinity, as shown in Equation 1, as molecules with tight binding interactions are often observed to have fast k_{on} and slow k_{off} rates.[84,85]

$$\frac{1}{K_d} = \frac{k_{on}}{k_{off}} \tag{1}$$

In addition, the thermodynamic analysis of an aptamer system can aid in determining the potential ligand recognition and binding mechanisms.[84,86,87] For instance, a measure of the Gibbs free energy (ΔG) can reveal the stability of an aptamer-ligand complex, as greater negative values are indicative of stronger associations between the molecules of interest.[84] From the ΔG, additional information regarding the change in enthalpy (ΔH) and change in entropy (ΔS) of the complex formation can be calculated and evaluated, as shown in Equation 2.

$$\Delta G = \Delta H - T\Delta S \quad (2)$$

The analysis of the ΔH can help one to understand the specificity of aptamer-ligand associations.[84,88,89] Negative enthalpies of large magnitudes are typically representative of energetically favourable interactions upon binding.[84,88] For instance, negative ΔH values represent a net gain of hydrogen bonds and electrostatic interactions between the interacting molecules.[84,90] It could also point towards the stacking of base pairs and nucleotides within target nucleic acid molecules.[91] Moreover, the analysis of the ΔS can reveal information regarding the degree of disorder present between interacting species within a target system.[84,89,92] Limited mobility and conformational rigidity within a biological complex is often characterized by negative values. Whereas values with positive signs are indicative of favourable entropy changes, which are associated with the release of water molecules from the complex's binding surface.[90,92] Positive ΔS values are also indicative of an increase in the intramolecular degrees of freedom and mobility within the target biomolecule system.[84] When analyzing the change in thermodynamics properties with respect to varying environmental conditions, such as pH and temperature, it can reveal the optimal binding conditions for an aptamer-ligand system.[86] Therefore, through an investigation of the binding affinity, as well as the kinetic and thermodynamic properties, a great deal of information can be gained regarding the interactions and overall behaviour of the aptamer-ligand complex. The resulting biochemical profile can a good indication of the next experimental steps that should be conducted, such as further optimizations to the aptamer sequence and the performed experimental conditions.

1.3 Fluorogen-Binding RNA Aptamers and their Applications

Over the last few of decades, researchers have selected for RNA aptamers that can bind to small molecules with fluorogenic properties.[93,94] Upon binding, these molecules display large increases in fluorescence. There are many examples of fluorogen-binding RNA sequences in literature, termed fluorescent light-up aptamers (FLAPs),[93] including the Malachite Green, Spinach, Broccoli, Mango, Corn, Chili and Pepper RNA aptamers.[78,95–100] Only a few model systems, however, have been summarized in **Table 1.1** and **Chapters 1.3.1** – **1.3.3** below. FLAPs have the potential to be used as building blocks for aptamer-based biosensors within commercial applications. These aptamer systems can be used as fluorescent tags to monitor cellular processes as well as bimolecular interactions,[46,93,101] in a similar mechanism to the label-free aptasensors discussed in **Chapter 1.2.2**.[73,77] For instance, studies conducted by Pothoulakis et al.[102] and Guet et al.[103] have demonstrated the ability of the 3,5-difluoro-4-hydroxybenzylidene imidazolinone (DFBHI)-binding Spinach RNA aptamer to act as a fluorescent tag for the localization of mRNA transcripts within live *Escherichia coli* and *Saccharomyces cerevisiae* cells.[93,102,103] In addition, researchers have produced FLAP-RNA aptamer fusion complexes which allow for the real-time visualization of the biorecognition event through fluorescence enhancement.[93,101] Functional FLAP-RNA constructs have been designed and synthesized for the Malachite Green and Spinach RNA aptamers, in which the fused RNA aptamers specifically bind to small molecules such as adenosine and S-adenosylmethionine (SAM).[77,93,101,104,105] Despite the many potential applications of FLAPs, the use of these aptamer systems has been mainly limited to *in vitro* and live cell systems.[93,101] Hence, further investigations and optimizations should be carried out to aid these FLAPs in becoming molecular tools for a broad range of commercial applications, including medical treatments and environmental conservation efforts.

Table 1.1: Examples of fluorogen-binding RNA aptamers in literature and their corresponding biochemical properties.

RNA Aptamer	Length (nt)	Fluorogen	Abbreviation	Kd (nM)	References
Malachite Green	38	Malachite Green	MG	800	[106]
				117	[107]
		Tetramethylrosamine	TMR	~ 40	[106]
		Pyronin Y	n/a	~ 225	[106]
Spinach	98	3,5-Difluoro-4-Hydroxybenzylidene Imidazolinone	DFBHI	537	[95]
Mango	29	Thiazole Orange 1-Biotin	TO1-Biotin	3.2	[97]

1.3.1 Malachite Green RNA Aptamer

Malachite green is a triphenyl methane-based dye (**Figure 1.7B**) that exhibits almost no fluorescence when unbound in solution.[77,106] In the year 1999, Grate and Wilson[78] performed *in vitro* selection and minimization experiments, which resulted in the production of a 38-nt RNA sequence that can specifically bind to the MG dye (**Figure 1.7A**). A year later, Baugh and Wilson[106] performed competitive inhibition assays between the RNA aptamer and analogs of the MG chromophore and monitored the resulting binding interactions by fluorescence anisotropy. Through these investigations, it was found that the MG aptamer binds to the MG dye with a dissociation constant of approximately 800 nM (**Table 1.1**). These experiments also revealed that the MG RNA aptamer preferentially binds to planar analogs of the dye.[106,107] For instance, the RNA aptamer was found to bind to tetramethylrosamine (TMR) (**Figure 1.7C**) and pyronin Y (**Figure 1.7D**) with dissociation constants of approximately 40 and 225 nM, respectively (**Table 1.1**).[106] Additional fluorescence titration experiments carried out by Babendure et al.[107] discovered that the MG RNA aptamer has stronger binding interactions with the MG dye than previously believed, at a K_d of 117 nM, within environments that contain higher ionic strengths and without the presence of competing ligands. The group also determined that the MG dye undergoes a 2400-

fold increase in fluorescence upon binding to the RNA sequence. The use of the MG RNA aptamer system for potential commercial applications, however, is not ideal. When exposed to laser irradiation, the MG dye may produce reactive oxygen species (ROS) that can be harmful to cells.[93,101] Moreover, the reduced form of MG, leucomalachite green, is toxic to aquatic ecosystems and humans.[108] Despite these disadvantages, the MG-binding RNA aptamer has become a model system that has helped pave the way for additional studies which focus on the development and optimization of FLAP systems.[93]

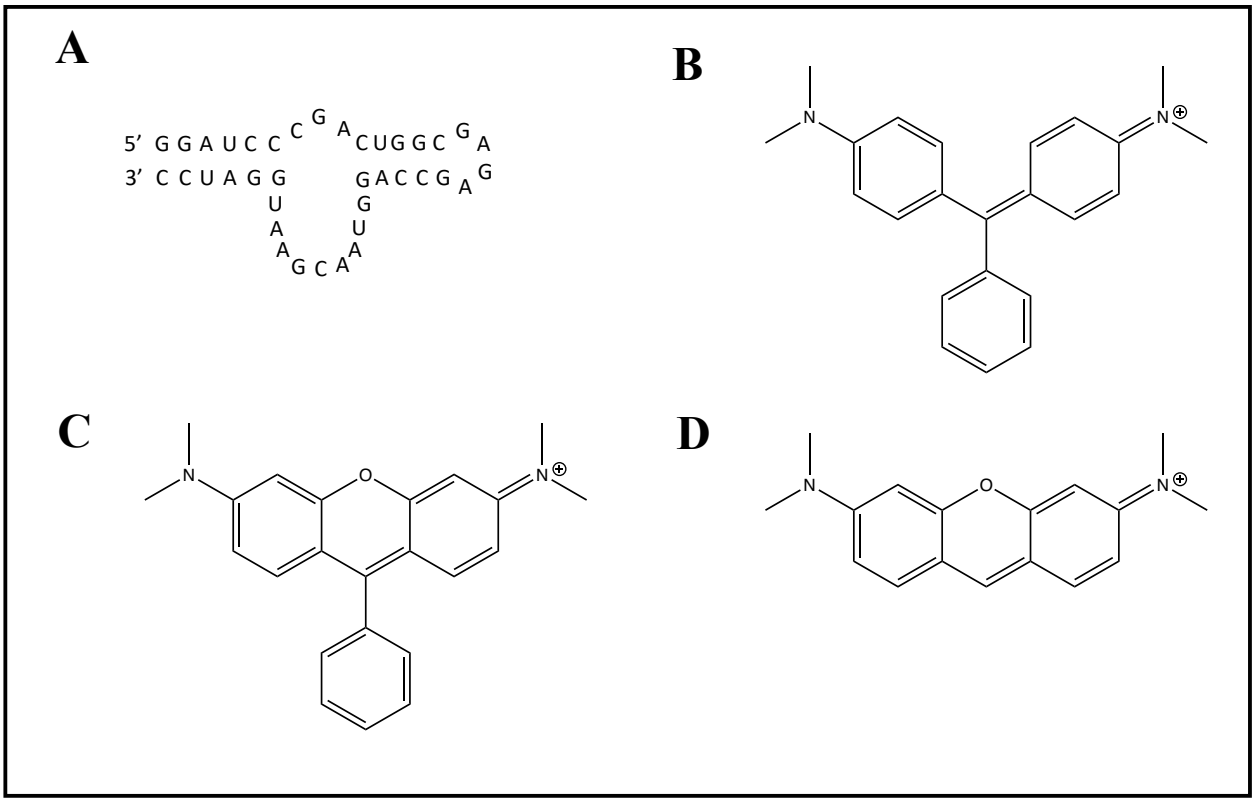


Figure 1.7: Malachite Green RNA aptamer. A) Secondary structure of the 38-nt MG RNA aptamer. The chemical structures of the **B)** MG, **C)** TMR, and **D)** pyronin Y dyes. Figure 1.7 was modified from Baugh et al.[106] using PowerPoint and Chemdraw.

1.3.2 Spinach RNA Aptamer

DFHBI (**Figure 1.8B**) is a derivative of 4-hydroxybenzlidene imidazolinone (HBI), the fluorophore within green fluorescent protein (GFP),[95,109] that was synthesized by Paige et al.[95] to mimic the spectral properties of enhanced green fluorescent protein (eGFP). The group went on to perform SELEX for the eventual selection of a 98-nt RNA aptamer, termed the Spinach aptamer (**Figure 1.8A**), that can bind to the DFHBI dye. Through a series of characterization experiments, it was revealed that the RNA aptamer selectively binds to DFHBI with a K_d of 537 nM (**Table 1.1**), even in the presence of similarly structured molecules, such as HBI. Upon binding to the RNA aptamer, the DFHBI dye was observed to display an approximate 2000-fold increase in fluorescence,[95] similar to that of the malachite green dye.[107] The group went on to demonstrate the potential *in vivo* applications of the Spinach aptamer, such as its use as a fluorescent tag for live-cell imaging.[95] Not only is DFHBI capable of permeating cell membranes, but it is also non-cytotoxic unlike the malachite green dye.[95,110] As a result, researchers have extensively characterized and further optimized the Spinach RNA aptamer system. For example, the Spinach2 aptamer was developed to improve the thermostability and folding of the RNA sequence when used within *in vivo* systems.[93,111] Furthermore, the Baby Spinach and iSpinach variants were developed to minimize the sequence length down to 51 and 69-nt, respectively.[93,110,112] Therefore, the development of the Spinach aptamer was integral for showcasing the promise of FLAPs as a molecular tool within *in vivo* systems.

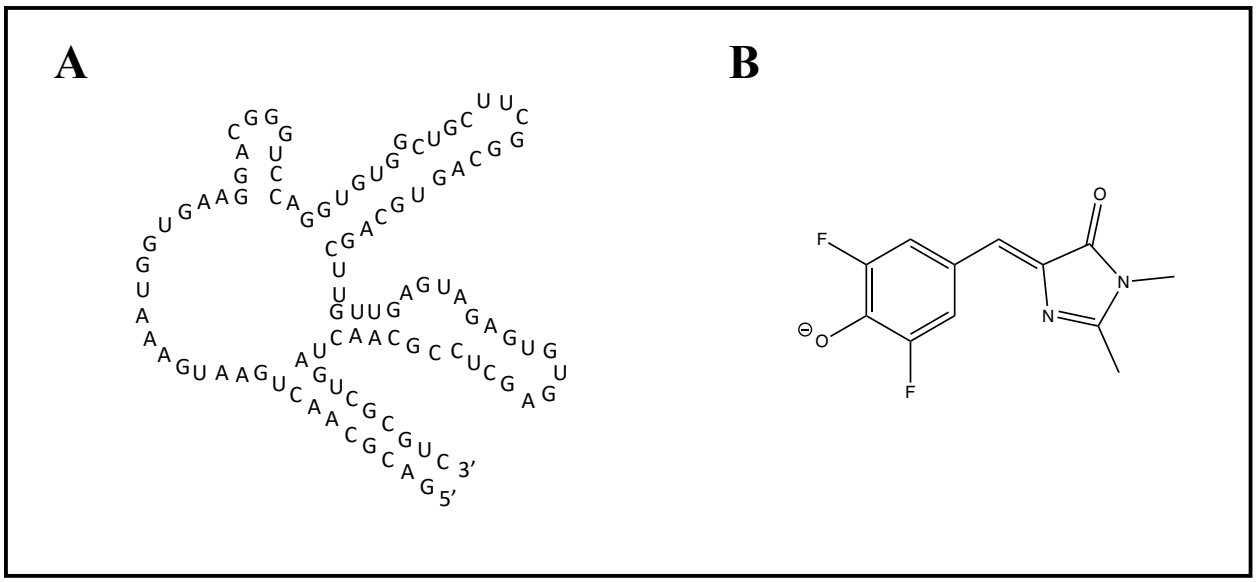


Figure 1.8: Spinach RNA aptamer. A) Secondary structure of the 98-nt Spinach RNA aptamer sequence and **B)** the chemical structure of the DFBHI dye. Figure 1.8 was modified Paige et al.[95] using PowerPoint and Chemdraw.

1.3.3 Mango RNA Aptamer

Similar to the DFHBI dye, thiazole orange (TO) is a low toxic asymmetric cyanine, that undergoes a large fluorescence enhancement upon interaction with double-stranded nucleic acids sequences.[97,113] In the year 2014, Dolgosheina et al.[97] synthesized a biotinylated derivative of the TO dye, named thiazole orange 1-biotin (TO1-Biotin) (**Figure 1.9A**), which prevents non-specific interactions with random nucleic acid sequences. The group performed SELEX and identified the Mango RNA aptamer sequence which contains a G-quadruplex forming 23-nt motif that participates in the specific binding to the TO1-Biotin dye. Characterization experiments revealed that the Mango RNA aptamer binds to the dye with a high affinity of 3.2 nM and the bound fluorophore exhibits an approximate 1100-fold increase in fluorescence. Similar to the Spinach aptamer, researchers have continued to optimize the Mango aptamer system through the development of the Mango II, III and IV RNA sequences.[101,114] These new Mango sequences were produced to not only optimize their biophysical properties but also their performance when used

for *in vivo* applications, such as the subcellular localization of RNA molecules.[114] Hence, the development and optimization of the Mango RNA aptamer has introduced an additional FLAP that can be used for molecular detection and visualization purposes within *in vitro* and *in vivo* systems.

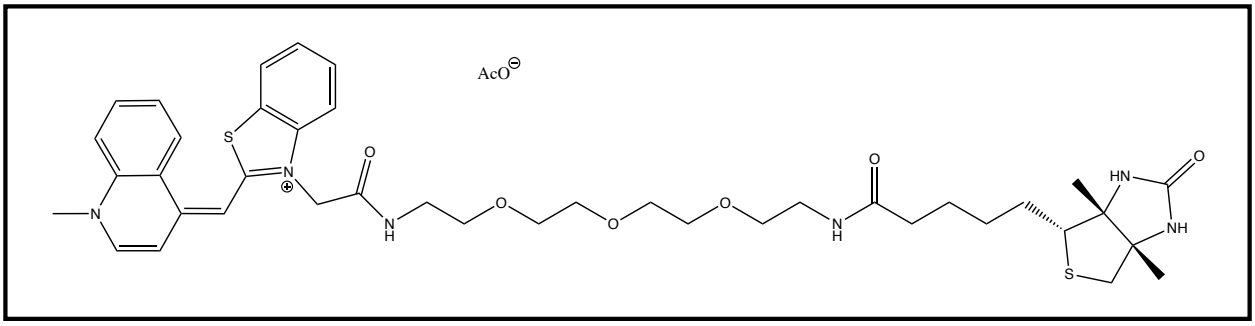


Figure 1.9: Chemical structure of the TO1-Biotin fluorophore. Figure 1.9 was modified from Dolgosheina et al.[97] using Chemdraw.

1.3.4 Derivative Hoechst Dyes

In addition to the fluorophores that were briefly discussed in **Chapter 1.3 – 1.3.3**, Hoechst dyes are another type of fluorescent molecule that have been traditionally used as a non-intercalating DNA stain within fixed and living cells.[115–117] Hoechst dyes are crescent-shaped molecules that consist of a methyl piperazine ring bound to two consecutive benzimidazole rings and a phenol ring, as shown in **Figure 1.10A**.[118] There are many derivatives of the Hoechst dye, which differ by the R-group on the terminal phenol ring.[117] Hoechst 33258 was the first derivative to be synthesized in the early 1970s by the German company Hoechst AG.[117,119] Since then, additional derivatives have been manufactured by the company, such as the Hoechst 33342 and Hoechst 34580 dyes. The modifications that were made to each of the Hoechst dye derivatives allow for slight variations in their function as a research tool. For instance, the Hoechst 33258 dye is often used for the staining of fixed cells while the Hoechst 33342 dye is often employed for the staining of live cells due to its heightened ability to permeate cell membranes.[117,120]

X-ray diffraction studies of the Hoechst 33258 and 33342 derivatives, conducted by Teng et al.[118] and Sriram et al.[121] respectively, have helped to visualize the binding interactions of the Hoechst dye to dsDNA. The Hoechst dye binds non-covalently within the minor groove of B-form helical DNA, specifically to regions rich in adenine-thymine (A-T) base pairs (**Figure 1.10B**).[118] Upon binding to dsDNA, the bonds within the Hoechst dye derivatives undergo a suppression in rotational freedom.[117,122] As a result, the Hoechst dyes display an approximate 30-fold increase in fluorescence when bound.[117,119] Due to their ability to display a large fluorescent signal upon binding to double-stranded DNA and low cytotoxicity, Hoechst dyes have become popular research tools for the visualization of DNA sequences.[117,120]

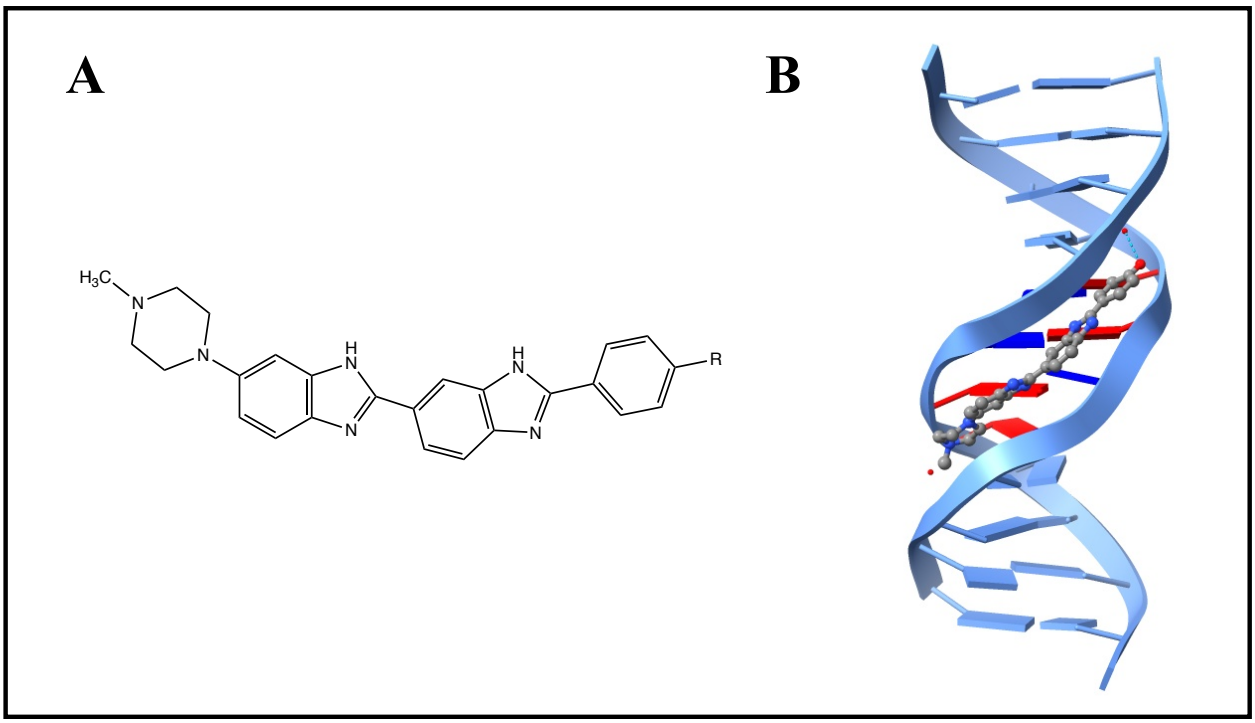


Figure 1.10: An example of a Hoechst-DNA complex. A) The molecular structure of the Hoechst dye, where the R group is -OH, -OCH_2CH_3 and -$N(CH_3)_2$ for the Hoechst 33285, 33342 and 34580 derivatives respectively.[117,119] **B)** An x-ray diffraction crystal structure, which shows the non-covalent binding of Hoechst 33258 to the minor groove of B-form helical DNA (PDB: 1DNH).[118] The adenine and thymine bases of the DNA sequence are shown in red and dark blue respectively. The molecular structure was created using Chemdraw and the molecular graphics of the Hoechst-DNA complex were created using ChimeraX.[31,32]

1.3.5 Selection of an RNA Aptamer Specific for Derivative Hoechst Dyes

In the year 2007, a study conducted by Sando et al.[123] synthesized a Hoechst dye derivative with bulky tert-Butyl (tBu) groups that prevents the non-specific binding to random dsDNA sequences. The group performed SELEX to identify and optimize a 25-nt DNA aptamer that can selectively bind to the tBu Hoechst dye. The group later went on to perform a second SELEX procedure to select for a 71-nt RNA aptamer, termed Aptamer II (**Figure 1.11A**), that can also bind to the tBu Hoechst dye (**Figures 1.11C** and **D**).[46] To characterize the molecular interactions within the RNA-tBu Hoechst complex, surface plasmon resonance (SPR) and fluorescence emission experiments were subsequently carried out by the group. Through these investigations, Aptamer II was determined to have a strong affinity for the tBu dye, with a K_d of 35 nM. Upon the formation of the aptamer-dye complex, a 13.1-fold increase in fluorescence intensity was also observed. Hence, to further optimize the RNA aptamer, truncations and nucleotide mutations were introduced to the sequence. The modified sequences were evaluated through fluorescence emission assays to pinpoint the sequence that produced the largest increase in fluorescence intensity upon interaction with the tBu Hoechst dye. Eventually, an optimized 29-nt sequence was produced, termed Aptamer II-mini3-4 (**Figure 1.11B**), which displayed a 28.2-fold increase in fluorescence intensity when bound to the tBu Hoechst dye.

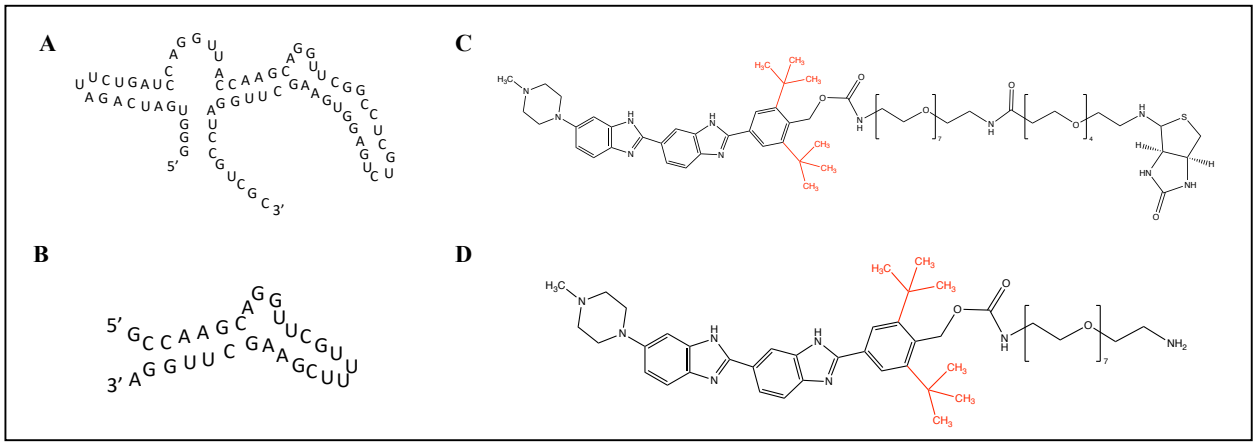


Figure 1.11: Sando selected RNA aptamers and their target derivative tBu Hoechst dyes. Predicted secondary structures of **A)** the 71-nt SELEX-selected RNA aptamer and **B)** the 29-nt Aptamer II-mini3-4 sequence that was optimized by Sando et al.[46] in the year 2008. The chemical structures of **C)** the Hoechst 1b dye derivative that was used by the group for SELEX and SPR experiments, as well as **D)** the Hoechst 1a derivative that was used for fluorescence emission experiments. The bulky tBu groups that were added to the phenol ring of the dye are shown in red. Figure 1.11 was modified from Sando et al.[46] using Chemdraw and PowerPoint.

During the optimization investigations performed by Sando et al.,[46] it was found that nucleotide modifications made to the bulge and head-stem regions of the predicted secondary structure of the Aptamer II-mini3-4 sequence significantly decreased the fluorescence emitted by the complex (**Figure 1.12**). This observation supported the hypothesis that the bulge region of the folded aptamer sequence likely accommodates the bulky tBu groups of the Hoechst dye. In a similar manner to the fluorogen-binding RNA aptamers that were discussed in **Chapter 1.3**, the group went on to suggest potential biosensor applications for the optimized RNA aptamer sequence. It was proposed and exemplified that the RNA sequence can be used as a blue-fluorescent tag for the visualization of luciferase transcription within live cells.

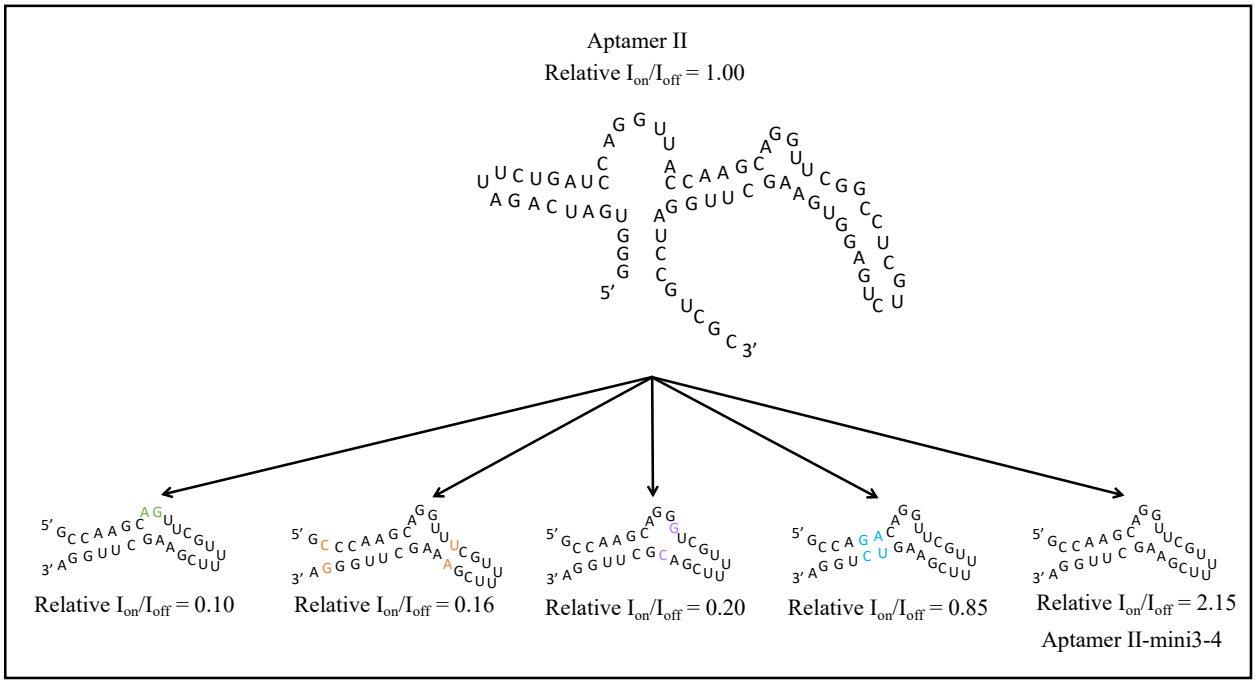


Figure 1.12: Optimization of the Hoechst-binding RNA sequence. Comparison of the nucleotide modifications that were made to the minimized RNA aptamer sequences and the evaluation of fluorescence intensity that was produced upon binding to the non-biotinylated Hoechst 1a derivative.[46] The group calculated the relative I_{on}/I_{off} values through comparison with the fluorescence intensity that was produced by the tBu-bound Aptamer II sequence. Figure 1.12 was modified from Sando et al.[46] using PowerPoint.

1.4 Research Objectives

As mentioned in **Chapter 1.3.5**, Sando et al.[46] selected for and optimized an RNA aptamer that is capable of specific binding to a tBu Hoechst dye derivative. The group conducted some preliminary biochemical studies (**Table 1.2**). However, the experiments performed were mainly focused on optimizing the tBu Hoechst-RNA aptamer's fluorescence through sequence minimization. Consequently, limited information is currently known regarding the molecular interactions and binding mechanisms between the optimized 29-nt Aptamer II-mini3-4 sequence and the tBu Hoechst dye. Therefore, the focus of this research project was to first obtain a complete biochemical profile of the Aptamer II-mini3-4 and Aptamer II RNA sequences that were previously selected by Sando et al.[46] This was done to develop an in-depth understanding of the

mechanisms present upon the formation of the optimized tBu Hoechst-Aptamer II-mini3-4 complex and how it differs from the non-optimized SELEX-selected aptamer sequence.

For this new research, additional RNA variants were also designed through nucleotide substitutions and sequence truncations to identify the tBu dye binding regions within the aptamer sequence as well as further optimize the aptamer system. Each of the RNA aptamer variants studied in this research project were evaluated through a combination of fluorescence emission, fluorescence titration, native polyacrylamide gel electrophoresis (PAGE), and isothermal titration calorimetry (ITC) experiments. These experiments were performed to determine the fluorescence enhancement, binding affinities, nucleic acid conformations, as well as the thermodynamic and kinetic properties of each of the variant RNA aptamers when complexed with the tBu Hoechst dye derivatives. Therefore, the biochemical experiments performed within this research project will hopefully lay the groundwork for the structure elucidation of the Aptamer II-mini3-4 sequence bound with the tBu Hoechst dye through nuclear magnetic resonance (NMR) spectroscopy experiments. The information gained from these experiments could also be helpful for the aptamer's potential development as a building block for an aptamer-based biosensor that can be used for commercial applications.

Table 1.2: Summary of the biochemical properties determined by Sando et al.[46] for the tBu Hoechst-binding RNA aptamers.

Aptamer Sequence	Length (nt)	K_d (nM)	I_{on}/I_{off} ratio	Relative I_{on}/I_{off} ratio
Aptamer II	71	35	13.1	1.00
Aptamer II-mini3-4	29	n/a	28.2	2.15

Chapter 2: Characterization of Derivative Hoechst-Binding RNA Aptamers through Fluorescence Methods

2.0 Introduction

As discussed in **Chapter 1.4**, the biochemical characterization of aptamer systems is important for understanding the specific molecular interactions and binding mechanisms between an aptamer and its target ligand.[80] This information can be used to determine the ideal working conditions of a selected aptamer for potential commercial applications.[86] It can also aid in identifying the specific modifications that can be made for the optimal function of an aptamer system. The tBu Hoechst-binding Aptamer II-mini3-4 RNA sequence has the potential to be developed as a FLAP for commercial applications, however extensive biochemical investigations must be first conducted on this aptamer system to understand its binding interactions. Sando et al.[46] performed brief fluorescence intensity experiments to compare the maximum fluorescence emitted by the tBu-bound RNA aptamer variants for the optimization of the RNA sequence. Fluorescence experiments are advantageous as these assays utilize the fluorescence produced by the sample and can be carried out quickly with low sample concentrations.[124] Therefore, the work done in **Chapter 2** focused to characterize the Sando-selected RNA aptamers and some newly designed RNA variants through fluorescence techniques, including fluorescence emission and titration assays.

When performing fluorescence emission assays, the emission spectra are obtained by exciting the sample with a series of excitation wavelengths and continuously recording the fluorescence emitted by the sample.[46,125,126] As stated above in **Chapter 1.3.4**, Hoechst dye derivatives are known to display an increase in fluorescence intensity upon binding to A:T rich regions of DNA sequences.[46,117] Therefore, an increase in fluorescence intensity at the corresponding emission wavelength is expected to be observed if binding is present between the tBu Hoechst dye and the RNA aptamer sequences. Moreover, fluorescence titration assays can be used to estimate the

dissociation constant between two molecules of interest.[127] Through this method, as described in a study by Wang et al.,[128] solutions of varying aptamer concentrations, ranging from zero to saturation, are prepared in a binding buffer and then incubated with a constant concentration of the fluorescent dye. Alternatively, the aptamer can be kept at a constant concentration while the dye concentrations vary. These aptamer-dye mixtures are then exposed to an excitation wavelength, and the fluorescence intensity produced by the complex is recorded based on the emission wavelength that produces the highest signal. The information that can be obtained from a fluorescence titration experiments, however, is limited to the binding affinity between the two molecules of interest. As a result, additional experiments must be conducted for a more in-depth molecular analysis of an aptamer-ligand complex.

2.1 Materials and Methods

2.1.1 RNA Aptamer Variants

To carry out the biochemical characterization of the tBu Hoechst-RNA aptamer complex, experiments were first performed on the SELEX-selected Aptamer II (**Figure 2.2A**) and optimized Aptamer II-mini3-4 (**Figure 2.2B**) RNA sequences that were discussed within the 2008 Sando et al.[46] publication. In addition, variations of the Aptamer II-mini3-4 sequence from the Sando et al. study were designed and synthesized, as shown in **Table 2.1** and **Figure 2.2** below. The nomenclature of the folded aptamer sequences that was used to discuss the RNA variants within this research project, including Helix 1 and 2, is depicted below in **Figure 2.1**.

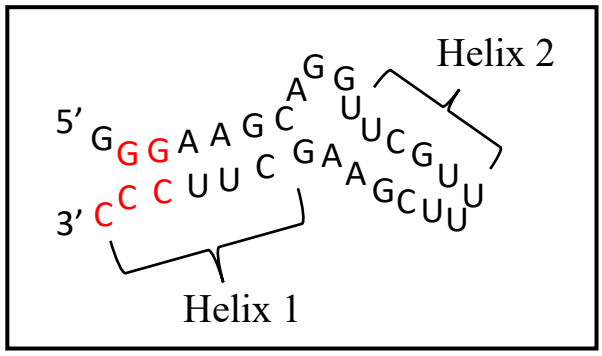


Figure 2.1: Nomenclature of the RNA aptamer variants. Depiction of Helix 1 and 2 of the folded aptamers using the Original RNA sequence as an example. Figure 2.1 was made using PowerPoint.

Each of RNA sequences that were used for experimentation were produced by *in vitro* transcription with T7 RNA polymerase (T7 RNAP). The Original RNA aptamer (**Figure 2.2C**) was the first variant to be designed. For this variant, the first three nucleotides of the 5’ end of the Aptamer II-mini3-4 sequence were changed to guanine for increased T7 RNAP activity and transcription yields.[129,130] Subsequently, the last three nucleotides of the 3’ end of the sequence were changed to cytosine in order to conserve the base pairing within Helix 1 of the predicted aptamer structure through Watson-Crick base pairing. In addition, when examining the predicted tetraloop portion of the RNA aptamer sequence, a four nucleotide UUUU tetraloop was observed. This tetraloop sequence can be difficult to observe through NMR spectroscopy as it does not adopt a single conformation due to its dynamic nature.[131] This was a concern for downstream experiments as this research project was focused on obtaining a biochemical profile that would eventually be used to support NMR spectroscopy experiments to study the structure of this tBu Hoechst-binding aptamer system. Therefore, two additional RNA aptamer variants were designed, one with a UNCG tetraloop and the other with a GNRA tetraloop, as shown in **Figures 2.2D** and **E**, respectively. These UNCG and GNRA tetraloop sequences have been very well characterized

in literature due to their stable structures and frequent presence in naturally occurring RNA sequences.[131,132] Therefore, conducting NMR spectroscopy experiments with these two RNA tetraloop variants would be helpful in identifying which nuclear Overhauser effect (NOE) signals correspond to the UUUU tetraloop nucleotides of the Original RNA aptamer. Moreover, it was previously predicted by Sando et al.[46] that the tBu groups of the Hoechst dye derivative interact with the internal bulge region of the folded RNA aptamer sequence. Hence, the Duplex RNA aptamer was designed in which the tetraloop portion of the aptamer was completely removed, as shown in **Figure 2.2F**. This was done to see if the tetraloop is required for the aptamer's binding to the tBu Hoechst dye. Similarly, the Elongated Duplex RNA aptamer was designed in which the length of both Helix 1 and 2 of the aptamer sequence were extended, as displayed in **Figure 2.2G**. This was done to ensure that the sequence had enough nucleotides for the T7 RNAP to transcribe a stable elongation complex.[129] It was hypothesized that extending these two stems would not interfere with the formation of the tBu Hoechst-RNA aptamer complex as the bulge region was believed to be the main binding region for the dye.[46] Finally, the Short Stem RNA aptamer variant was designed in which Helix 1 was almost entirely removed from the sequence, as shown in **Figure 2.2H**. This was done to determine if Helix 1 is involved in binding to the tBu Hoechst dye and to help identify which NOE signals arise solely from the first stem portion of the aptamer. Therefore, each of these aptamer variants were first subjected to biochemical characterization experiments to determine if the applied modifications affect binding to the tBu Hoechst dye and to ultimately gain deeper insights of the molecular interactions that are present in the tBu Hoechst dye-Aptamer II-mini3-4 complex.

Table 2.1: Variant Hoechst RNA aptamer sequences used for biochemical characterization experiments.

Variant Hoechst RNA Aptamer	Sequence
Aptamer II*	5'-GGGUGAUCAGAUUCUGAUCCAGGUUACCAAGCAGGUUCGGCCUCGUCUGAGGUGAAGCUUGGAUCCGUCGC-3'
Aptamer II-mini3-4*	5'-GCCAAGCAGGUUCG**UUUU**CGAAGCUUCCA-3'
Original	5'-GGGAAGCAGGUUCG**UUUU**CGAAGCUUCCC-3'
UUCG Tetraloop	5'-GGGAAGCAGGUUCG**UUCG**CGAAGCUUCCC-3'
GAAA Tetraloop	5'-GGGAAGCAGGUUCG**GAAA**CGAAGCUUCCC-3'
Duplex 5'-half	5'-GCCAAGCAGGUUCG-3'
Duplex 3'-half	5'-CGAAGCUUCCA-3'
Elongated Duplex 5'-half	5'-GGCCAAGCAGGUUCGCC-3'
Elongated Duplex 3'-half	5'-GGCGAAGCUUGGCC-3'
Short Stem	5'-GGCAGGUUCG**UUUU**CGAAGCC-3'

The * indicates the SELEX-selected and optimized Hoechst RNA aptamer sequences that were originally discussed within the 2008 Sando et al.[46] publication. The **bolded** bases indicate the location of the predicted tetraloop portion within the aptamer sequences.

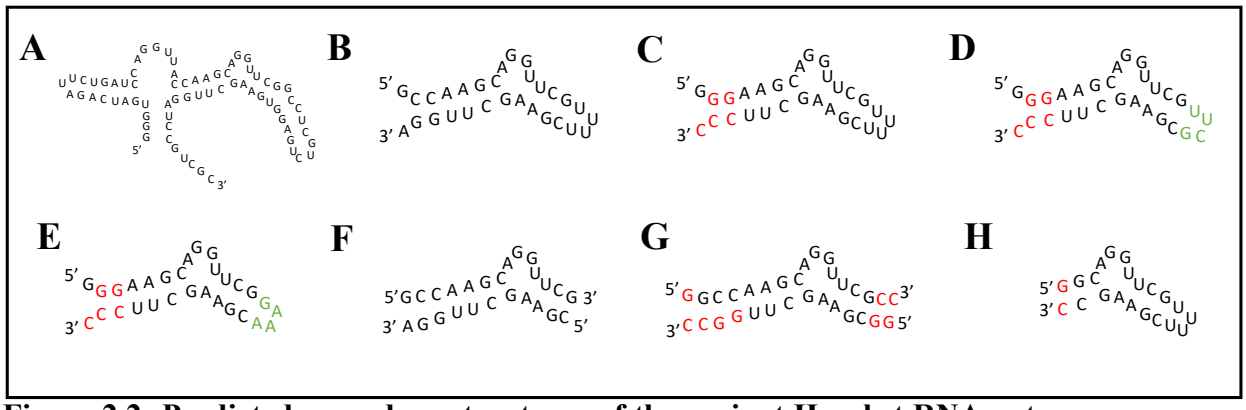


Figure 2.2: Predicted secondary structures of the variant Hoechst RNA aptamer sequences used for experimentation. A) Aptamer II,[46] **B)** Aptamer II-mini3-4,[46] **C)** Original, **D)** UUCG Tetraloop, **E)** GAAA Tetraloop, **F)** Duplex, **G)** Elongated Duplex, and **H)** Short Stem RNA aptamers. The modifications that were made to the Helix 1 of the published Aptamer II-mini3-4 sequence are shown in red and the modifications that were made to the predicted tetraloop portion are shown in green. Figure 2.2 was made using PowerPoint.

2.1.2 Derivative Hoechst Dyes

The tBu Hoechst dye derivatives used for the biochemical experiments shown in **Figure 2.3** below were synthesized by PhD candidate Avery To in Dr. Graham Murphy's lab at the University

of Waterloo following the methodology developed by Sando et al.[46,123] Two variations of the tBu Hoechst dye were studied, the tBu (PEG) Hoechst (**Figure 2.3A**) and the biotinylated tBu (PEG) Hoechst dye (**Figure 2.3B**). As it was previously discovered by Kyla Egerdeen, the addition of a PEG7 tail to the terminal phenol group of the tBu Hoechst dye was necessary for its solubility in water.[133,134] It was predicted that the addition of this PEG tail would have little effect on the existing interactions present within the tBu Hoechst dye-Aptamer II-mini3-4 complex. This is due to the fact that the added PEG7 tail contains a similar chemical composition as the side chain of the Hoechst 1a and 1b derivatives (**Figures 1.11C** and **D**) that were originally used by Sando et al.[46,133] for the selection of the RNA aptamer sequence and the subsequent biochemical experiments.

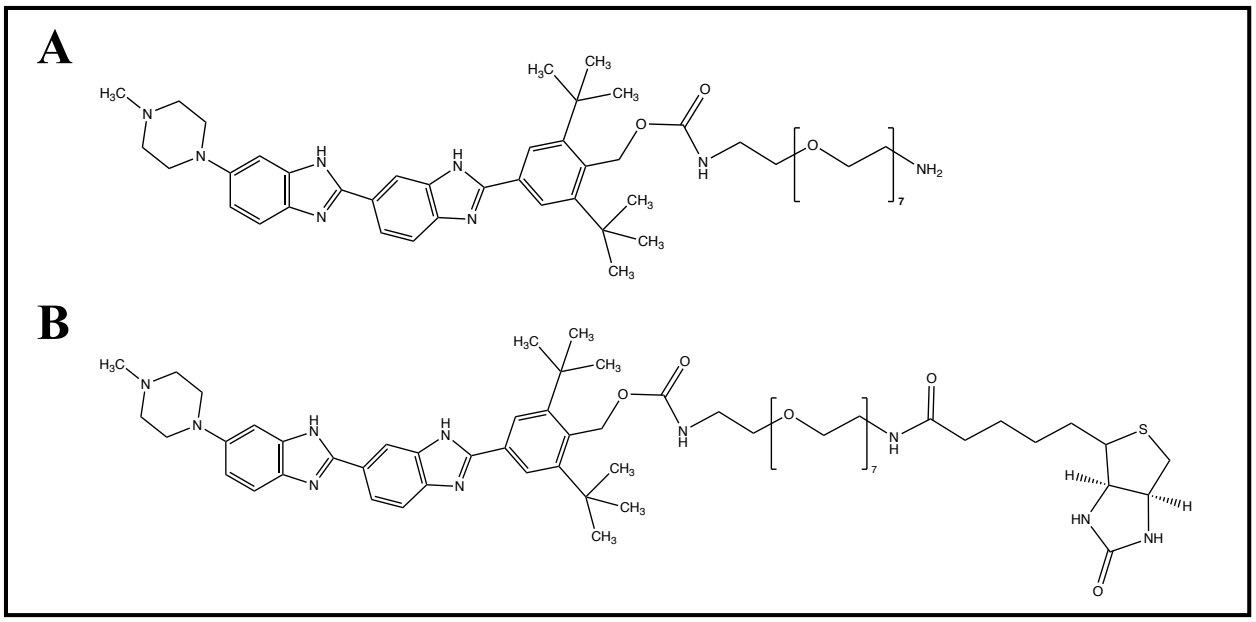


Figure 2.3: Comparison of the chemical structures of the tBu Hoechst dye derivatives. A) The tBu (PEG) Hoechst (molecular weight (MW) = 945.22 g/mol) and **B)** the biotinylated tBu (PEG) Hoechst (MW = 1171.51 g/mol) dye derivatives that were used for experimentation. The chemical structures were created using ChemDraw.

2.1.3 RNA Transcription

The RNA sequences used for biochemical characterization were enzymatically transcribed *in vitro* using the transcription mixture summarized in **Table 2.2**, which was modified from the method described by Milligan and Uhlenbeck.[135] The buffer used for transcription was a Tris-buffered saline (TBS), which consisted of 10 mM NaCl and 40 mM Tris at pH 8.3. The addition of low concentrations of dimethyl sulfoxide (DMSO) was used to increase transcription yields by altering the structure of T7 RNAP, which in turn enhances its activity.[136,137] PEG 8000 was also added to improve transcription yields by acting as a crowding reagent to help improve the molecular interactions between the various reaction components.[135,138,139] Moreover, since the T7 RNAP is known to slowly lose activity over the course of the transcription reaction,[140] an additional 0.125 – 0.135 mg/mL of enzyme was added to the transcription mixture halfway through the reaction to revive the enzyme's activity and once again improve RNA yields. The DNA template strands that were used for transcription were custom designed for each RNA variant, as exemplified in **Figure 2.4A**, and were synthesized by Integrated DNA Technologies (IDT) (IDT, Coralville, Iowa). The template strands were annealed to a T7 promoter sequence for 4 min at 90°C to create the DNA transcription template, as shown in **Figure 2.4B**.[135] The T7 RNAP was obtained through the overexpression of His-tagged T7 RNAP in *E. coli* cells and the purification of the target protein on a nickel affinity column.[135,141] Therefore, to obtain between 1-2 mM of the desired RNA aptamer in a final volume of 500 µL, a 10 mL RNA transcription mixture (**Table 2.2**) was incubated in a 37°C water bath for 4-5 hours.[135,138,142]

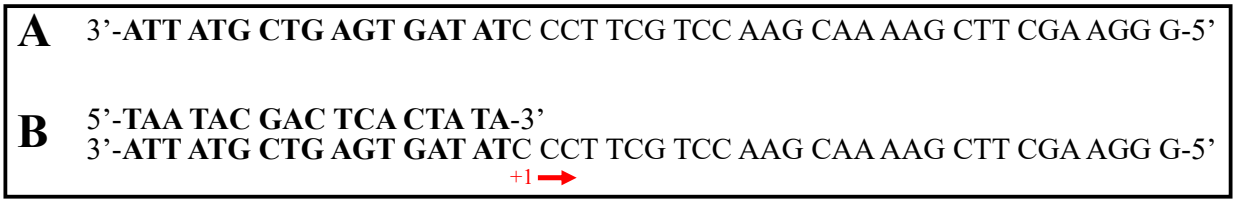


Figure 2.4: DNA template examples. A) A DNA template strand that was designed for the Original RNA aptamer sequence and **B)** the corresponding DNA transcription template that was annealed for RNA transcription. The T7 promoter portion of the sequence is shown in bold, and the start of transcription is indicated by the red +1. Figure 2.4 was modified from Milligan and Uhlenbeck[135] using PowerPoint.

Table 2.2: Recipe for a 10 mL RNA transcription mixture to produce 1-2 mM of the target RNA aptamer in a final volume of 500 µL.

Reagent	Stock Concentration	Volume Added (µL)	Target Concentration
MQW	--	850	--
DMSO	100% v/v	2000	20% v/v
TBS Buffer	10×	1000	1x
$MgCl_2$	1000 mM	450	45 mM
DTT	100 mM	500	5 mM
PEG 8000	40% w/v	400	1.6% w/v
NTPs	100 mM	750	7.5 mM
DNA Template	20 µM	800	1.6 µM
T7 RNAP	2.5 – 3.5 mg/mL	1000	0.25 – 0.35 mg/mL
		500*	0.125 – 0.175 mg/mL

The * indicates the additional T7 RNAP that was added halfway through the transcription reaction to revive the enzyme's activity and increase transcription yields. The 10× TBS buffer consisted of 100 mM NaCl and 400 mM Tris (pH 8.3).

2.1.4 RNA Purification

Once the RNA transcription reaction was complete, an equal volume of 10 M urea was added to the transcription mixture in order to halt the activity of the T7 RNAP[143] and denature the secondary structure of the transcribed RNA.[144] Moreover, 20-50 µL of bromophenol blue (BB) dye was added to the transcription mixture to act as a dye marker for downstream purification methods.[145] The transcribed RNA was then run on a denaturing urea PAGE gel to isolate the

desired RNA aptamer from contaminants, such as erroneous transcription products, as shown in **Figure 2.5**.[129,146] The percentage of acrylamide (19:1 acrylamide: bis-acrylamide) chosen for the denaturing gels was based on the number of bases present within the variant RNA aptamer sequences, as shown in **Table 2.3**, similar to the percent recommendations provided in the protocol by Green and Sambrook.[147]

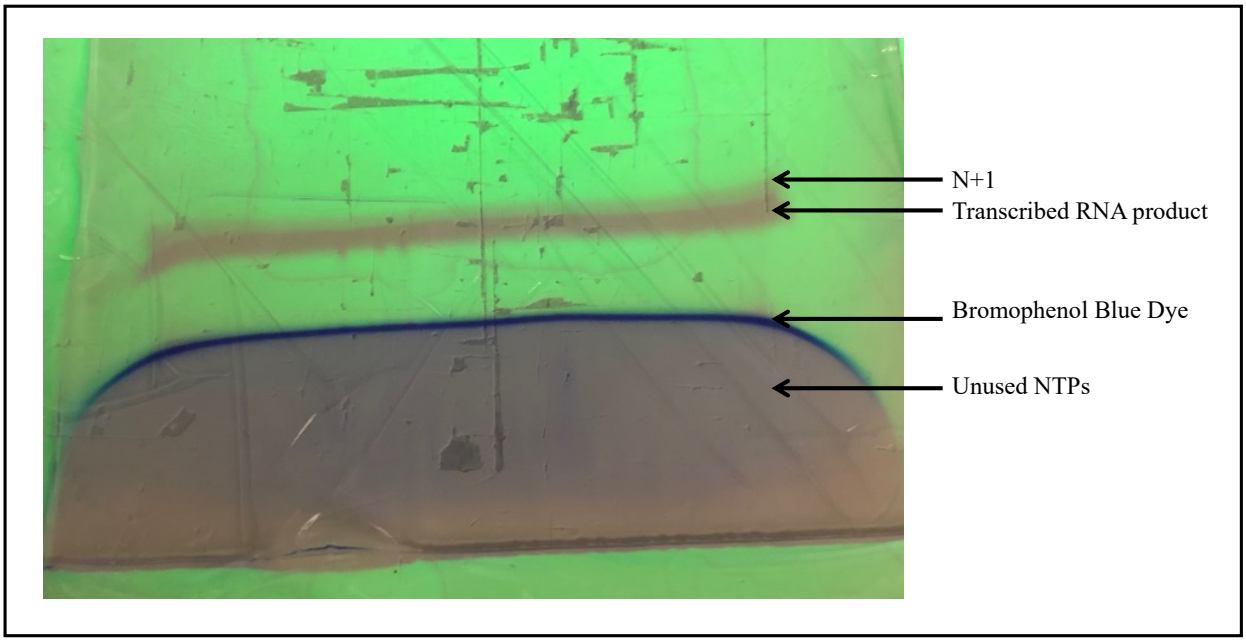


Figure 2.5: Example of an intermediate UREA PAGE gel under ultraviolet (UV) shadowing using experimental data. The positions of the transcribed RNA product, as well as the positions of the erroneous transcription product (N+1), BB dye and unused nucleoside triphosphates (NTPs) on the gel.

Table 2.3: Percent acrylamide chosen for the UREA PAGE gels that were run for each of the variant Hoechst RNA aptamers.

Variant Hoechst RNA Aptamer	Number of Bases	% Acrylamide
Aptamer II	71	10
Aptamer II-mini3-4	29	13
Original		
UUCG Tetraloop		
GAAA Tetraloop		
Duplex 5'-half	14	20
Duplex 3'-half	11	
Elongated Duplex 5'-half	17	
Elongated Duplex 3'-half	14	
Short Stem	21	15

Once the gel had finished running, the band for the transcribed RNA product was then cut out of the gel, crushed and the RNA was extracted using 300 mM NaCl for 24 h at 4 °C.[135,148] The extracted RNA was then isolated from the gel pieces using a sterile 0.45 µm filter, and the RNA was subjected to ethanol precipitation with 2.5 volumes of ice-cold 100% ethanol for 24 h at -20 °C.[135,148,149] To further increase the RNA yield, the gel pieces underwent a second round of the crush and soak as well as ethanol precipitation procedures, as previously described above. The precipitated RNA was subsequently pelleted by centrifugation at 19680 × g for 45 min at 4 °C and the supernatant was discarded.[148,149] The RNA pellet was resuspended in Milli-Q water (MQW). The ÄKTA purifier fast performance liquid chromatography (FPLC) system (Cytiva, Marlborough, Massachusetts) was then used with a 25 mL HiPrep diethylaminomethyl (DEAE) FF 16/10 weak anion-exchange column (GE Healthcare, Uppsala, Sweden) to separate the target RNA sequence from contaminant acrylamide through a low to high salt gradient from 0.150 M to 2 M NaCl, as shown in **Figure 2.6A**.[150,151] The sample was then subjected to another round of ethanol precipitation for 24 h at -20 °C and was once again pelleted by centrifugation at 19680 × g for 45

min at 4 °C.[148,149] The resulting RNA pellet was dissolved in MQW and the salt was removed from the sample through size exclusion chromatography, using a 53 mL HiPrep 26/10 desalting column (GE Healthcare, Uppsala, Sweden) on the ÄKTA FPLC system, as shown in **Figure 2.6B**.[152] The purified RNA was then lyophilized, re-dissolved in MQW and the concentration was determined using the RNA-40 setting on a Nanodrop 2000 spectrophotometer (Thermo Fisher Scientific, Waltham, Massachusetts).[153]

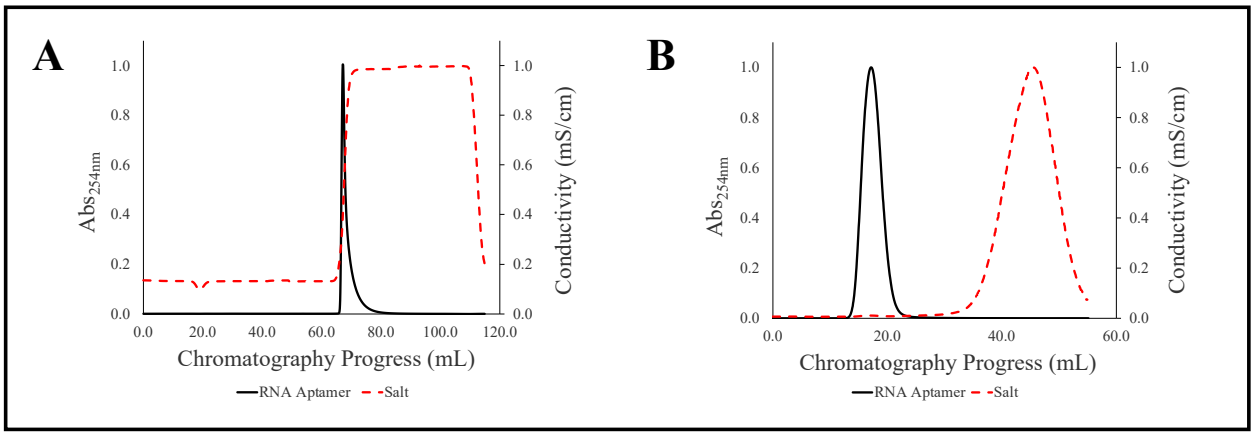


Figure 2.6: Example chromatograms of nucleic acids purified using the FPLC system. **A)** Depiction of the nucleic acid being eluted from the DEAE anion column through increasing salt concentrations and **B)** depiction of the removal of salt from the nucleic acid by running it through a size exclusion column. The values for the Abs_{254nm} and conductivity axes were normalized for ease of read. Figure 2.6 was generated in Excel using example experimental data.

2.1.5 Ultraviolet Absorption Spectra

UV absorption spectra were obtained to determine the wavelengths at which the tBu Hoechst dye derivatives absorb maximally and hence the excitation wavelengths (λ_{ex}) to be used for the subsequent fluorescence experiments.[154,155] Two sets of the tBu dye samples were prepared, one dissolved in MQW and the other dissolved in 1× phosphate-buffered saline (PBS) (20 mM NaCl, 2.7 mM KCl, 10 mM Na_2HPO_4, 1.8 mM KH_2PO_4, pH 7.4). The samples contained approximately 13 µM of the tBu Hoechst dye derivatives to keep the absorbance readings under 1.0 a.u. for accurate spectrophotometer measurements.[156,157] The absorbances were measured from 250-500

nm in 1 nm steps, using UV-Vis semi-micro rectangular quartz cuvettes (Agilent, Santa Clara, California) and a Cary 4000 UV-Vis spectrophotometer (Varian, Palo Alto, California).[158,159]

2.1.6 Determination of the Molar Extinction Coefficients by Ultraviolet Spectroscopy

To determine the molar extinction coefficient of the tBu Hoechst dye derivatives, dilution series were performed in a similar manner to the method described by Cavaluzzi and Borer.[157] The dye concentrations were determined by dry weight[160] and the dye was dissolved in MQW. For accurate UV measurements, serial dilutions were carried out to obtain sample concentrations ranging from 25 – 1.56 µM and 30 – 1.87 µM for the tBu (PEG) Hoechst and biotinylated tBu (PEG) Hoechst dyes, respectively.[157] The samples were prepared in triplicates for reliable data. A Cary 4000 UV-Vis spectrophotometer (Varian, Palo Alto, California) was zeroed with MQW and the absorbances were measured at 345 nm, using UV-Vis semi-micro rectangular quartz cuvettes (Agilent, Santa Clara, California). The wavelength used for absorbance measurements was determined through the performed UV absorption spectra experiments described in **Chapter 2.1.5**. The molar extinction coefficients of the tBu Hoechst dyes were calculated using the Beer-Lambert law (Equation 3), where A, ε, C and l represent the sample absorbance, molar extinction coefficient, concentration, and cuvette pathlength, respectively.[157,161]

$$A = \varepsilon \cdot C \cdot l \tag{3}$$

2.1.7 Fluorescence Emission Spectra

To obtain the fluorescence emission spectra and analyze the increase in fluorescence produced upon binding of the variant RNA aptamers to the tBu Hoechst dye derivatives, the samples were prepared with 40 µM of the variant RNA aptamer, 13 µM of the tBu (PEG) Hoechst dye and 1×

PBS buffer (20 mM NaCl, 2.7 mM KCl, 10 mM Na_2HPO_4, 1.8 mM KH_2PO_4, pH 7.4), similar to the method previously described by Sando et al.[46] To ensure that the RNA aptamers were properly folded and existed as a single conformation in the sample solution, the RNA sequences mixed with 1× PBS buffer were heat-treated according to **Table 2.4**, prior to the addition of the tBu Hoechst dye.[162,163] Control samples were prepared with 13 μM of the tBu (PEG) Hoechst dye and 1× PBS buffer to observe the fluorescence emitted by the unbound tBu dye.[46] The PBS buffer used in this study was similar to the selection buffer originally used by Sando et al.; however, it contained lower salt concentrations and no Mg^{2+} ions. The dye concentrations were determined using absorbance values obtained from a Cary 4000 UV-Vis spectrophotometer (Varian, Palo Alto, California) set to an λ_{ex} of 345nm. The λ_{ex} was experimentally determined through the performed UV absorption experiments as discussed in **Chapter 2.1.5**. The concentrations of the biotinylated and non-biotinylated tBu (PEG) Hoechst dyes were calculated using molar extinction coefficients of 30000 cm^{-1} M^{-1} and 34700 cm^{-1} M^{-1}, respectively. These values were experimentally determined through the performed dilution series discussed in **Chapter 2.1.6**. The samples were loaded into a 96-well black U-bottom microplate (Greiner Bio-One, Kremsmünster, Upper Austria) and the fluorescence measurements were conducted using a SpectraMax M5 microplate reader (Molecular Devices, San Jose, California). Similar to the method described by Sando et al.,[46] the emission spectra were collected by exciting the sample with a λ_{ex} of 345 nm and recording the relative fluorescence units (RFU) produced over emission wavelengths (λ_{em}) ranging from 405-505 nm with 1 nm spacing.[46,125] The I_{on}/I_{off} ratios were calculated for each sample by dividing the maximum fluorescence produced by the variant RNA-tBu Hoechst dye complex by the maximum fluorescence produced by the control tBu Hoechst dye sample.[46] For a more accurate comparison,

the data were normalized relative to the Original RNA aptamer-tBu (PEG) Hoechst complex, which was set to a relative I_{on}/I_{off} ratio of 1.00.

Table 2.4: Heat-treatment of the RNA aptamers prior to experimentation to ensure proper folding.

Variant Hoechst RNA Aptamer	Heat-Treatment
Aptamer II	70°C for 2 min in a water bath Fast cool on ice for 5 min
Aptamer II-mini3-4	
Original	
UUCG Tetraloop	
GAAA Tetraloop	
Short Stem	
Duplex	70°C for 1 min in a water bath Slow cool at 1°C/min in a water bath for 1 hour
Elongated Duplex	

2.1.8 Fluorescence Titration Assays

To determine the binding affinities between the variant RNA aptamers and the tBu Hoechst dye derivatives, fluorescence titration assays were conducted.[164] Prior to performing fluorescence titration tests on each of the RNA aptamer variants, however, a brief investigation was carried out to identify the optimal buffer conditions for binding using the Original RNA aptamer and tBu (PEG) Hoechst dye, as shown in **Table 2.5**. Buffer A (1× PBS with high salt and Mg^{2+} ions) was the original buffer used by Sando et al.[46] to select for the RNA aptamer and conduct subsequent biochemical characterization experiments. Buffers B and C were variations of the original selection buffer that were used in this research project to test the effects of varying ionic strengths and the presence of Mg^{2+} ions on the aptamer system's binding. Buffer B (1× PBS with low salt and without Mg^{2+} ions) was ultimately chosen for subsequent fluorescence titration experiments.

Table 2.5: Summary of the buffer conditions tested for the fluorescence titration experiments to optimize the binding system.

Buffer	Conditions Tested	Buffer Type	Composition	pH
A	High salt, Mg^{2+}	1× PBS	137 mM NaCl, 2.7 mM KCl, 10 mM Na_2HPO_4, 1.8 mM KH_2PO_4 and 2.5 mM Mg^{2+}	7.4
B	Low salt, no Mg^{2+}	1× PBS	20 mM NaCl, 2.7 mM KCl, 10 mM Na_2HPO_4, and 1.8 mM KH_2PO_4	
C	Low salt, Mg^{2+}	1× Tris-KCl	20 mM NaCl, 2.7 mM KCl, 25 mM Tris, and 2.5 mM Mg^{2+}	

The fluorescence titration samples were prepared with varying RNA concentrations ranging from 30 – 0.469 μM by serial dilution at a fixed tBu Hoechst concentration of 1.33 μM and in the presence of Buffer B (1× PBS with low salt and no Mg^{2+}).[128,165] The RNA concentrations used for the Aptamer II RNA variant were modified to 1250 – 19.5 nM, following the observation of stronger binding interactions with the tBu (PEG) Hoechst dye. The samples were prepared in triplicates and a buffer blank, which consisted of Buffer B in MQW, was prepared to subtract the background fluorescence from the sample readings.[166] Like the fluorescence emission experiments, prior to the addition of the tBu Hoechst dye, the RNA aptamers mixed with Buffer B were heat-treated according to the procedures listed in **Table 2.4** to ensure proper RNA folding.[162,163] The samples were once again loaded in a 96-well black U-bottom microplate (Greiner Bio-One, Kremsmünster, Upper Austria) and the fluorescence measurements were carried out using a SpectraMax M5 microplate reader (Molecular Devices, San Jose, California). Endpoint readings of the samples were read at λ_{ex} and λ_{em} of 345 nm and 465 nm, respectively.[122,167] These wavelengths were experimentally determined through the performed UV absorption and fluorescence emission experiments as discussed in **Chapters 2.1.5** and **2.1.7**. The raw fluorescence readings were processed using equation (4), where F_i represents the relative fluorescence intensity of the sample and F_{max} represents the fluorescence intensity produced at saturation.[164]

$$F_i = \frac{[ligand] \times F_{max}}{K_d + [ligand]} \quad (4)$$

The relative fluorescent intensities were normalized by dividing the values with the corresponding F_{max}. The results were plotted on the graphing software, GraphPad Prism (GraphPad, San Diego, California), using non-linear regression and the one site-specific binding model to determine the dissociation constant between the variant RNA aptamers and the tBu Hoechst dye, as previously done by Jeon et al.[164]

2.2 Results and Discussion

2.2.1 Ultraviolet Absorption Spectra

UV absorption spectra were obtained for both the tBu (PEG) Hoechst and the biotinylated tBu (PEG) Hoechst dyes to determine the wavelength at which the dye absorbs light maximally (λ_{max}).[155] Hence, the λ_{ex} to use for the following fluorescence experiments. The tBu (PEG) Hoechst dye was found to absorb maximally at 339 nm when the dye was dissolved in water (**Figure 2.7A**) and in a 1× PBS solution (**Figure 2.7B**). Meanwhile, the biotinylated tBu (PEG) Hoechst dye was found to absorb maximally at 344 nm and 342 nm when dissolved in water (**Figure 2.7C**) and a 1× PBS solution (**Figure 2.7D**), respectively. These experimental λ_{max} were similar to the λ_{ex} of 345 nm that was previously reported by Sando et al.[46,123] for the tBu Hoechst dye's fluorescence. In addition, the presence of salts in the buffer solutions appeared to have little effect on the dye's λ_{ex}. Therefore, to remain consistent with the methods performed by Sando et al.,[46] a wavelength of 345 nm was used to excite the dye samples within this research project.

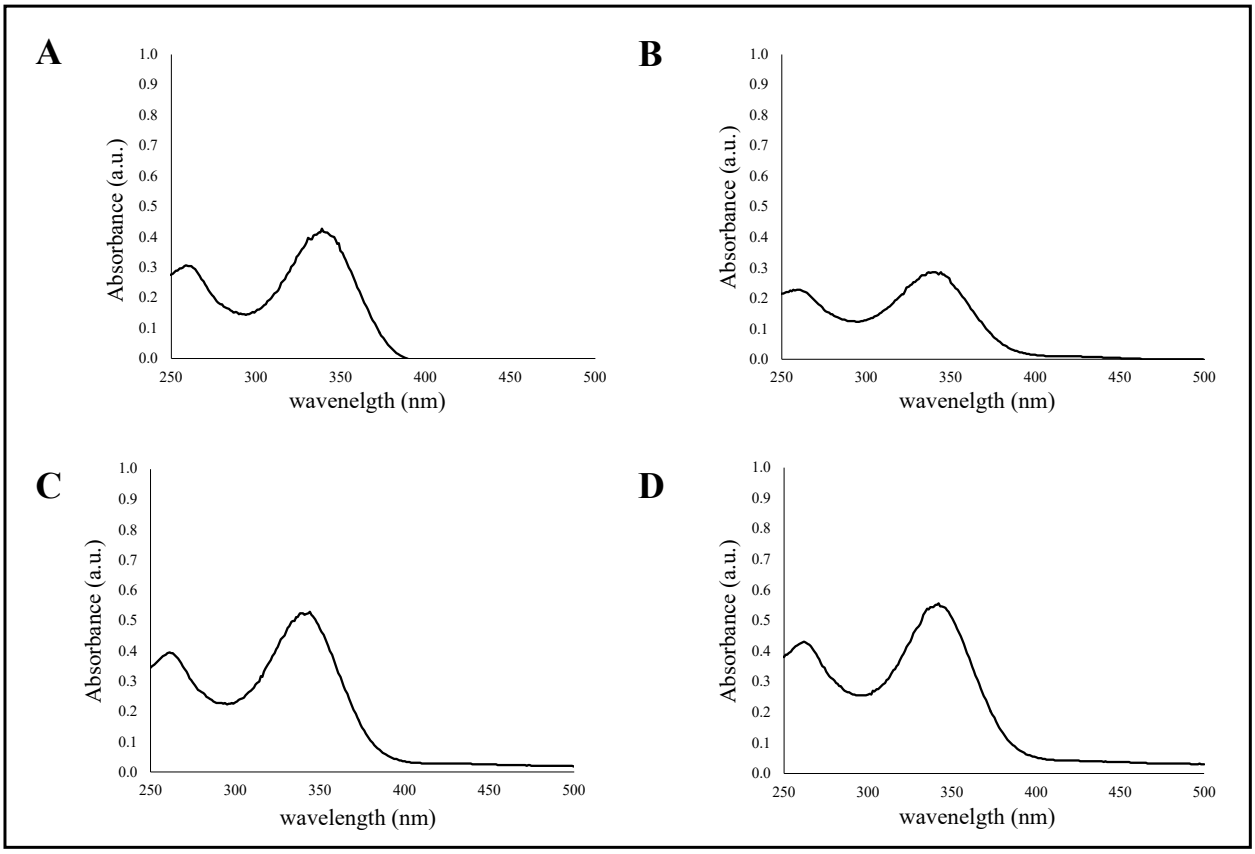


Figure 2.7: UV absorption spectra to determine the λ_{max}. The tBu (PEG) Hoechst dye dissolved in **A)** MQW and **B)** 1× PBS. The biotinylated tBu (PEG) Hoechst dye dissolved in **C)** MQW and **D)** 1× PBS.

2.2.2 Determination of the Molar Extinction Coefficients by Ultraviolet Spectroscopy

A brief dilution series was performed on the unbound tBu Hoechst dye samples to determine their molar extinction coefficients through UV spectroscopy methods.[157] The molar extinction coefficients of the dyes dissolved in water were determined to be 34700 $cm^{-1} M^{-1}$ and 30000 $cm^{-1} M^{-1}$ for the tBu (PEG) Hoechst and the biotinylated tBu (PEG) Hoechst dyes at an λ_{ex} of 345 nm (**Table 2.6** and **Appendix A Figure 4.1**). Sando et al.[46,123] previously used the molar extinction coefficient of the Hoechst 33342 dye to estimate the concentrations of their newly synthesized tBu Hoechst dye derivatives. As a result, there is currently no published data for the molar extinction coefficients of the tBu Hoechst dye derivates. When compared to other commercially available

Hoechst dyes, however, the experimentally determined tBu Hoechst dye extinction coefficients are considerably lower. For instance, the molar extinction coefficient of the Hoechst 33258 dye dissolved in water was previously determined to be 46000 cm^{-1} M^{-1} at 345 nm.[168] A study by Paul et al.[169] found that the addition of tBu groups to aromatic compounds slightly increases the molar extinction coefficient. The added tBu groups increase the electron density around the aromatic rings, which subsequently enhances the sample's ability to absorb light.[170] The addition of the PEG7 tail and biotin motif to the phenol ring of the tBu Hoechst dyes, however, may have negated the effects of the tBu groups and hindered the sample's light absorption. These large and bulky side chains likely acted as crowding agents in the solution and proceeded to shield the light beam, hence reducing the sample's measured absorbance and calculated molar extinction coefficient.[171]

Table 2.6: Comparison of the experimentally determined molar extinction coefficients for the tBu Hoechst dye derivatives in water.

Hoechst Dye Derivative	Molar Extinction Coefficient (cm^{-1} M^{-1})	λ_{ex} (nm)	Solvent
tBu (PEG) Hoechst	34700	345	Water
Biotinylated tBu (PEG) Hoechst	30000		

2.2.3 Fluorescence Emission Spectra of the RNA aptamer variants with tBu (PEG) Hoechst

It is well known that unbound Hoechst dyes are almost nonfluorescent and will exhibit large increases in fluorescence intensity, approximately 30-fold, upon binding to DNA sequences.[46,117,119] This trend was observed by Sando et al.,[46] where a 28.2-fold increase in fluorescence intensity was observed upon binding of Aptamer II-mini3-4 to Hoechst 1a. Therefore, obtaining fluorescence emission spectra for each aptamer system was deemed an efficient way to determine if binding was present between the variant RNA aptamers and tBu (PEG) Hoechst dye. As can be seen in **Figures 2.8A-D**, each of the variant RNA aptamers appear to bind to the tBu

(PEG) Hoechst dye, with maximum fluorescence intensities that range from approximately 2500 – 5000 RFU. It was noted that the experimental λ_{em} of the tBu dye was found to be 465 nm, which was slightly off from the literature λ_{em} of 470 nm that was previously determined by Sando et al.[46] This difference likely arose from the minor deviations between the chemical compositions of the tBu Hoechst dye's PEG tail that was used within this research project (**Figure 2.3**) and the Sando et al. published study (**Figures 1.11C-D**).

For a more effective comparison of the fluorescent enhancements produced by the tBu dye upon binding to each of the variant RNA aptamers, the relative I_{on}/I_{off} ratios were calculated as shown in **Table 2.7**. Since the Original RNA aptamer was the first variant to be produced and has the closest sequence similarity to Aptamer II-mini3-4, it was set to a relative I_{on}/I_{off} ratio of 1.0. Aptamer II-mini3-4 was found to display a comparable relative I_{on}/I_{off} ratio to the Original RNA aptamer at 0.956. These two aptamer sequences only differ by the substitution of three GC base pairs in Helix 1 of the folded aptamer. Therefore it can be assumed that these changes do not affect the overall conformation of the RNA aptamer that was formerly selected and optimized by Sando et al.[46] Likewise, the Short Stem RNA aptamer was observed to exhibit a slightly greater fluorescence enhancement than the Original RNA aptamer when bound to the tBu (PEG) Hoechst dye, as can be seen through a relative I_{on}/I_{off} ratio of 1.09. This indicated that the almost complete removal of Helix 1 has little to no impact on the overall tertiary structure of the RNA aptamer. Hence, it was hypothesized that tBu Hoechst dye likely sits within a groove located in Helix 2 of the folded aptamer sequence. When analyzing the fluorescence emission spectra for the UUCG Tetraloop, GAAA Tetraloop, Duplex, Elongated Duplex and Aptamer II RNA aptamer variants, they were all found to have lower relative I_{on}/I_{off} ratios than the Original RNA aptamer at 0.788, 0.887, 0.775, 0.440 and 0.285, respectively. The fluorescence emission results observed for the

Aptamer II RNA sequence agree with the data that was previously obtained by Sando et al.[46] Within the published study the Aptamer II-mini3-4 sequence was found to display a 2.15× increase in fluorescence intensity upon binding to the tBu Hoechst dye when compared to the Aptamer II RNA sequence (**Table 1.2**). Similarly, the fluorescence emission experiments performed in this research project yielded a 3.35× fluorescence increase when comparing the fluorescence of the tBu-bound Aptamer II-mini3-4 and Aptamer II RNA sequences. It should be noted, however, that the relative I_{on}/I_{off} ratios are not an indication of how tightly the molecules of interest are interacting with each other. These values may instead provide some information regarding how the aptamer is bound to the dye.[172] Upon binding to the minor grooves of nucleic acid sequences, the bonds within the Hoechst dye experience reduced rotational freedom, which in turn gives rise to the dye's increased fluorescence intensity.[117,122] Therefore, the discussed sequence modifications that were made to the RNA variants may have altered the overall geometry of the aptamer's tertiary structure, through a change in the conformational stability of the major and minor grooves within Helix 2 of the aptamer. This may have changed the way the dye was able to lock into place within the folded aptamer sequence and ultimately reduced the amount of fluorescence emitted upon binding.[122]

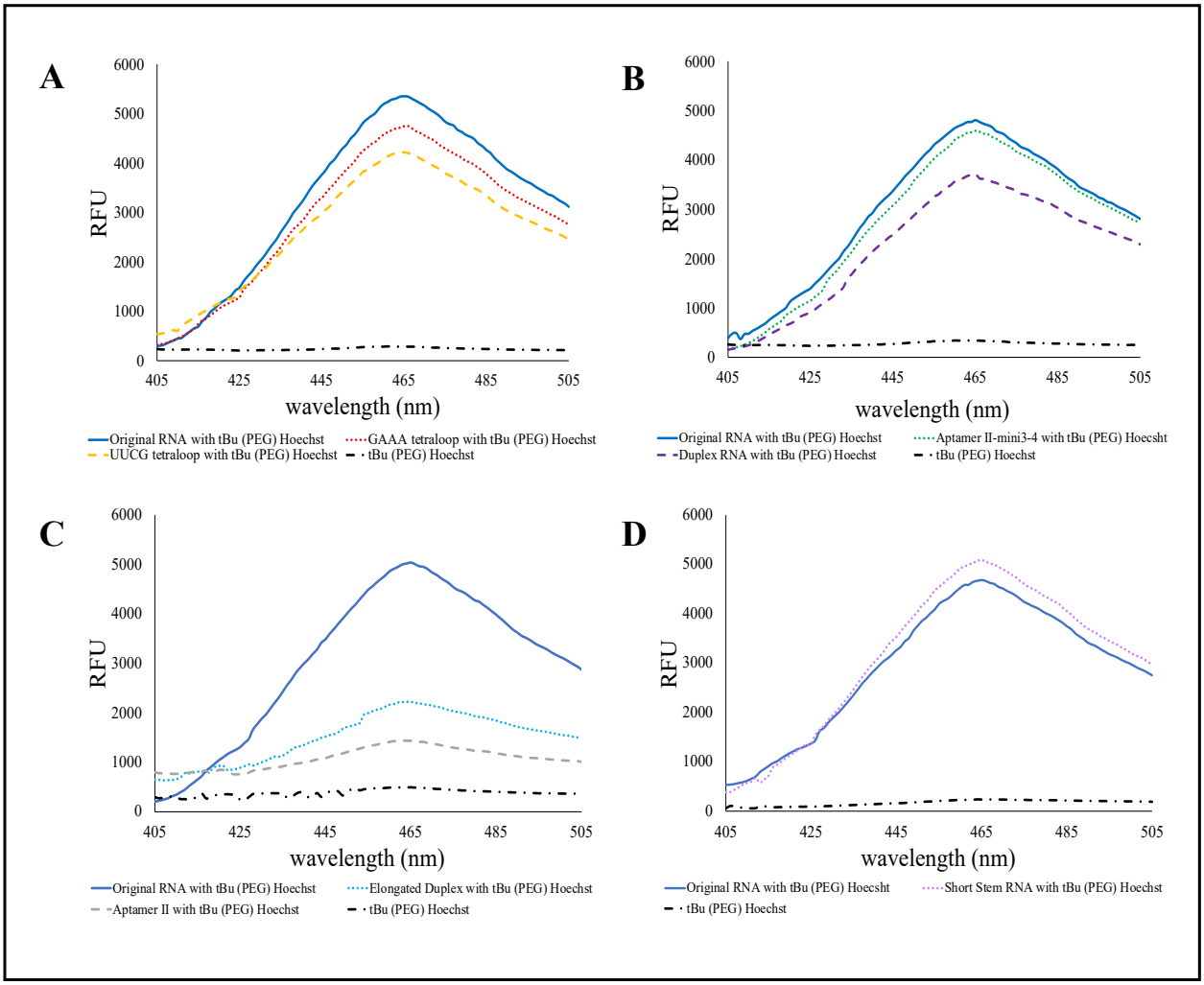


Figure 2.8: Fluorescence emission assays of the variant RNA aptamers. Comparison of the fluorescence enhancement produced upon binding of the tBu (PEG) Hoechst dye to the Original RNA aptamer with the fluorescence intensity produced upon binding of the tBu dye to the **A)** UUCG and GAAA tetraloop, **B)** Aptamer II-mini3-4 and Duplex, **C)** Elongated Duplex and Aptamer II, and **D)** Short Stem RNA aptamer variants.

Table 2.7: Comparison of the relative I_{on}/I_{off} ratios produced by the tBu (PEG) Hoechst - variant RNA aptamer complexes.

Variant Hoechst RNA Aptamer	Relative I_{on}/I_{off}
Original	1.00
Aptamer II	0.285
Aptamer II-mini3-4	0.956
UUCG Tetraloop	0.788
GAAA Tetraloop	0.887
Duplex	0.775
Elongated Duplex	0.440
Short stem	1.09

2.2.4 Fluorescence Emission Spectra of the Original RNA aptamer with biotinylated tBu (PEG) Hoechst

When analyzing the fluorescence emission spectra of the Original RNA aptamer interacting with the biotinylated tBu (PEG) Hoechst dye (**Figure 2.9**), the maximum fluorescence signal was also found to be produced at 465 nm. Additionally, the fluorescence enhancement observed upon binding of the Original RNA aptamer to the biotinylated dye was once again lower, with a relative I_{on}/I_{off} ratio of 0.711 (**Table 2.8**), than when bound to the non-biotinylated tBu dye. This indicated that the addition of the biotin group to the end of the tBu dye's PEG7 side chain likely altered the way that the dye is able to sit within the Helix 2 grooves of the folded RNA aptamer sequence.[122]

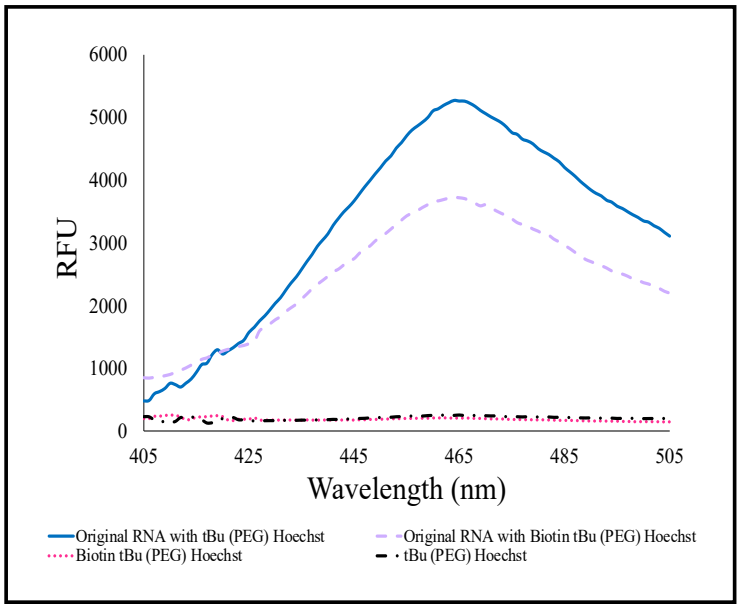


Figure 2.9: Fluorescence emission assay of the variant tBu Hoechst dyes. Comparison of the fluorescence intensity emitted by the biotinylated versus non-biotinylated version of the tBu Hoechst dye when bound to the Original RNA aptamer.

Table 2.8: Comparison of the relative I_{on}/I_{off} ratios produced upon the interaction of the Original RNA with the biotinylated and non-biotinylated tBu (PEG) Hoechst dye.

Variant Hoechst Dye	Relative I_{on}/I_{off}
tBu (PEG) Hoechst	1.00
Biotinylated tBu (PEG) Hoechst	0.711

2.2.5 Fluorescence Titration Binding Buffer Optimization

Prior to conducting fluorescence titration assays on each of the variant aptamer systems, a brief investigation was conducted using the Original RNA aptamer and tBu (PEG) Hoechst dye to determine the optimal binding conditions, as shown in **Figure 2.10**. The use of Buffer A, which contained 137 mM NaCl and 2.5 mM Mg^{2+}, resulted in relatively weak binding interactions with a K_d of 17.5 μM, as can be observed in **Table 2.9**. This result was not expected since Buffer A was the buffer that was originally used by Sando et al.[46] to select for the RNA aptamer and perform subsequent biochemical characterization studies. As stated above, the group only performed SPR binding affinity studies on the SELEX-selected 71-nt Aptamer II with the biotinylated Hoechst 1b dye, which yielded a K_d of 35 nM (**Table 1.2**). Each of the sequence substitutions and minimizations that were made to Aptamer II was tested by the group solely through fluorescence emission assays. As a result, there are no literature values that can be used to compare the experimentally produced binding affinities for the variant RNA aptamers that were obtained within this research project.

It has been previously reported that selection buffers do not always offer the best binding conditions for aptamer systems; however, they can be improved by modifying the buffer's existing component concentrations.[173] Hence, to test the effects of reduced ionic strength on the binding interactions of the Original RNA-tBu (PEG) Hoechst complex, a second fluorescence assay using Buffer B, which contained only 20 mM NaCl and 0 mM Mg^{2+} ions, was carried out. The magnesium ions were excluded from this buffer due to difficulties with magnesium phosphate precipitation when preparing the 10× stock buffer solution.[174] From this test, it was found that Buffer B gave rise to improved binding conditions with a K_d of 1.38 μM, as shown in **Table 2.9**. Therefore, these results suggest that the binding mechanisms of the Original RNA aptamer to the

tBu (PEG) Hoechst dye may be heavily dependent on its electrostatic interactions and environments with reduced salt concentrations yield the best binding results.[173] Moreover, magnesium ions are often required for the stabilization of folded RNA aptamers, which can in turn improve the binding interactions between the aptamer and its target molecule.[175,176] Since magnesium was previously excluded from Buffer B, another test was performed to determine if the presence of magnesium ions would also affect binding. Therefore, Buffer C, a tris buffer that contained 20 mM NaCl and 2.5 mM Mg^{2+} was tested on the aptamer system. The addition of Mg^{2+} ions to the low salt environment was found to produce a K_d of 2.54 μM (**Table 2.9**), which was slightly weaker than the binding affinity observed when Buffer B was used. This indicated that the binding interactions between the Original RNA aptamer and the tBu (PEG) Hoechst dye are not dependent on the presence of magnesium ions. Therefore, since it was found that reduced ionic strength is optimal and magnesium ions are not required for binding, Buffer B was chosen for future biochemical experiments since it had the closest chemical composition to the buffer originally used by Sando et al.[46]

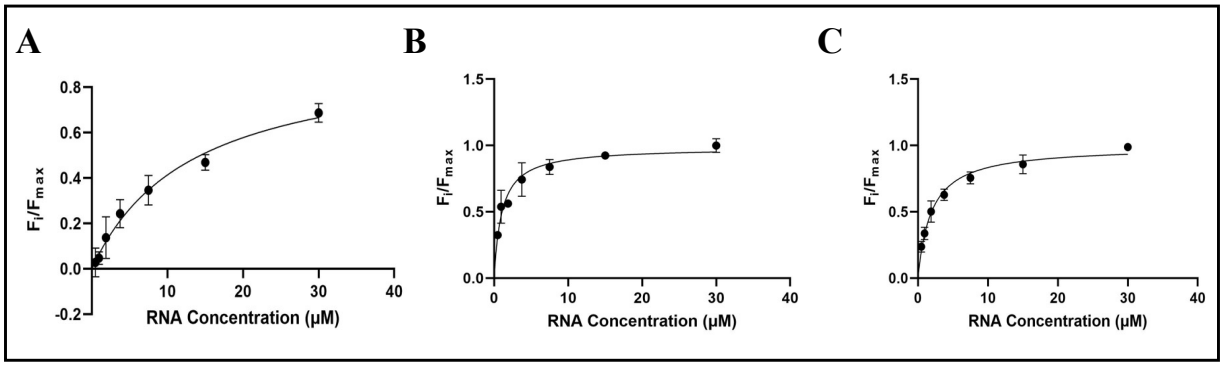


Figure 2.10: Binding buffer optimization through fluorescence titration assays. Comparison of the fluorescence titration curves for the Original RNA aptamer with tBu (PEG) Hoechst under different buffer conditions using **A)** Buffer A **(**high salt with Mg^{2+}), **B)** Buffer B (low salt without Mg^{2+}), and **C)** Buffer C **(**low salt with Mg^{2+}).

Table 2.9: Comparison of the dissociation constants produced for the complex formation of the Original RNA aptamer with tBu (PEG) Hoechst under different buffer conditions.

Buffer	Buffer Conditions Tested	K_d (μM)	95% Confidence Interval (μM)
A	High salt, Mg^{2+}	17.5	11.1 – 29.3
B	Low Salt, no Mg^{2+}	1.38	0.983 – 1.90
C	Low salt, Mg^{2+}	2.54	1.99 – 3.23

2.2.6 Fluorescence Titration of the Variant RNA Aptamers with tBu (PEG) Hoechst

To determine the approximate binding affinities of the variant RNA aptamers with the tBu (PEG) Hoechst dye, fluorescence titration experiments were performed as shown in **Figure 2.11** and **Table 2.10**. Through the analysis of the results, Aptamer II (**Figure 2.11B**) was found to have the tightest binding with the tBu (PEG) Hoechst dye, as can be seen through an experimentally determined K_d of 58.2 nM (**Table 2.10**). This result agrees with the literature value of 35 nM that was previously discussed in the Sando et al.[46] publication (**Table 1.2**). Moreover, the Short Stem RNA aptamer (**Figure 2.11H**) was found to have the second strongest binding affinity for the tBu (PEG) Hoechst dye at a K_d of 0.895 μM (**Table 2.10**). The Short Stem sequence differs from the Original RNA aptamer by the removal of four base pairs from Helix 1 of the predicted secondary structure, as can be seen in **Figure 2.2H**. Therefore, the removal of Helix 1 appears to improve the aptamer's binding interactions with the tBu (PEG) Hoechst dye. This hypothesis agrees with the fluorescence emission results previously discussed in **Chapter 2.2.3**, in which the formation of the Short Stem-tBu (PEG) Hoechst complex was found to produce a greater increase in fluorescence intensity than the Original RNA aptamer at a relative I_{on}/I_{off} ratio of 1.09 (**Table 2.7**). Additionally, the Original, Aptamer II-mini3-4, UUCG Tetraloop and GAAA Tetraloop RNA aptamers (**Figures 2.11A, C-E**) were all determined to have comparable binding affinities for the tBu (PEG) Hoechst dye, ranging from 1.38 – 2.10 μM (**Table 2.10**). These results make sense as minimal sequence changes were made to each of these variants. As briefly mentioned in **Chapter 2.2.3**, the Original

RNA and Aptamer II-mini3-4 sequences are identical apart from the substitution of three base pairs in Helix 1 of the aptamer (**Figures 2.2B** and **C**). In addition, only the nucleotides of the predicted tetraloop portion of the Original RNA aptamer were changed within the UUCG and GAAA Tetraloop RNA sequences (**Figures 2.2D** and **E**). Therefore, since the binding affinities for each of these variant RNA aptamers were similar, this indicated that the discussed sequence changes did not affect the binding regions of the aptamer. These results are interesting, however, when comparing the Original RNA aptamer with the Tetraloop RNA aptamer sequences. As discussed in **Chapter 2.2.3**, the UUCG and GAAA Tetraloop RNA variants were found to have lower relative I_{on}/I_{off} ratios than the Original RNA aptamer at 0.788 and 0.887 (**Table 2.7**); however, the binding affinities are approximately the same for these three aptamer sequences. This suggests that the although the change from the dynamic UUUU tetraloop of the Original RNA aptamer to the stable UUCG and GAAA motifs likely increases the overall conformational rigidity of Helix 2, it did not affect the internal bulge binding region. Finally, when analyzing the molecular interactions between the Duplex and Elongated Duplex RNA aptamers and the tBu (PEG) Hoechst dye (**Figures 2.11F** and **G**), weaker binding interactions were observed compared to the other RNA aptamer variants, as was seen through determined K_d values of 8.51 μM and 3.40 μM, respectively (**Table 2.10)**. Similar to the Tetraloop RNA variants, the relative I_{on}/I_{off} ratios for the Duplex and Elongated Duplex RNA aptamers were found to be 0.775 and 0.533, as shown in **Table 2.7**. Therefore, this indicates that although the tetraloop portion is not required for binding to the dye, its removal from Helix 2 consequently increases the conformational flexibility of the aptamer's helical structure and reduces the binding interactions.

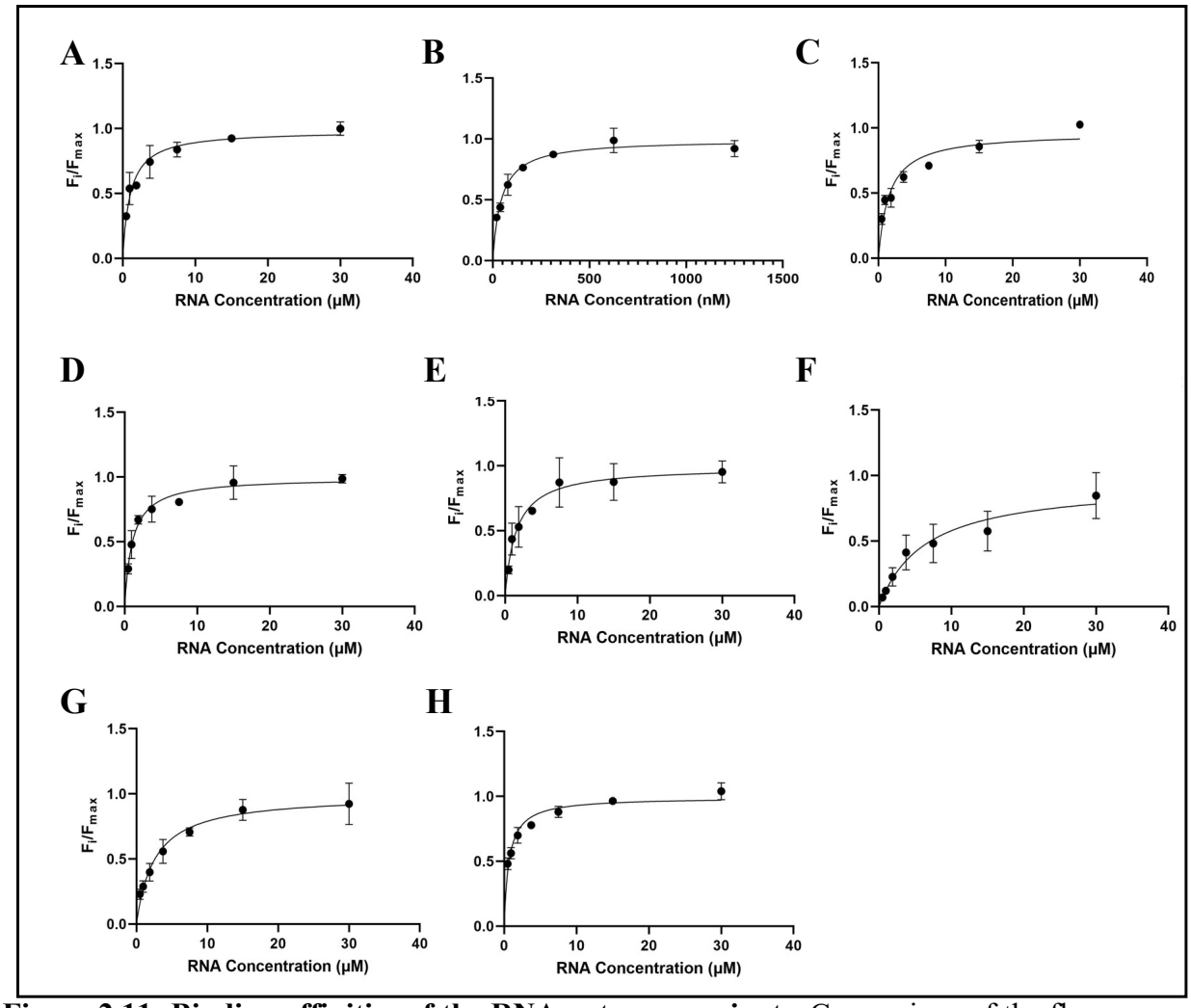


Figure 2.11: Binding affinities of the RNA aptamer variants. Comparison of the fluorescence titration curves produced for the **A)** Original, **B)** Aptamer II, **C)** Aptamer II-mini3-4, **D)** UUCG Tetraloop, **E)** GAAA Tetraloop, **F)** Duplex, **G)** Elongated Duplex, and **H)** Short Stem RNA Aptamers with the tBu (PEG) Hoechst dye under low salt conditions and in the absence of Mg^{2+} ions.

Table 2.10: Comparison of the dissociation constants obtained for the variant RNA aptamers with tBu (PEG) Hoechst dye under low salt conditions and in the absence of Mg^{2+} ions.

Variant Hoechst RNA Aptamer	K_d (μM)	95% Confidence Interval (μM)
Original	1.38	0.983 – 1.90
Aptamer II	0.0582	0.0452 – 0.0741
Aptamer II-mini3-4	2.10	1.38 – 3.15
UUCG tetraloop	1.42	1.05 – 1.89
GAAA tetraloop	2.05	1.30 – 3.18
Duplex	8.51	4.27 – 18.0
Elongated Duplex	3.40	2.35 – 4.88
Short Stem	0.895	0.672 – 1.17

2.2.7 Fluorescence Titration of the Original RNA Aptamer with Biotinylated tBu (PEG) Hoechst

An additional fluorescence titration assay was carried out to determine the binding affinity between the Original RNA aptamer with the biotinylated version of the tBu Hoechst dye as shown in **Figure 2.12**. The binding affinity of this aptamer system was found to be weaker at a K_d of 6.31 μM (**Table 2.11**) than when bound to the non-biotinylated version of the dye. Similarly, as shown in **Chapter 2.2.4**, the relative I_{on}/I_{off} ratio for this molecular interaction was determined to be 0.711 (**Table 2.8**). The biotinylated tBu (PEG) Hoechst dye differs from the tBu (PEG) Hoechst dye by the addition of a carbonyl group, a four-carbon chain, and a biotin group to the end of the PEG7 tail, as depicted in **Figure 2.3**. Hence, this once again supports the hypothesis that the addition of the biotin motif changes the way the tBu dye can interact with Helix 2 of the folded aptamer and consequently reduces its binding interactions.

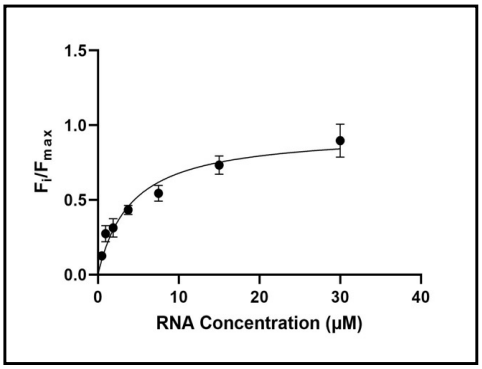


Figure 2.12: Binding affinity of the tBu Hoechst variants. Fluorescence titration curve of the Original RNA aptamer with the biotinylated tBu (PEG) Hoechst dye under low salt concentrations and without Mg^{2+} ions.

Table 2.11: Comparison of the dissociation constants produced upon interaction of the Original RNA aptamer with the tBu Hoechst dye derivatives under low salt conditions and in the absence of Mg^{2+} ions.

Hoechst Dye Derivative	K_d (μM)	95% Confidence Interval (μM)
tBu (PEG) Hoechst	1.38	0.983 – 1.90
Biotinylated tBu (PEG) Hoechst	6.31	4.14 – 9.61

2.3 Conclusions

The experiments performed in **Chapter 2** focused on the biochemical characterization of the variant RNA aptamers complexed with the tBu Hoechst dyes through fluorescence techniques. This was done to determine if binding was present within each aptamer system and to evaluate the molecular interactions of the binding reaction. It also served to lay the groundwork for the structure determination of the Aptamer II-mini3-4 sequence complexed with the tBu (PEG) Hoechst dye. These experiments also allowed for the identification of specific regions within the RNA aptamer that are required for binding to the tBu dye and the potential conformational changes that may arise from the applied sequence modifications. Through the fluorescence emission and titration experiments, it was found that each of the designed RNA aptamer variants can bind to the tBu (PEG) Hoechst dye with nano to micromolar affinities at low salt concentrations and in the absence of Mg^{2+} ions.

From the fluorescence data, the Aptamer II sequence was found to have the tightest binding interactions with the tBu (PEG) Hoechst dye, which was consistent with literature results.[46] Out of all the minimized RNA aptamers that were studied within this research project, the Original and Short Stem sequences were found have the highest affinities for the tBu (PEG) Hoechst dye. These results were expected as the Original RNA aptamer most closely resembles the Aptamer II-mini3-4 sequence that was originally selected and optimized by Sando et al. (2008).[46] Additionally, the Helix 1 region of the RNA aptamer appears to not be involved in binding to the tBu dye. Therefore, its almost complete removal in the Short Stem RNA sequence had little to no effect on the aptamer's binding and fluorescence properties. The stabilization of the tetraloop within the UUCG and GAAA Tetraloop RNA variants appears to increase the conformational rigidity of Helix 2, leading to a reduction in the fluorescence intensity produced by the dye. The complete removal of

the tetraloop from the Duplex and Elongated Duplex RNA aptamers appears to increase the conformational flexibility of the RNA helix and destabilizes the interactions with the tBu (PEG) Hoechst dye. Moreover, the biotinylation of the tBu (PEG) Hoechst dye seems to also decrease the aptamer's ability to recognize and bind to the dye. To complement the data obtained through fluorescence methods and develop a more in-depth understanding of the molecular interactions, additional biochemical experiments through alternative techniques should be carried out.

Chapter 3: Conformational, Thermodynamic, and Kinetic Analysis of Derivative Hoechst-Binding RNA Aptamers

3.0 Introduction

As discussed in **Chapters 2.2.6** and **2.2.7**, fluorescence titration assays were performed to assess the binding affinities between the variant RNA aptamers and the derivative tBu Hoechst dyes. Performing these assays was advantageous as they allowed for the rapid determination of the dissociation constants with minimal sample quantities.[127,177] It should be noted, however, that using fluorescence titration for the evaluation of binding affinities is faced with some limitations. Through this assay, the molecular interactions are assessed solely based on the intensity of the fluorescence produced upon binding at each given sample concentration.[164] As a result, fluorescence-determined K_d values may not be a true representation of the specific binding mechanisms present within the aptamer systems. For instance, this method is not sensitive enough to detect the potential conformational changes of the RNA aptamer, such as the rise of structural heterogeneity upon binding to the target ligand.[178] Moreover, if the RNA sequence forms multiple conformations in solution, the target ligand may bind to the various conformations with different fluorescence enhancements.[179] This would likely result in an averaged-out fluorescence intensity[180] that is recorded through the single endpoint measurements of the fluorescence titration experiment.[167] This would consequently affect the calculated binding affinity for the interacting molecules.

Isothermal titration calorimetry is an alternative biophysical method that analyzes the molecular interactions of a reaction based on the heat released or absorbed upon binding.[178,181] Not only can ITC experiments obtain the binding affinity of a reaction with a higher degree of accuracy than fluorescence-based techniques, but it also calculates the various entropic and enthalpic contributions that arise from the molecular interactions.[182] For instance, a single sample run can obtain information regarding the stoichiometry of the binding sites (N), the association constant

(K_a), as well as thermodynamic properties including the ΔH, ΔS and ΔG of a reaction.[92] Methods have also been developed which allow for the calculation of the kinetic parameters, including the k_{on} and k_{off} rates, from the equilibration time of each sample injection.[85,183] Moreover, through the visual inspection of the endothermic and exothermic peaks produced during the sample titrations, one can gain some additional insight regarding the conformational stability of a folded aptamer sequence.[184]

The information gained from these ITC investigations can be used to complement native PAGE experiments. These native gels aid in the visualization of a biomolecule's native conformation in solution and under the desired experimental conditions.[185] For instance, an RNA aptamer may exist as a monomer or it may form a multimeric structure, such as a dimer, trimer or tetramer.[186–188] It is also possible for multiple conformations to co-exist within the same sample solution.[186] Understanding the conformation of an RNA aptamer in its unbound and ligand-bound states can reveal an abundance of information regarding the overall structure and binding mechanisms of an aptamer system.[185] Therefore, the work discussed in **Chapter 3** was to conduct ITC and native gel experiments as additional methods to evaluate the binding affinities that were obtained through fluorescence titration assays and to compare the unbound versus tBu Hoechst-bound conformations of the variant RNA sequences.[189]

3.1 Materials and Methods

3.1.1 RNA Aptamer Variants

The RNA aptamer variants used for experimentation were the same as those described in **Chapter 2.1.1**, except for the Aptamer II-mini3-4 sequence. This RNA sequence was excluded from investigations due to its similarity to the Original RNA aptamer.

3.1.2 Derivative Hoechst Dyes

The derivative Hoechst dyes used for experimentation were the same as those described in **Chapter 2.1.2**.

3.1.3 RNA Transcription

The RNA transcription was performed as described in **Chapter 2.1.3**.

3.1.4 RNA Purification

The purification of the RNA sequences was performed as described in **Chapter 2.1.4**.

3.1.5 Native PAGE for the Comparison of the Bound and Unbound RNA Conformations

To compare the tBu-bound and unbound conformations of the Aptamer II, Original and Short Stem RNA variants, a 15% native gel was made with acrylamide solution (19:1 acrylamide: bis-acrylamide), 1× tris-borate ethylenediamine tetraacetic acid (EDTA) (TBE) buffer (0.892 M Tris, 0.890 M Boric acid and 20 mM EDTA, pH 8.0) and MQW, similar to the method described by Arndt et al.[190] For the tBu-bound RNA, samples containing 1.1 µg of the variant RNA aptamer and 1.1 µg of tBu (PEG) Hoechst dye, with 1× PBS buffer (20 mM NaCl, 2.7 mM KCl, 10 mM Na_2HPO_4, 1.8 mM KH_2PO_4, pH 7.4) were prepared in a final volume of 5 µL[191] and heat treated according to the conditions listed in **Table 2.4**.[162,163] An equal volume of 100% glycerol was added to the RNA samples and the samples were promptly loaded into the native gel, as modified from the method described by Woodson and Koculi.[191] Control RNA samples, which were used to observe the native conformation of the unbound RNA aptamers, were prepared by loading 1.1 µg of the RNA in 1× PBS buffer with 50% glycerol into the native PAGE gel. A low MW DNA size

marker (New England Biolabs, Ipswich, Massachusetts), ranging from 25 to 766 base pairs (bp) was also loaded into the native gel and used as a standard to analyze the resulting conformations of the bound and unbound RNA aptamer sequences.[190,191] The gel was run at a constant voltage of 260 V for approximately 30 min until the dye front of the MW ladder reached the bottom of the gel.[192] To visualize the fluorescence of the RNA-bound tBu (PEG) Hoechst dye, the gel was imaged on a FluorChem FC2 Imaging System (Alpha Innotech, San Leandro, California), similar to the method described by Chew et al.[193] A DRC III Fiber Optic Light Source Illuminator (Schott, Mainz, Germany) fastened with a blue excitation filter (433-517 nm) was used to excite the samples at 365 nm. The fluorescence emitted by the samples at 465 nm was visualized through a SYBR green emission filter (502-572 nm) on the gel imager system. For the imaging of the RNA bands, the same gel was then stained for 30 min at 50 rpm on an Ocelot Rotator (Boekel Scientific, Feasterville Trevose, Pennsylvania) with a 1× staining solution, which was prepared by diluting a 10 000× SYBR Safe DNA stock stain solution (Invitrogen, Waltham, Massachusetts) with 1× TBE buffer.[193,194] The stained gel was imaged once again on the FluorChem FC2 Imaging System using the same blue excitation and green emission filters to visualize the RNA bands.[193]

3.1.6 Native PAGE Time Experiment

A brief time experiment was also conducted to monitor the change in binding interactions between the RNA aptamer and tBu (PEG) Hoechst dye over time. Samples containing 1.1 µg of the heat treated Original RNA aptamer (**Table 2.4**) and 1.1 µg of tBu (PEG) Hoechst dye, with 1× PBS buffer were prepared and loaded into 15% native PAGE gels with 50% glycerol.[191] The native gels were run at a constant voltage of 260 V[192] for different lengths of time (5 and 10 min). The imaging of the unstained gel to visualize the tBu (PEG) Hoechst dye's fluorescence, the subsequent

staining of the gel with 1× SYBR safe solution and the imaging of the stained RNA bands were carried out as described above in **Chapter 3.1.5**.[193,194]

3.1.7 Native PAGE for the Comparison of the Unbound Conformation of the RNA Aptamer Variants

For a direct conformational comparison of the unbound RNA aptamer variants used in this study, a final native gel experiment was conducted. Samples containing 1.1 µg of the heat treated RNA (**Table 2.4**) in 1× PBS buffer were prepared for each of the RNA aptamer variants and were loaded into the native gels with 50% glycerol.[191] The percent acrylamide used for the RNA variants is listed in **Table 3.1** and was once again chosen based on the effective range of separation suggested by Green and Sambrook.[147] As described in **Chapter 3.1.5**, a low MW DNA size marker was also loaded into the gel[190,191] and the samples were run at a constant voltage of 260 V until the dye marker reached the bottom of the gel.[192] The native gels were promptly stained with 1× SYBR stain solution[194] and imaged with a blue excitation and SYBR green emission filter on the FluorChem FC2 Imaging System.[193]

Table 3.1: Percent acrylamide chosen for the native PAGE experiments based on the number of bases present within the variant RNA aptamer sequences.

Variant Hoechst RNA Aptamer	Number of Bases	% Acrylamide
Aptamer II	71	15
Aptamer II-mini3-4 Original UUCG Tetraloop GAAA Tetraloop	29	
Short Stem	21	
Duplex 5'-half	14	20
Duplex 3'-half	11	
Elongated Duplex 5'-half	17	
Elongated Duplex 3'-half	14	

3.1.8 Isothermal Titration Calorimetry of the RNA Aptamer Variants

ITC experiments were conducted as an additional method to evaluate the binding affinities between the variant RNA aptamer-tBu Hoechst dye complexes, as well as to investigate the thermodynamic and kinetic properties of the aptamer systems.[189,195] The experiments were conducted on a MicroCal iTC_{200} system (Malvern Panalytical, Malvern, Worcestershire), and the samples were prepared in a 1× PBS binding buffer (20 mM NaCl, 2.7 mM KCl, 10 mM Na_2HPO_4, 1.8 mM KH_2PO_4, pH 7.4) according to the concentrations listed in **Table 3.2** below.[196–198] These concentrations were optimized based on the dissociation constants that were determined from the performed fluorescence titration experiments (**Table 2.10**), similar to how previously described by Gilbert et al.[197] Once again, the samples containing the RNA mixed with 1× PBS buffer were heat-treated according to the procedure listed in **Table 2.4**.[162,163] The samples were degassed for 5 minutes at room temperature using a Microcal Thermovac (Malvern Panalytical, Malvern, Worcestershire).[197,198]

Table 3.2: RNA and tBu Hoechst dye sample concentrations that were prepared for the ITC experiments at 25 °C.

RNA System		RNA Concentration (μM)	Dye Concentration (μM)
RNA aptamer	**Dye**		
Original RNA	tBu (PEG) Hoechst	50	600
UUCG Tetraloop			
GAAA Tetraloop			
Duplex		50	730
Elongated Duplex		50	
Short stem		30	860
Aptamer II		20	400
Original RNA	Biotinylated tBu (PEG) Hoechst	550	80

Each of the ITC runs was performed at 25 °C using the ITC parameters listed **Table 3.3**. For the experiments where the tBu (PEG) Hoechst dye was used, the tBu dye was titrated into the sample cell containing the variant RNA aptamers.[198,199] Whereas, for the experiments where the biotinylated tBu (PEG) Hoechst dye was used, the Original RNA aptamer was titrated into the sample cell containing the biotinylated dye.

Table 3.3: ITC experimental and injection parameters that were used for each of the variant RNA aptamer-tBu dye systems at 25 °C.

Experimental parameters	Total number of Injections	80
	Reference Cell Power (μcal/s)	3
	Initial delay (s)	180
	Stirring Speed (rpm)	750
Injection parameters	Volume (μL)	0.5
	Duration (s)	1
	Spacing (s)	180
	Filter Period (s)	5

Control experiments were also performed to determine the heat produced by the titration of the dye into the sample cell containing 1× PBS buffer as well as the titration of 1× PBS buffer into the sample cell containing the RNA aptamer.[198] The control experiments were conducted as

single trials and the concentrations used for these experiments (**Table 3.4**) were chosen to best reflect the sample parameters that were used for the RNA aptamer-tBu Hoechst dye ITC experiments. The ITC runs were performed in duplicates for the variant RNA aptamers. Both the resulting data and standard deviations were reported as averaged values from the duplicate runs. The raw ITC files were processed using the AFFINImeter KinITC software (AFFINImeter, Santiago de Compostela, Spain) to extract the thermodynamic and kinetic information.[200] For each ITC experiment, the first 1-4 injections were removed from the data set due to decreased magnitudes of heat produced, which were caused by anatomical limitations of the titrating syringe.[197,201] To generate an equilibration time curve (ETC) that would be used for the determination of the kinetic rates,[85,200] the raw ITC data was manually processed by setting the integration region and end of the signal for each sample peak.[200] To properly fit the ETC curve, the kinetic data was processed such that the error was one magnitude lower than the association and dissociation rates.

Table 3.4: Preparation of the tBu Hoechst dye and RNA control samples titrated into 1× PBS.

Sample type	Sample	Concentration (μM)
RNA control	Original RNA	50
tBu dye control	tBu (PEG) Hoechst	670
	Biotinylated tBu (PEG) Hoechst	840
		80

3.1.9 Isothermal Titration Calorimetry Temperature Series

A multitemperature experiment of the Original RNA aptamer with tBu (PEG) Hoechst dye was performed at 5, 15, 25 and 35 °C using the same concentrations and ITC parameters as listed in **Tables 3.2** and **3.3**, to analyze how the molecular interactions change with varying temperatures.[199,202] The ITC experiments were performed in duplicates and processed on the

AFFINImeter kinITC software as described in **Chapter 3.1.8** to extract the thermodynamic and kinetic parameters. Once again both the resulting data and standard deviations were reported as averaged values from the duplicate ITC experiments. The temperature dependence of ΔH, van't Hoff and Eyring linear plots were also generated from the multitemperature data series using the kinITC software.[200] The change in heat capacity (ΔC_p) was calculated by the kinITC software from the linear slope of the ΔH temperature dependence plot, which correlated the experimentally determined enthalpy changes with the corresponding reaction temperatures.[92,203] Moreover, the enthalpic and entropic contributions of the binding reaction were determined using the van't Hoff equation (5), where K_{eq} and R represent the equilibration and gas constants, and T represents the temperature.[204,205]

$$ln(K_{eq}) = -\frac{\Delta H}{RT} + \frac{\Delta S}{R} \quad (5)$$

To determine the enthalpy of activation ($\Delta^{\ddagger}H$) and entropy of activation ($\Delta^{\ddagger}S$) for the association and dissociation reactions, the multitemperature data was further processed on the kinITC software using the Eyring equation (6), where R, h, k and k_B, represent the gas, Planck, rate and Boltzmann constants and T represents the temperature.[206]

$$ln\left(\frac{k}{T}\right) = -\frac{\Delta H^{\ddagger}}{RT} + ln\left(\frac{k_B}{h}\right) + \frac{\Delta S^{\ddagger}}{R} \quad (6)$$

3.2 Results and Discussion

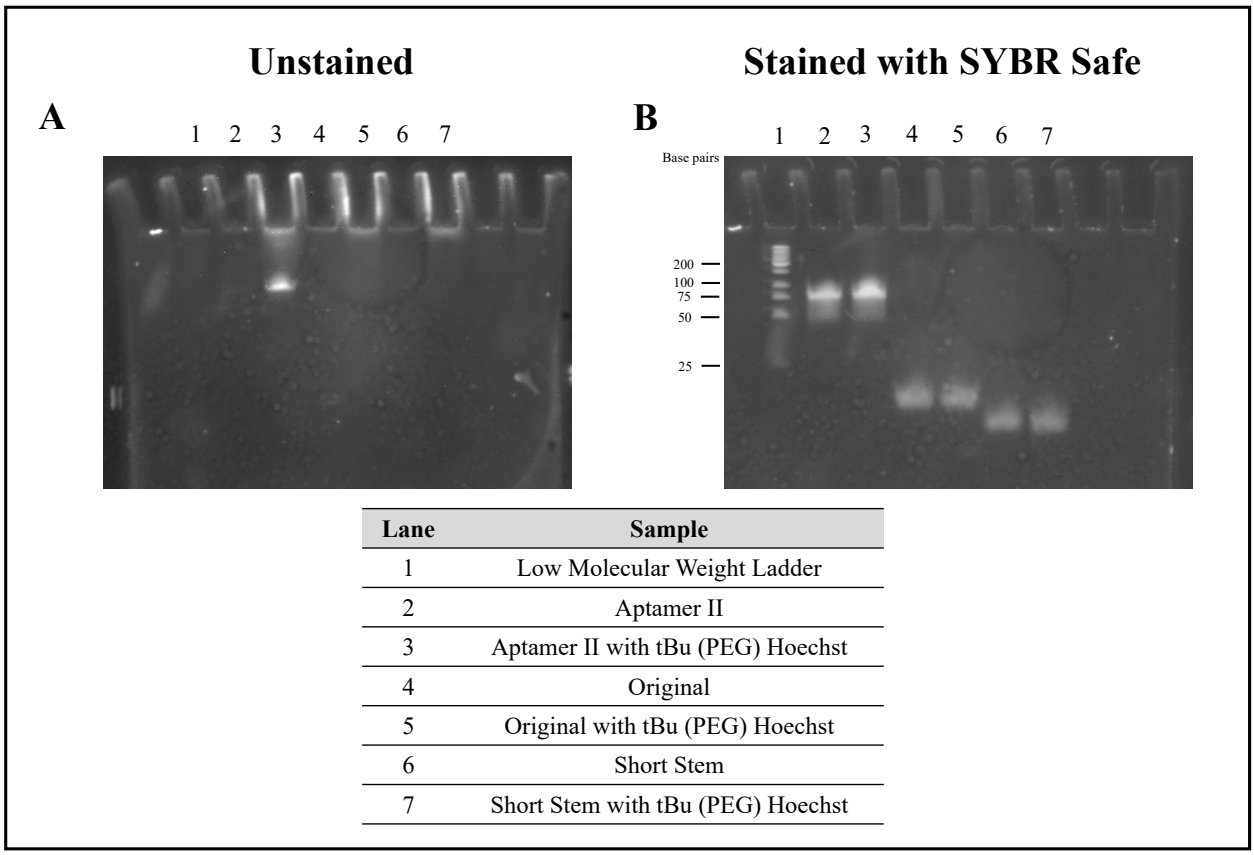
3.2.1 Native PAGE for the Comparison of the Bound and Unbound RNA Conformations

To compare the conformations of the tBu Hoechst-bound and unbound RNA aptamers, a native gel was run and imaged.[191] Similar to the native gels that were previously obtained by Ryder et al.[207] and Yakhnin et al.[208] for the visualization of protein-RNA interactions, distinct bands were expected to be seen for both the tBu-bound and unbound RNA sequences. In addition, since the

tBu (PEG) Hoechst dye fluoresces when interacting with the RNA variants, as demonstrated through the fluorescence emission experiments in **Figure 2.8**, bright fluorescent bands were expected to be observed under UV illumination for the bound samples within the unstained native gel. When analyzing the unstained native gel (**Figure 3.1A**), however, a single fluorescent band was observed in Lane 3 for the tBu-bound Aptamer II sequence. No bands were observed in Lanes 5 or 7 of the unstained native gel which contained the tBu-bound Original and Short Stem RNA aptamers, respectively. The native gel was run at a high voltage of 260V, which caused the gel to heat up during electrophoresis.[209] The prolonged exposure of the RNA-dye complex to a high-heat environment likely reduced the binding strength between the interacting molecules.[210] Therefore, tight nanomolar interactions with slow dissociation rates were required for the complex to be visualized within the gel.[207,208,211,212] Since the molecular interactions between Aptamer II and the tBu (PEG) Hoechst dye were determined to have a K_d of 58.2 nM (**Table 2.10**), these interactions were strong enough for the complex to remain bound while travelling through the heated native gel. The Original and Short Stem RNA aptamers on the other hand, have significantly weaker binding affinities at 1.38 μM and 0.895 μM (**Table 2.10**), respectively. These binding interactions were further reduced during electrophoresis which likely caused the complexes to fall apart.

When comparing the tBu-bound and unbound conformations of the Aptamer II sequence in Lanes 2 and 3 of the SYBR safe-stained native gel (**Figure 3.1B**), little to no changes in the overall hydrodynamic properties were observed. In addition, only the unbound forms of the Original and Short Stem RNA aptamers were imaged, as can be observed in Lanes 4 – 7 of the SYBR-stained gel shown in **Figure 3.1B**. Therefore, native gel experiments to compare the tBu dye-bound and unbound conformations of the UUCG Tetraloop, GAAA Tetraloop, Duplex and Elongated Duplex RNA sequences were not carried out since each of these aptamer variants were determined to have

micromolar affinities for the tBu dye (**Table 2.10**). Therefore, the RNA-tBu dye complexes would likely not be visualized within the unstained gel.



Lane	Sample
1	Low Molecular Weight Ladder
2	Aptamer II
3	Aptamer II with tBu (PEG) Hoechst
4	Original
5	Original with tBu (PEG) Hoechst
6	Short Stem
7	Short Stem with tBu (PEG) Hoechst

Figure 3.1: Bound versus unbound conformations of the RNA aptamer variants. A 15% native gel to compare the tBu-bound and unbound conformations of the Aptamer II, Original and Short Stem RNA aptamers. The same gel was imaged **A)** unstained and **B)** stained with 1× SYBR Safe dye.

3.2.2 Native PAGE Time Experiment

To test the hypothesis that micromolar binding affinities are not strong enough for the RNA-tBu dye complex to remain intact during high voltage electrophoresis, a brief time experiment was conducted using two separate 15% native gels that were run for 5 and 10 minutes, as can be seen in **Figure 3.2**. From the results, it can be clearly seen that while the electrical current was applied, the Original RNA aptamer migrated into the gel, while the tBu (PEG) Hoechst dye remained in the well. Since the dye could not enter the gel, it was gradually repulsed from the well as time went

on. This was observed in **Figures 3.2B** where only trace amounts of the tBu (PEG) Hoechst dye remained in the well after the native gel had been run for 10 minutes and the RNA sequence had long since separated from the dye. To prevent the heating of the gel and ensure that the RNA-tBu Hoechst complex remains intact for imaging, it would have been best to run the native gel experiment in a cold room.[213] In addition, the electrophoresis should have been run for a longer length of time at a lower voltage, such as 100 or 150 V, to further reduce the heat produced by the electrical current.[190,209,213]

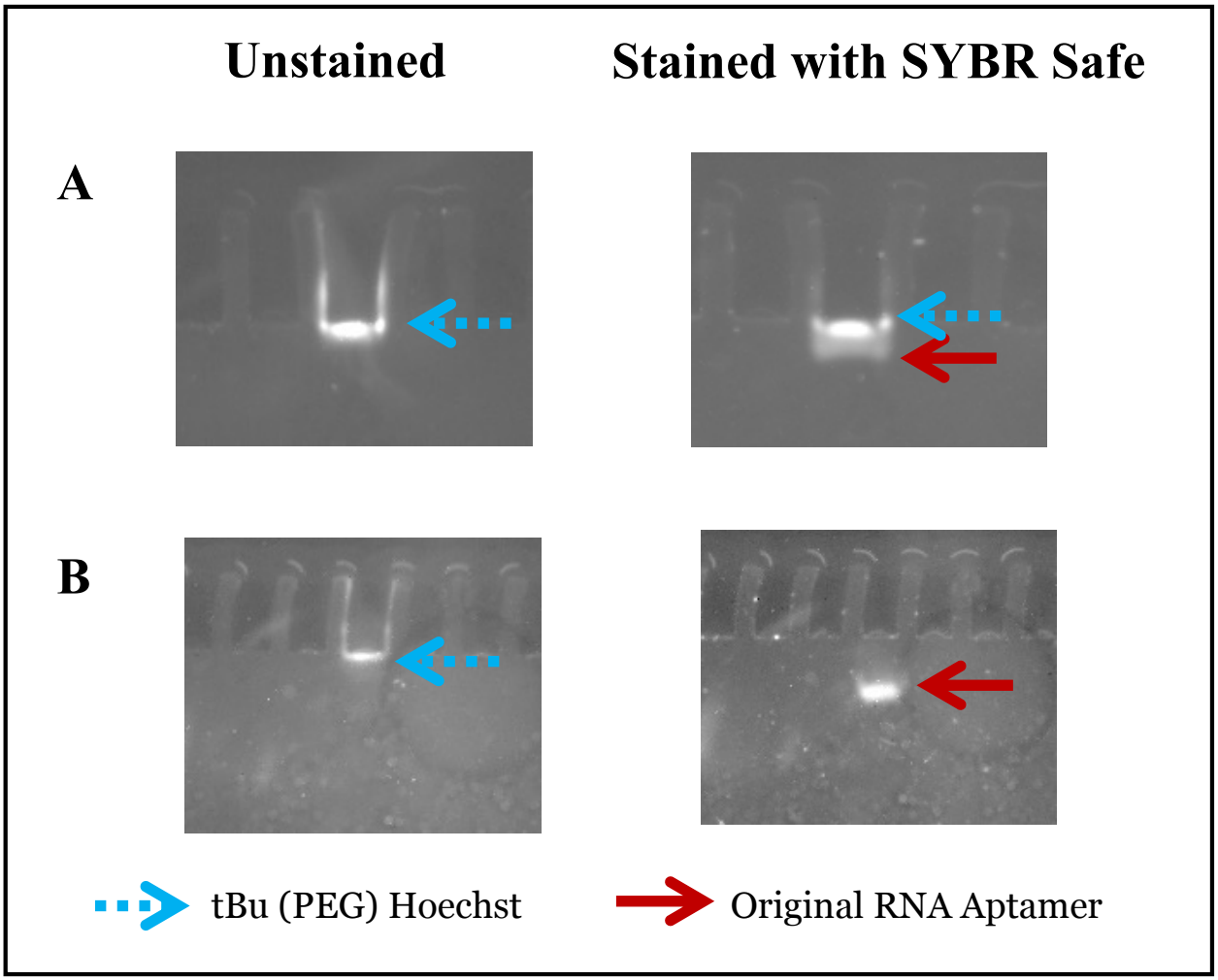
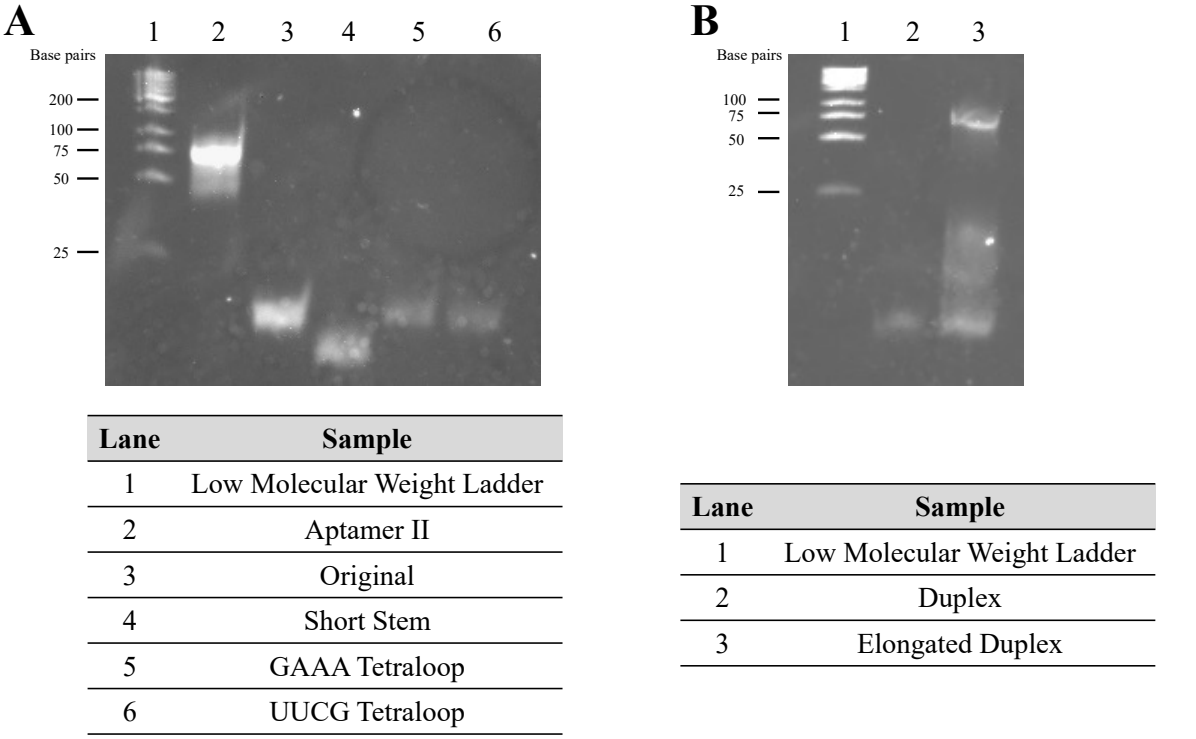


Figure 3.2: Time experiment to monitor the conformational changes over time. 15% native gels containing the tBu-bound RNA aptamers that were run for **A)** 5 and **B)** 10 minutes. At each time point, the unstained gels were imaged to observe the fluorescence of the tBu (PEG) Hoechst dye. The same gels were then stained with 1× SYBR safe dye and imaged again to view the RNA aptamer band.

3.2.3 Native PAGE for the Comparison of the Unbound Conformations of the RNA Aptamer Variants

As the conformation of the tBu-bound complex could only be visualized for the Aptamer II sequence (**Figure 3.1A**), one final native gel experiment was performed to compare the unbound conformations of all the RNA aptamer variants that were used within this research project. From the 15% native gel shown in **Figure 3.3A**, the 71-nt Aptamer II sequence was observed to mainly exist in a dimeric conformation around the 75-bp size marker. Due to the large size of the aptamer sequence some variations in folding were present, as evident from the smearing observed in Lane 2.[191] In addition, the Original, Short Stem, UUCG Tetraloop and GAAA Tetraloop RNA aptamers were found to exist as monomeric structures and in a folded stem-loop conformation. This was apparent as distinct singular bands were imaged in Lanes 3 – 6 of the 15% native gel (**Figure 3.3A**). In addition, when comparing the RNA bands with the low MW DNA size markers in Lane 1 of the gel, their positions were well below the 25-bp marker. From the movement of the 29-nt Original (Lane 3), GAAA Tetraloop (Lane 5) and UUCG Tetraloop (Lane 6) RNA aptamers and their respective secondary structures (**Figure 2.2C-E**), their folded conformations likely form approximately 11 base pairs. This agrees with the predicted secondary structure that was hypothesized by Sando et al.[46] for the Aptamer II-mini3-4 sequence. Additionally, based on the predicted secondary structure of the 21-nt Short Stem RNA aptamer (Lane 4) and the observation that it migrated slightly further down the gel than the Original, GAAA Tetraloop and UUCG Tetraloop RNA variants, its folded conformation likely forms approximately 8 base pairs. From the analysis of the 20% native gel imaged in **Figure 3.3B**, the Duplex RNA aptamer appears to also form a monomeric structure with potentially 10 base pairs, as evident by a single band in Lane 2 of the gel. The addition of the extra base pairs to Helix 1 and 2 of the Elongated Duplex causes

it to form two very distinct conformations, a monomer at approximately 14 base pairs and a multimeric structure at the 75-bp size marker, as can be seen in Lane 3 of the native gel (**Figure 3.3B)**. Similar to the Aptamer II sequence, variations in folding were also observed for the Elongated Duplex through the large smear on the gel.



Lane	Sample
1	Low Molecular Weight Ladder
2	Aptamer II
3	Original
4	Short Stem
5	GAAA Tetraloop
6	UUCG Tetraloop

Lane	Sample
1	Low Molecular Weight Ladder
2	Duplex
3	Elongated Duplex

Figure 3.3: SYBR Safe-stained native gels for the comparison of the unbound RNA aptamer variant conformations. A) A 15% native gel comparing the Aptamer II, Original, Short Stem, GAAA Tetraloop and UUCG Tetraloop RNA aptamers. **B)** A 20% native gel comparing the Duplex and Elongated Duplex RNA aptamers.

3.2.4 Isothermal Titration Calorimetry of the RNA Aptamer Variants with tBu (PEG) Hoechst

From the analysis of the control experiments, where 1× PBS buffer was titrated into the Original RNA aptamer and the tBu (PEG) Hoechst dye was titrated into 1× PBS buffer, the heats produced were found to be minimal (<0.1 µcal/s) as can be seen in **Appendix A Figures 5.2A** and

B. The endothermic peaks observed within the tBu Hoechst dye control experiment (**Figure 5.2B**) likely arose from the PEG7 tail that was added to the terminal phenol ring of the dye.[214] When comparing the dissociation constants for the variant RNA aptamers that were obtained through ITC (**Table 3.5**) and fluorescence titration (**Table 2.10**), the results agree with each other as similar K_d values were observed. For instance, the Aptamer II RNA sequence was found to have the strongest binding interactions with the tBu (PEG) Hoechst dye, as can be seen through K_d values of 340 ± 30 nM (**Table 3.5**) and 58.2 nM (**Table 2.10**), which were obtained through ITC and fluorescence experiments respectively. In addition, the Short Stem RNA aptamer was once again found to have the second strongest binding affinity for the tBu (PEG) Hoechst dye at a K_d of 1.35 ± 0.08 μM (**Table 3.5**). This ITC result agrees with the K_d value of 0.895 μM that was determined through fluorescence titration (**Table 2.10**). Similarly, the Original RNA aptamer-tBu (PEG) Hoechst dye complex has an ITC-determined K_d value of 6.9 ± 0.4 μM (**Table 3.5**), which was slightly weaker than the fluorescence-determined K_d of 1.38 μM (**Table 2.10**). Through the fluorescence titration of the UUGC and GAAA Tetraloop sequences with the tBu (PEG) Hoechst dye, the binding affinities were found to be 1.42 μM and 2.10 μM (**Table 2.10**), respectively. Therefore, the ITC experiments for these two tetraloop variants were expected to yield dissociation constants of approximately 6 μM to match the results obtained for the Original RNA aptamer. When performing the ITC experiments for the UUCG and GAAA Tetraloop RNA aptamers however, weaker binding interactions were observed at 9 ± 1 μM and 13 ± 1 μM (**Table 3.5**), respectively. Despite the difference in binding affinities between the two methods, these ITC results make sense when compared to the fluorescence emission results (**Table 2.7**) in which weaker fluorescent enhancements were observed in comparison to the Original RNA aptamer. As it was previously discussed in **Chapter 2**, the tetraloop stabilization of the UUCG and GAAA

Tetraloop variants likely increases the conformational rigidity of Helix 2. Currently, the bulge[46] and Helix 2 regions of the folded Tetraloop sequences are the hypothesized binding regions for the tBu (PEG) Hoechst dye. Therefore, the decrease in binding interactions between Helix 2 of the Tetraloop RNA aptamers and the tBu Hoechst dye is reflected within the ITC data. Interestingly, the ITC experiments also revealed that the Duplex RNA aptamer has tighter binding interactions with the tBu (PEG) Hoechst dye than the Original RNA aptamer at a K_d of 3.8 ± 0.2 μM (**Table 3.5**). These results were not expected as the fluorescence titration assay yielded a relatively weak binding affinity of 8.51 μM (**Table 2.10**). Upon further analysis of the processed ITC data in **Figure 3.4E**, large positive endothermic peaks were observed. Since it is known that the formation of biomolecule complexes is typically an exothermic process,[215] these endothermic peaks may have arisen from conformational changes within the ligand-RNA aptamer complex.[184] For example, the complete removal of the tetraloop sequence greatly decreases the stability of the Duplex complex. The Duplex strands likely break apart and then quickly reform prior to binding with the tBu Hoechst dye. These conformational rearrangements likely hindered the fluorescence of the tBu dye,[216] which would explain why the fluorescence titration assay yielded such a high dissociation constant. Finally, the Elongated Duplex RNA aptamer was found to have a similar dissociation constant as the Original RNA aptamer, at a K_d of 6 ± 1 μM (**Table 3.5**). This ITC-determined binding affinity was once again not expected as the fluorescence titration assay yielded a K_d of 3.40 μM (**Table 2.10**), which was slightly weaker than what was found for the Original RNA aptamer. When looking at the raw data in **Appendix A Table 5.1**, large variations in the dissociation constants were observed. For instance, replicates 1 and 2 of the ITC experiments produced K_d values of 10 ± 2 μM and 1.8 ± 0.3 μM, respectively. As it was previously discovered from the native gel experiments, the Elongated Duplex aptamer contains two main conformations,

a monomer and a multimeric structure (**Figure 3.3**). Without a more in-depth investigation, however, it is difficult to know the exact concentrations of the species populations and how they varied within each of the sample solutions that were prepared for ITC analysis. The fluctuations in the Elongated Duplex's binding affinity likely arose from slight variations in the heat and cool procedure, which were caused by using a water bath and ice to anneal the RNA sequences, as described in **Table 2.4**. It should also be noted that the ITC experiments performed for the Elongated Duplex resulted in significant levels of noise, which may have affected the fit and reliability of the data (**Figure 3.4F** and **Appendix A Figure 5.4F**). Therefore, additional optimizations should be carried out to ensure that dependable and consistent ITC results are obtained for the biochemical analysis of this aptamer system.

In addition to the Duplex RNA aptamer, the UUCG Tetraloop and Elongated Duplex aptamer sequences were also observed to produce positive endothermic peaks with each sample injection, as can be seen in **Figures 3.4C** and **F**. As mentioned above, these endothermic peaks are indicative of conformational changes within the ligand-aptamer system.[184] These ITC results were particularly interesting when compared to the native gel experiments for the Duplex and UUCG Tetraloop aptamers. These two RNA sequences were found to form monomeric structures with no evidence of additional conformations in their unbound states (**Figure 3.3**). Therefore, the production of these endothermic peaks likely suggests that these two RNA sequences undergo conformational rearrangements only upon interaction with the tBu (PEG) Hoechst dye. Moreover, through the fluorescence emission experiments, the Duplex, Elongated Duplex and UUCG Tetraloop aptamer sequences were found to have low relative I_{on}/I_{off} ratios in comparison to the Original RNA aptamer, ranging from 0.440 – 0.788 (**Table 2.7**). The conformational rearrangements of these RNA aptamers upon interaction of the tBu (PEG) Hoechst dye were likely

caused by both the stabilization of the aptamer's tetraloop and its complete removal from the folded sequence. Hence, this subsequently affected the how the dye interacts with Helix 2 of the aptamer sequences and reduced the fluorescence emitted by the bound complexes.

Through the performed ITC experiments, the thermodynamic properties of the aptamer systems were also evaluated, as shown in **Table 3.5**.[189] When analyzing the enthalpy change at 25 °C (ΔH_{25}) for the RNA aptamer variants bound with the tBu (PEG) Hoechst dye (**Table 3.5**), the Original RNA aptamer was found to have the most favourable binding interactions, as can be seen through a ΔH_{25} of -18.8 ± 0.5 kcal mol^{-1}. This suggests that the conformation of the Original RNA aptamer is optimal for non-covalent interactions with the tBu (PEG) Hoechst dye.[217] The Short Stem RNA aptamer was found a similar ΔH_{25} with a value of -16.2 ± 0.7 kcal mol^{-1}. This was expected as the fluorescence data suggested that the removal of Helix 1 causes minimal conformational changes within the aptamer's binding region. Moreover, the UUCG Tetraloop, GAAA Tetraloop and Duplex RNA aptamers were found to have slightly less favourable binding interactions than the Original RNA aptamer, with ΔH_{25} values of -14 ± 1 kcal mol^{-1}, -13.7 ± 0.6 kcal mol^{-1} and -11.5 ± 0.2 kcal mol^{-1}, respectively. This data further supports the hypothesis that the change in the conformational stability of Helix 2 reduces the dye's binding interactions with the aptamer sequence. Finally, the Aptamer II and Elongated Duplex sequences were found to have significantly less favourable binding interactions, through increased ΔH_{25} values of -5.49 ± 0.06 kcal mol^{-1} and -2.1 ± 0.1 kcal mol^{-1}, respectively. Once again, the trends observed for the ΔH_{25} make sense as these two aptamer sequences form multiple conformations in solution. The tBu Hoechst dye likely binds interchangeably to the various conformations, which would consequently disrupt the noncovalent interactions within the binding sites and contribute to the increased ΔH_{25} values.[84]

In addition to the ΔH_{25}, the change in entropy at 25 °C ($T\Delta S_{25}$) was analyzed for each of the RNA aptamer variants, as shown in **Table 3.5**. When analyzing the $T\Delta S_{25}$ of the variant RNA aptamers, the Original, Short Stem, UUCG Tetraloop, GAAA Tetraloop and Duplex RNA sequences were found to produce negative $T\Delta S_{25}$ values ranging from approximately -4 to -12 K kcal mol^{-1}. The negative values indicate that the formation of these tBu dye-RNA complexes appears to be an enthalpy-driven process.[218] Upon binding of the tBu (PEG) Hoechst dye to these RNA sequences there is a loss in rotational and translational freedom, which contributes to the net negative entropy change.[84,89] The Aptamer II and Elongated Duplex sequences on the other hand were found to have positive entropy change at 3.35 ± 0.08 K kcal mol^{-1} and 5.2 ± 0.2 K kcal mol^{-1}, respectively. Therefore, the formation of these aptamer complexes appear to be entropy-driven,[218] which is likely a result of their structural heterogeneity. The concurrent stabilization and destabilization of the different tBu Hoechst-bound conformations likely increases the degree of disorder present within the aptamer system.[84] This increased disorder is evidently large enough to overcompensate for the mobility loss that arises from the complex formation. As a result, the molecular interactions yielded a positive ΔS, as observed for the two aptamer systems.

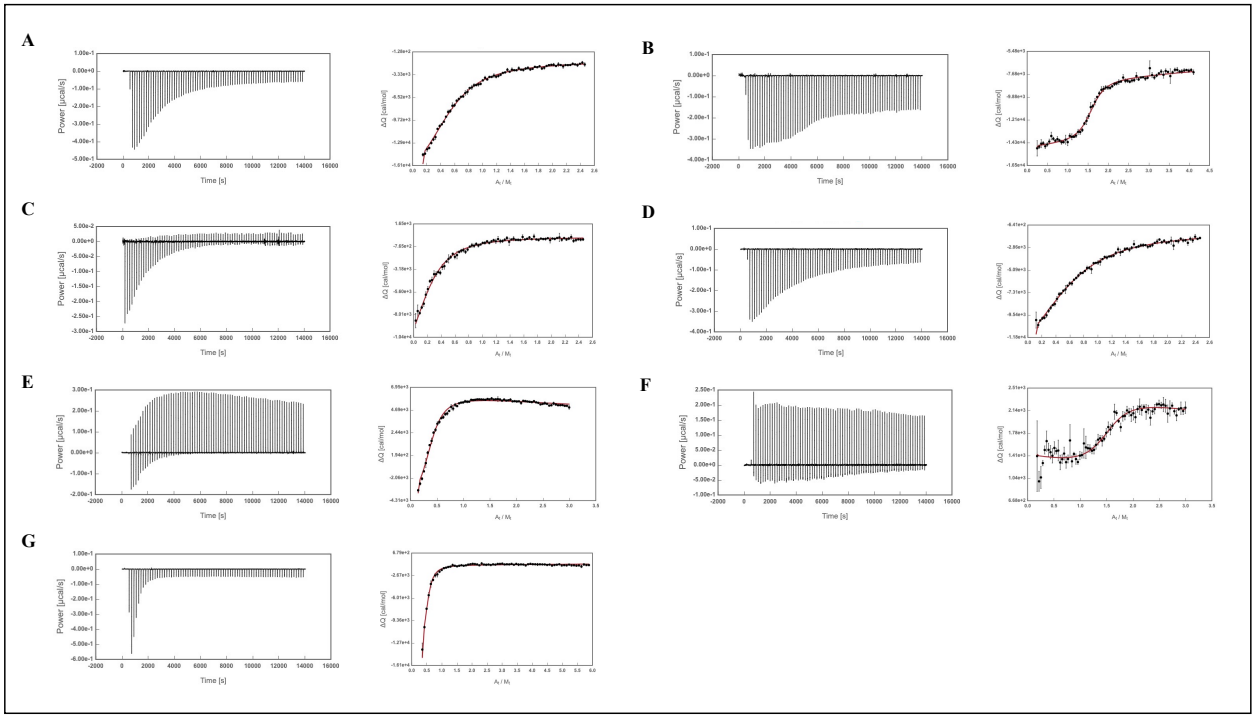


Figure 3.4: Processed ITC and equilibrium isotherm data for the RNA aptamer variants. The titration of the tBu (PEG) Hoechst dye into the **A)** Original, **B)** Aptamer II, **C)** UUCG Tetraloop, **D)** GAAA Tetraloop**, E)** Duplex, **F)** Elongated Duplex, and **G)** Short Stem RNA aptamers at 25 °C. The data for the duplicate runs are presented in **Appendix A Figures 5.4A-G**.

Table 3.5: Comparison of the averaged data for the binding affinities and thermodynamic properties of the variant RNA aptamers with the tBu (PEG) Hoechst dye at 25 °C.

Variant RNA Aptamer	$\mathbf{K_A\ (\mu M^{-1})}$	$\mathbf{K_D\ (\mu M)}$	$\mathbf{\Delta H_{25}}$ **(kcal mol^{-1})**	$\mathbf{T\Delta S_{25}}$ **(K kcal mol^{-1})**
Original RNA	0.151 ± 0.009	6.9 ± 0.4	-18.8 ± 0.5	-11.7 ± 0.5
Aptamer II	3.1 ± 0.3	0.34 ± 0.03	-5.49 ± 0.06	3.35 ± 0.08
UUCG Tetraloop	0.11 ± 0.01	9 ± 1	-14 ± 1	-7 ± 1
GAAA Tetraloop	0.084 ± 0.007	13 ± 1	-13.7 ± 0.6	-7.0 ± 0.6
Duplex	0.28 ± 0.01	3.8 ± 0.2	-11.5 ± 0.2	-4.1 ± 0.2
Elongated Duplex	0.32 ± 0.06	6 ± 1	-2.1 ± 0.1	5.2 ± 0.2
Short stem	0.96 ± 0.06	1.35 ± 0.08	-16.2 ± 0.7	-8.2 ± 0.7

The ITC data were further processed through the AFFINImeter kinITC software to determine the equilibration times of each injection, which were then used to generate an equilibration time curve.[85] This ETC plot was used to calculate the kinetic parameters, k_{on} and k_{off}, of the binding interactions.[85,219] Through the analysis of the ETC plots for the RNA aptamer variants with the

tBu (PEG) Hoechst dye (**Figure 3.5**) and their derived kinetic properties (**Table 3.6**), the Aptamer II RNA sequence was determined to have the fastest association rate with the tBu dye, with a k_{on} value of $(1.4 \pm 0.2) \times 10^5$ M^{-1} s^{-1}. This result agrees with the fluorescence and ITC-determined binding affinities as Aptamer II was found to have tight nanomolar binding interactions with the tBu (PEG) Hoechst dye. As mentioned in **Chapter 1.2.3**, strong binding interactions are often accompanied with fast association rates.[84,85] In addition, it was found that the Original, Short Stem, UUCG Tetraloop, GAAA Tetraloop, Duplex and Elongated Duplex RNA aptamers all have similar association rates with k_{on} values in the 10^4 M^{-1} s^{-1} range. This indicated that each of the RNA aptamer variants have similar recognition mechanisms and specificities for the tBu (PEG) Hoechst dye.[217] When compared to literature results, these experimental k_{on} values fall within the expected range of approximately $10^3 – 10^8$ M^{-1} s^{-1} for biomolecules that have micromolar affinities for their targets; however, they are among the slower association rates.[87,220]

When analyzing the dissociation constants produced from the ETC plots (**Table 3.6**), the Aptamer II, Original, Short Stem, Duplex and Elongated Duplex RNA aptamers were found to have similar dissociation rates, with k_{off} values in the 10^{-2} s^{-1} range. Meanwhile the UUCG and GAAA Tetraloop variants were discovered to have dissociation rates that were a magnitude faster, with k_{off} values in the 10^{-1} s^{-1} range. It should be noted that these RNA aptamers have fast dissociation rates when compared to literature values, where 10^{-1} s^{-1} is considered a fast dissociation and 10^{-6} s^{-1} is considered a slow dissociation rate.[220] Therefore, the comparable dissociation rates observed for the Aptamer II, Original, Short Stem, Duplex and Elongated Duplex RNA aptamers suggest that these folded sequences have similar geometric complementarities with the tBu (PEG) Hoechst dye, which increases their complex stability and subsequent dissociation half-lives.[87,217,221] The faster dissociation rates observed for the Tetraloop variants once again

supports the hypothesis that the stabilization of the tetraloop sequence results in the conformational rigidity of Helix 2, which reduces the aptamer's ability to adapt for ligand binding. This causes the tBu (PEG) Hoechst dye to dissociate from the bound Tetraloop variant complexes at a slightly faster rate than the other aptamer systems studied within this research project.

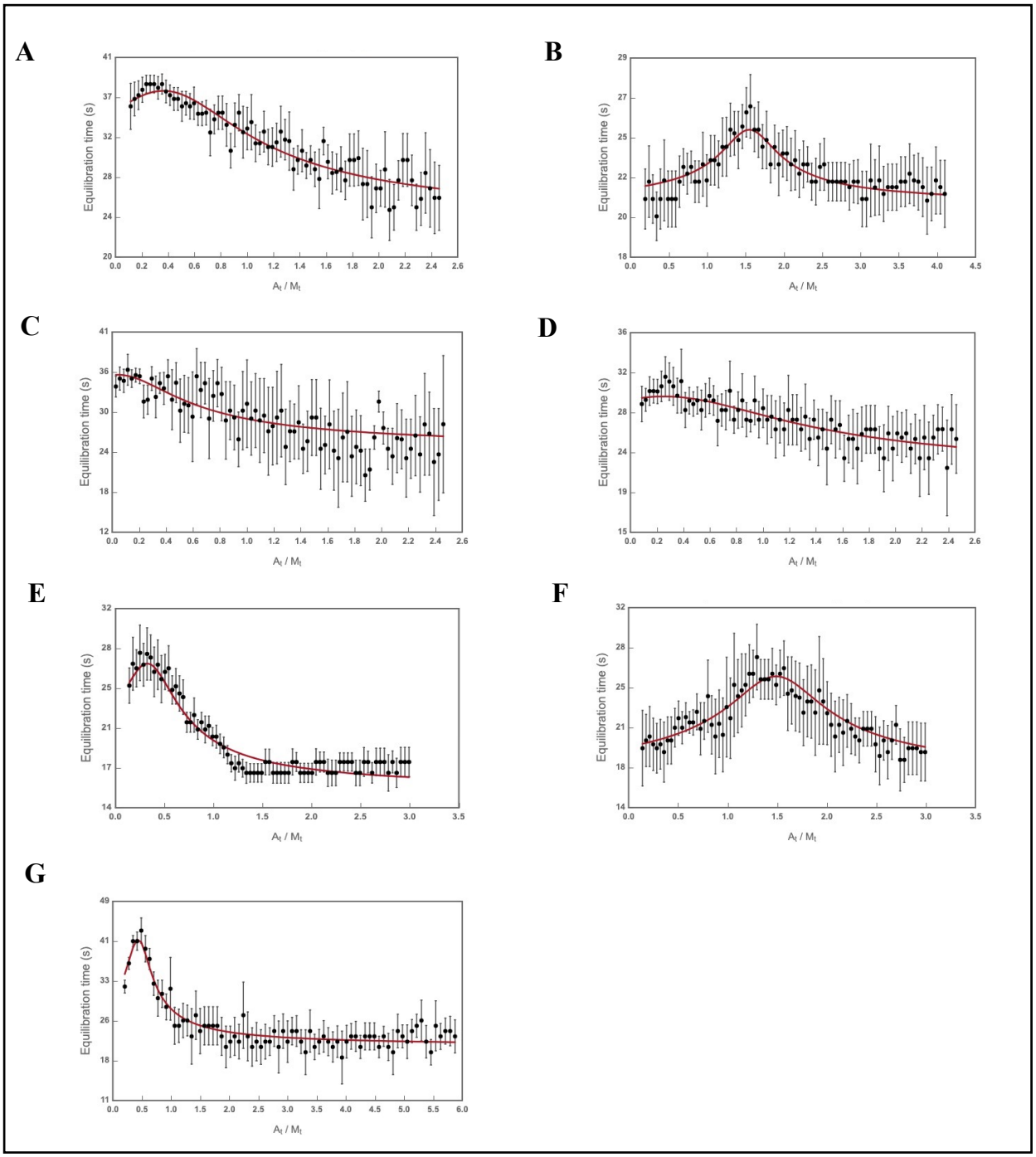


Figure 3.5: Processed ETC for the RNA aptamer variants. The titration of tBu (PEG) Hoechst dye into the **A)** Original, **B)** Aptamer II, **C)** Aptamer II-mini3-4, **D)** UUCG Tetraloop, **E)** GAAA Tetraloop**, F)** Duplex, **G)** Elongated Duplex, and **H)** Short Stem RNA aptamers at 25 °C. The data for the duplicate runs is presented in **Appendix A Figures 5.5A-G**.

Table 3.6: Comparison of the averaged data for the kinetic properties of the RNA aptamer variants with the tBu (PEG) Hoechst dye at 25 °C.

Variant RNA Aptamer	k_{on} ($M^{-1}s^{-1}$)	k_{off} (s^{-1})
Original RNA	$(1.4 \pm 0.1) \times 10^4$	$(9.3 \pm 0.7) \times 10^{-2}$
Aptamer II	$(1.4 \pm 0.2) \times 10^5$	$(4.9 \pm 0.8) \times 10^{-2}$
UUCG Tetraloop	$(1.8 \pm 0.3) \times 10^4$	$(1.7 \pm 0.3) \times 10^{-1}$
GAAA Tetraloop	$(1.2 \pm 0.2) \times 10^4$	$(1.5 \pm 0.2) \times 10^{-1}$
Duplex	$(2.4 \pm 0.2) \times 10^4$	$(8.7 \pm 0.6) \times 10^{-2}$
Elongated Duplex	$(1.2 \pm 0.2) \times 10^4$	$(3.9 \pm 0.6) \times 10^{-2}$
Short Stem	$(2.9 \pm 0.2) \times 10^4$	$(3.4 \pm 0.2) \times 10^{-2}$

3.2.5 Isothermal Titration Calorimetry of the Original RNA Aptamer with Biotinylated tBu (PEG) Hoechst

Initially, when optimizing the ITC experiments for the Original RNA aptamer and the biotinylated tBu (PEG) Hoechst dye, the dye was first titrated into the sample cell containing the RNA sequence, like the experiments that were performed for each of the RNA aptamer variants as described in **Chapter 3.1.8**. Upon analysis of the raw ITC data, it was noticed that the binding curves never reached saturation, even when higher concentrations of the biotinylated dye were titrated into the RNA sample, which resulted in large error bars (data not included in this thesis). Therefore, a control experiment was conducted where 840 μM of the biotinylated tBu (PEG) Hoechst dye was titrated into the sample cell containing 1× PBS to see if there were any unusual peaks of large magnitudes. As can be seen in **Appendix A Figure 5.3A**, the control run looked normal, and the heats produced were minimal (<0.02 μcal/s). This problem of aptamer saturation was solved by titrating the Original RNA aptamer into the sample cell containing the biotinylated tBu (PEG) Hoechst dye. Therefore, this suggested that at high concentrations, the biotinylated tBu (PEG) Hoechst dye may undergo self-aggregation and interfere with the complex's binding interactions.[222] It can be noted that the heats produced by the second control experiment, where

1× PBS was titrated into the sample cell containing 80 µM of the biotinylated dye were also minimal (<0.02 µcal/s), as shown in **Appendix A Figure 5.3B**.

When analyzing the ITC data for heats produced upon the interaction of the Original RNA aptamer with the biotinylated tBu (PEG) Hoechst dye (**Figure 3.6**), the results once again make sense and agrees with the fluorescence data. For instance, the fluorescence titration assay was found to produce an estimated K_d of 6.31 µM (**Table 2.11**), while the ITC experiments yielded a K_d of 13.3 ± 0.6 µM (**Table 3.7**). Moreover, through the analysis of the ΔH_{25}, the interactions between the Original RNA aptamer and the biotinylated tBu (PEG) Hoechst dye were found to be less favourable at -14.6 ± 0.3 kcal mol^{-1} than when bound to the non-biotinylated dye (**Table 3.7**). In addition, although the entropy change for the biotinylated-Original aptamer system was also determined to be unfavourable, the magnitude was slightly lower than the non-biotinylated system, as can be seen through a $T\Delta S_{25}$ of -7.9 ± 0.3 K kcal mol^{-1} (**Table 3.7**). Therefore, these thermodynamic properties agree with the performed fluorescence experiments which suggested that the addition of the biotin tag to the biotinylated tBu Hoechst dye interferes with its ability to form binding interactions with Helix 2 of the folded aptamer, hence hindering complex formation.

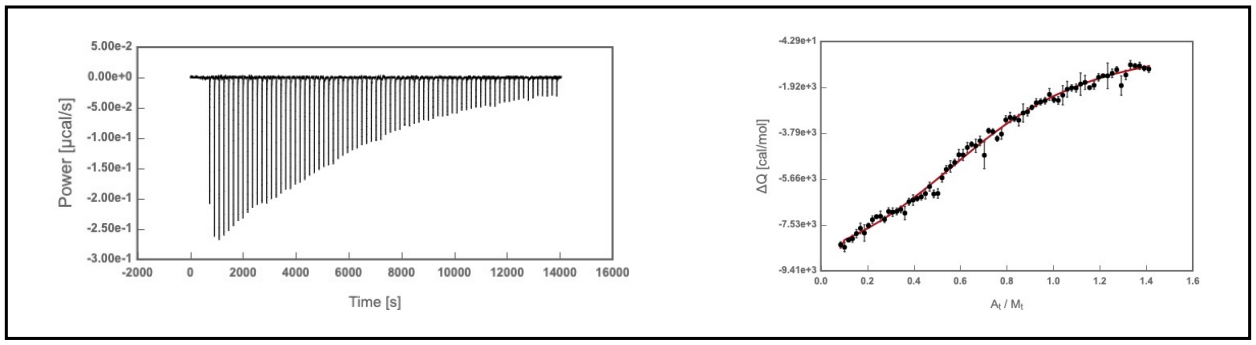


Figure 3.6: Processed ITC and equilibrium isotherm data for the tBu Hoechst dye derivatives. the titration of the Original RNA aptamer into the biotinylated tBu (PEG) Hoechst dye at 25°C. The duplicate run is shown in **Appendix A Figure 5.6**.

Table 3.7: Comparison of the averaged data for the binding affinities and binding enthalpies of the Original RNA aptamer with biotinylated versus non-biotinylated tBu Hoechst dye at 25 °C.

Hoechst Dye Derivative	K_A (μM^{-1})	K_D (μM)	ΔH_{25} (kcal mol^{-1})	$T\Delta S_{25}$ (K kcal mol^{-1})
tBu (PEG) Hoechst	0.151 ± 0.009	6.9 ± 0.4	-18.8 ± 0.5	-11.7 ± 0.5
Biotinylated tBu (PEG) Hoechst	0.077 ± 0.003	13.3 ± 0.6	-14.6 ± 0.3	-7.9 ± 0.3

Through the analysis of the ETC plot (**Figure 3.7**) and its derived kinetic properties (**Table 3.8**), the association rate for the binding of the Original RNA aptamer to the biotinylated tBu (PEG) Hoechst dye was found to be slightly slower than when the aptamer binds to the non-biotinylated dye. For instance, the k_{on} values were determined to be $(4.7 \pm 0.5) \times 10^3$ M^{-1} s^{-1} and $(1.4 \pm 0.1) \times 10^4$ M^{-1} s^{-1} for the binding of the biotinylated and non-biotinylated dye, respectively. In comparison, the dissociation constants fell within the 10^{-2} s^{-1} range for both of the derivative tBu Hoechst dye-Original RNA complexes. Therefore, these results once again support the theory that the biotin motif reduces the recognition and binding mechanisms of the Original RNA aptamer to the biotinylated dye.[217] Once bound however, the interacting molecules remain a stable complex due to the overall geometrical compatibility of the binding region.

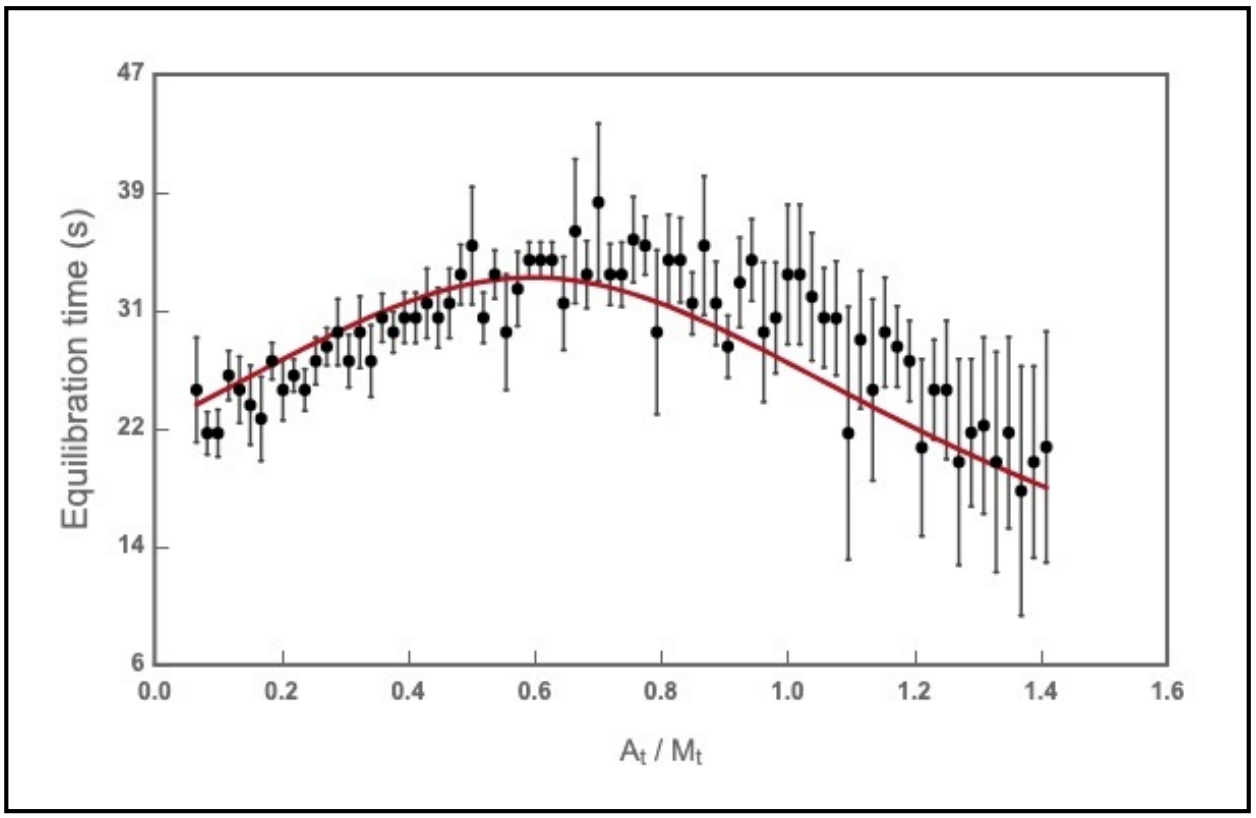


Figure 3.7: Processed ETC for the tBu Hoechst dye derivatives. The titration of the Original RNA aptamer into the biotinylated tBu (PEG) Hoechst dye at 25 °C. The data for the duplicate run can be found in **Appendix A Figure 5.7**.

Table 3.8: Comparison of the averaged data for the kinetic properties of the Original RNA aptamer with biotinylated versus non-biotinylated tBu Hoechst dye at 25 °C.

Hoechst Dye Derivative	k_{on} ($M^{-1}s^{-1}$)	k_{off} (s^{-1})
tBu (PEG) Hoechst	$(1.4 \pm 0.1) \times 10^4$	$(9.3 \pm 0.7) \times 10^{-2}$
Biotinylated tBu (PEG) Hoechst	$(4.7 \pm 0.5) \times 10^3$	$(6.3 \pm 0.7) \times 10^{-2}$

3.2.6 Isothermal Titration Calorimetry Temperature Series of the Original RNA aptamer with tBu (PEG) Hoechst

To determine the effects of temperature on the binding interactions and potential conformation changes of the Original RNA aptamer-tBu (PEG) Hoechst dye complex, ITC experiments were performed at 5, 15, 25 and 35 °C (**Figure 3.8**).[181,217,223] As can be observed from the results in **Table 3.9**, the binding interactions were the strongest at 5 °C with a K_d of 180 ± 30 nM. As the

temperature increased, the binding affinities gradually became weaker, until a 100-fold decrease in the binding affinity was observed at 35 °C with a K_d of 29 ± 2 μM. This trend of increasing binding affinities with decreasing temperatures has been previously observed in other biomolecule systems.[224,225] When looking at the kinetic properties of the binding interactions with varying temperatures in **Table 3.10** and **Figure 3.9**, it was found that the k_{on} rates increased and the k_{off} rates decreased with reducing temperatures. Therefore, this indicates that reduced temperatures may stabilize the tertiary structure of the Original RNA aptamer by reducing its conformational flexibility,[226] thus increasing the speed at which it can recognize and bind to the tBu (PEG) Hoechst dye.[217] Similarly, the increased stability of the aptamer may allow for the best geometrical fit of the dye within the aptamer's groove, hence reducing the dissociation rate.

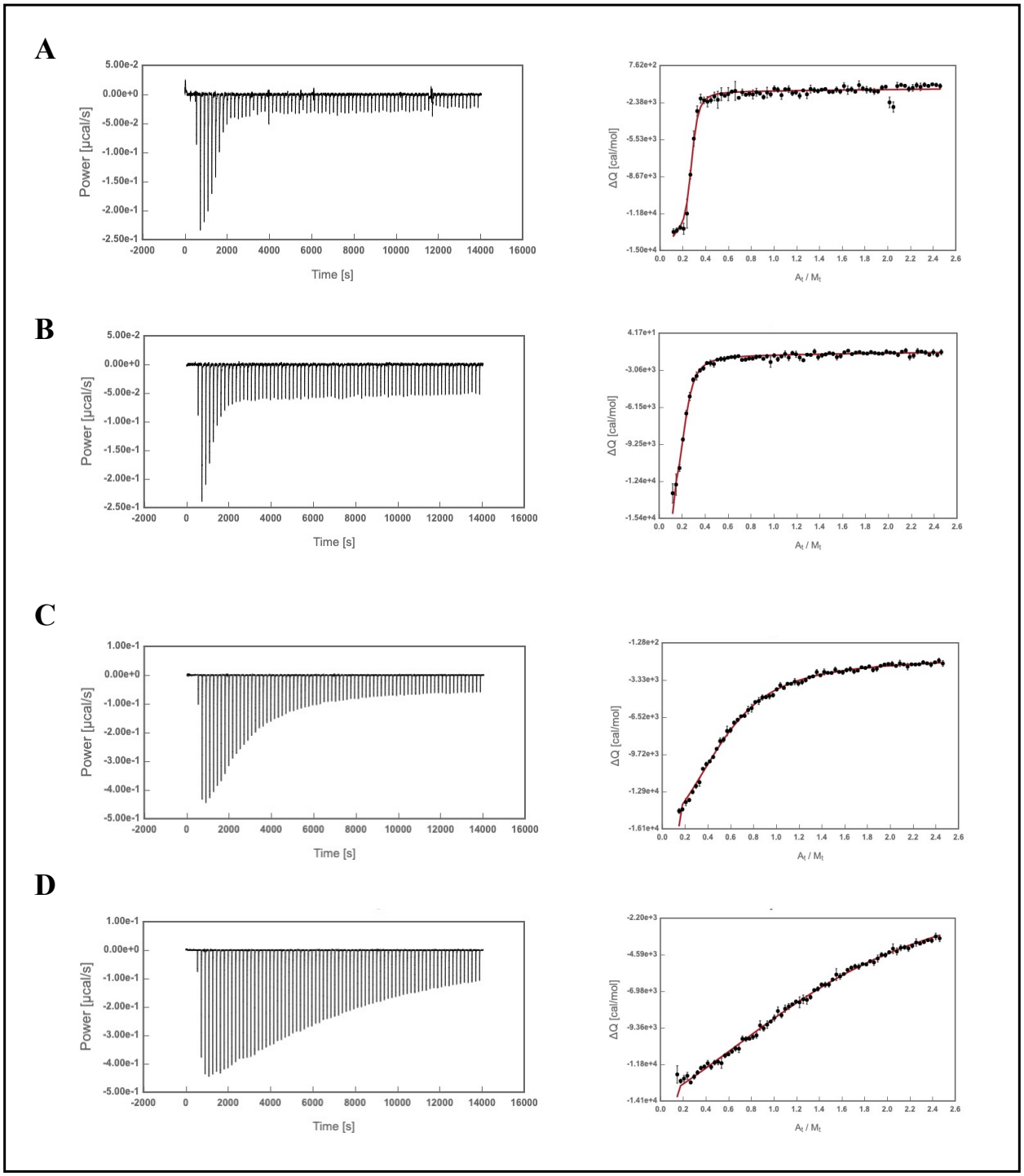


Figure 3.8: Processed ITC and equilibrium isotherm data for the temperature series. Titration of the tBu (PEG) Hoechst dye into the Original RNA aptamer at **A)** 5 °C, **B)** 15 °C **C)** 25 °C and **D)** 35 °C. The duplicate runs are displayed in **Appendix A Figures 5.8A-D**.

Table 3.9: Averaged data for the binding affinities and thermodynamic properties obtained from the titration of 600 µM tBu (PEG) Hoechst into 50 µM Original RNA at different temperatures.

Temperature (°C)	K_A (M^{-1})	K_D (µM)	ΔH_{25} (kcal mol^{-1})	$T\Delta S_{25}$ (K kcal mol^{-1})
5	5.6 ± 0.9	0.18 ± 0.03	-11.4 ± 0.3	-2.8 ± 0.3
15	1.4 ± 0.2	0.73 ± 0.08	-16 ± 1	-8 ± 1
25	0.151 ± 0.009	6.9 ± 0.4	-18.8 ± 0.5	-11.7 ± 0.5
35	0.035 ± 0.002	29 ± 2	-18.5 ± 0.4	-12.1 ± 0.4

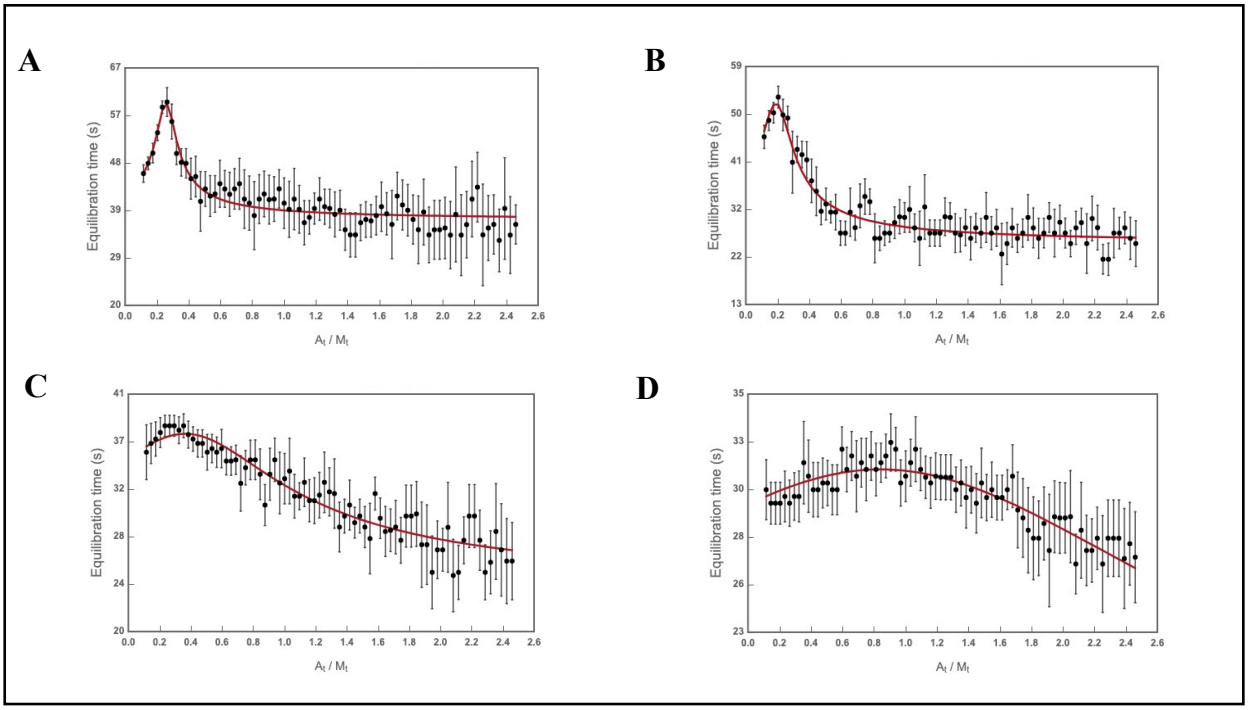


Figure 3.9: Processed ETC for the temperature series. The Original RNA aptamer titrated with tBu (PEG) Hoechst dye at **A)** 5 °C, **B)** 15 °C **C)** 25 °C and **D)** 35 °C. The duplicate run is in **Appendix A Figures 5.9A-D**.

Table 3.10: Averaged data for the kinetic parameters obtained from the titration of 600 µM tBu (PEG) Hoechst into 50 µM Original RNA at different temperatures.

Temperature (°C)	k_{on} ($M^{-1}s^{-1}$)	k_{off} (s^{-1})
5	$(5.4 \pm 0.6) \times 10^4$	$(1.0 \pm 0.1) \times 10^{-2}$
15	$(3.8 \pm 0.3) \times 10^4$	$(2.8 \pm 0.3) \times 10^{-2}$
25	$(1.4 \pm 0.1) \times 10^4$	$(9.3 \pm 0.7) \times 10^{-2}$
35	$(2.0 \pm 0.3) \times 10^3$	$(5.8 \pm 0.8) \times 10^{-2}$

Through the analysis of the temperature variance of ΔH (**Figure 3.10A**), the ΔC_p was calculated to be -250 ± 0.01 cal mol^{-1} K^{-1} (**Table 3.11**), which is indicative that the reaction becomes more exothermic with increasing temperatures.[203] The negative ΔC_p also points towards specific binding with some conformational rearrangements upon the interaction of the Original RNA aptamer with the tBu (PEG) Hoechst dye.[181,203,217] These conformational rearrangements likely arise from the dynamic UUUU tetraloop of the Original RNA aptamer, which increases the flexibility of the dye's binding region in Helix 2. Moreover, the negative sign of the calculated change in heat capacity is also indicative of the exposure of polar surfaces within the folded RNA aptamer sequence, which likely play a role in the complex's binding interactions.[227,228] For instance, upon binding to the tBu (PEG) Hoechst dye the aptamer's bulge region may protrude outwards to help accommodate for the bulky tBu groups.

Upon closer inspection of the ΔH values (**Table 3.9**), the binding interactions appear to become more exothermic with increasing temperatures until a maximum ΔH of -18.8 ± 0.5 kcal mol^{-1} was observed at 25 °C, which is consistent with the calculated ΔC_p (**Table 3.11**). When the temperature was further increased to 35 °C the change in enthalpy was observed to slightly increase, through an averaged ΔH value of -18.5 ± 0.4 kcal mol^{-1}. Despite this slight increase, the temperatures studied within this research project produced a linear trend for the temperature dependence of enthalpy change, as shown in **Figure 3.10A**. Similarly, when analyzing the TΔS values produced from the multitemperature experiments, the entropy change gradually becomes more negative from 5 to 35 °C (**Table 3.9**). This makes sense as at higher temperatures there should be an increase in the molecular movement of the free RNA molecules in the sample solution.[229] Upon formation of the bound complex from the dynamic free molecules there would be a greater decrease in entropy within the aptamer system,[84] which would contribute to the reduced ΔS values

observed at higher temperatures. In addition, the observation of more negative ΔS values with increasing temperature could be indicative of the formation of hydrophobic interactions between the tBu (PEG) Hoechst dye and the hydrophobic interior of the aptamer's groove.[230]

The production of the van't Hoff plot (**Figure 3.10B**) from the multitemperature experiments revealed a ΔH_{VH} of -30.6 ± 0.5 kcal mol^{-1} (**Table 3.11**) which is significantly larger than the ΔH_{25} of -18.8 ± 0.5 kcal mol^{-1} (**Table 3.9**) that was previously determined through calorimetric methods. It has been noted in a study by Horn et al.[205] that the enthalpy change determined through the two methods should yield similar results and any differences are not indicative of structural changes within the aptamer system. Therefore, the difference observed between the ΔH values that were calculated from the two methods may have arisen from experimental error. Moreover, the entropy change extracted from the van't Hoff plot (ΔS_{VH}) was found to be unfavourable at -79 ± 2 cal mol^{-1} K^{-1}, as shown in **Table 3.11**. The large and negative value ΔS_{VH} suggests that the complex is quite stable with limited conformational rearrangements, as negative values are indicative of reduced degrees of freedom within the bound system.[84,122,203,204]

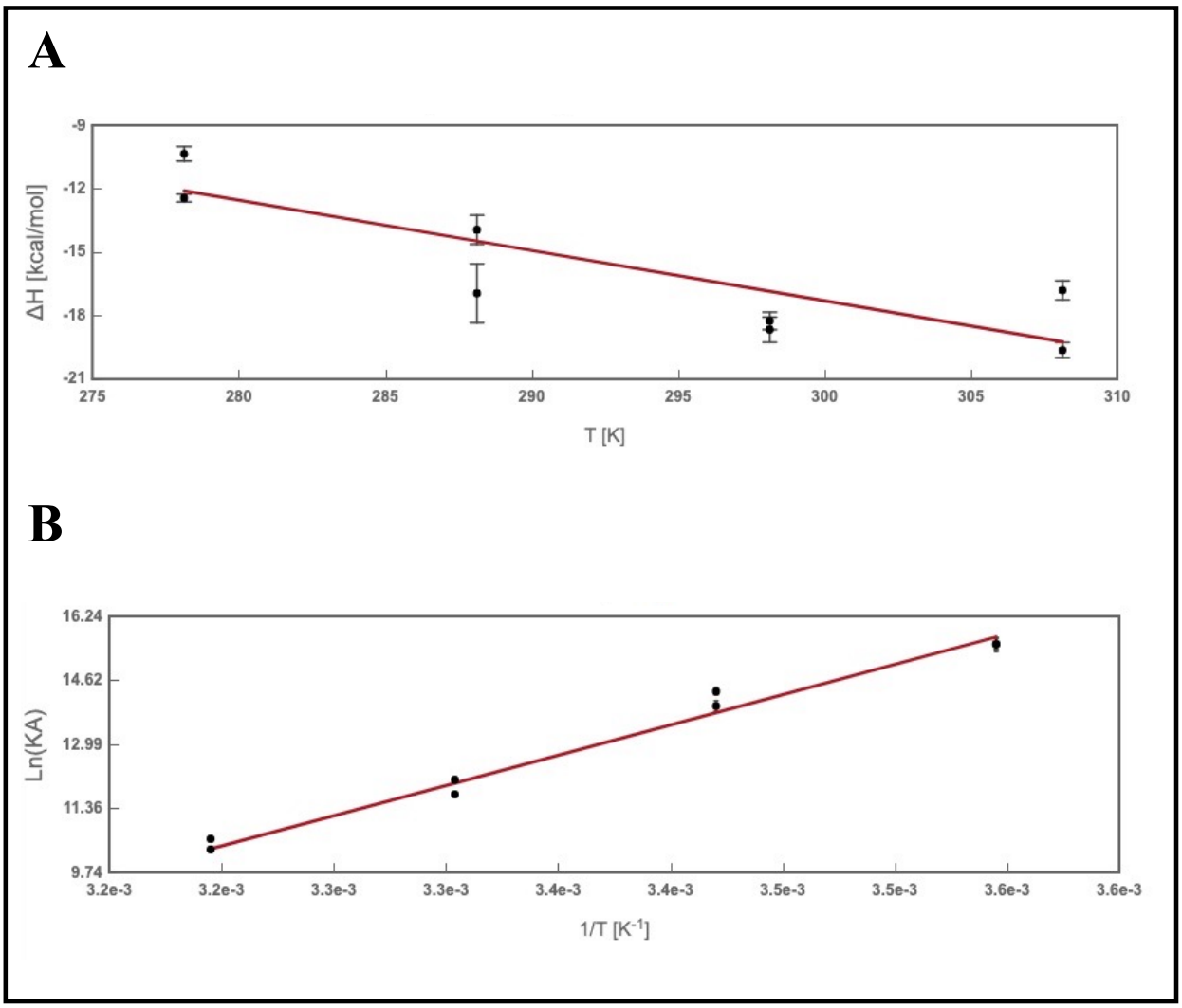


Figure 3.10: Plotted temperatures series. A) Temperature dependence of ΔH and **B)** van't Hoff plot for the Original RNA aptamer with tBu (PEG) Hoechst dye, generated by the kinITC software from the multitemperature ITC experiments.

Table 3.11: Thermodynamic properties calculated from the temperature dependence of ΔH and van't Hoff plots.

ΔC_p (cal mol^{-1} K^{-1})	ΔH_{VH} (kcal mol^{-1})	ΔS_{VH} (cal mol^{-1} K^{-1})
-250 ± 0.01	-30.6 ± 0.5	-79 ± 2

Linear Eyring plots, such as those produced in **Figure 3.11**, are often used to characterize the activation energies and transition state entropies for the thermodynamic profile of the association and dissociation reactions.[204,206] From the plots, the $\Delta^{\ddagger}H_{on}$ was found to be -17.1 ± 0.6 kcal mol^{-1}

(**Table 3.12**) thus indicating that there is essentially no enthalpic barrier to overcome upon formation of the transition state from the unbound reactants.[204,231] The $\Delta^{\ddagger}H_{off}$, on the other hand was determined to be 14.1 ± 0.6 kcal mol^{-1} (**Table 3.12**), which represents a large enthalpic barrier that is required to overcome for the formation of the transition state from the bound products. Therefore, these enthalpies of activation for the association and dissociation reactions support the hypothesis of a stable Original RNA-tBu dye complex and agree with the enthalpic data obtained in **Tables 3.9** and **3.11**. Additionally, the $\Delta^{\ddagger}S_{on}$ and the $\Delta^{\ddagger}S_{off}$ were found to be -97 ± 2 cal mol^{-1} K^{-1} and -17 ± 2 cal mol^{-1} K^{-1}, respectively (**Table 3.12**). This indicated that the entropy contributions towards the transition state formation are unfavourable for both the association and dissociation reactions.[204] It has been previously noted that the interpretation of the $\Delta^{\ddagger}S$ may be difficult as the formation of the transition state may be affected by external factors, such as steric hindrance or solvation effects.[232,233] Nevertheless, the observation of an increased $\Delta^{\ddagger}S_{off}$ in comparison to the $\Delta^{\ddagger}S_{on}$ indicates that the formation of the transition state from the bound products results in increased disorder within the aptamer system.[234] This is consistent with previously discussed entropic data (**Table 3.9**) and current understandings of the interactions within the Original RNA aptamer-tBu (PEG) Hoechst complex.

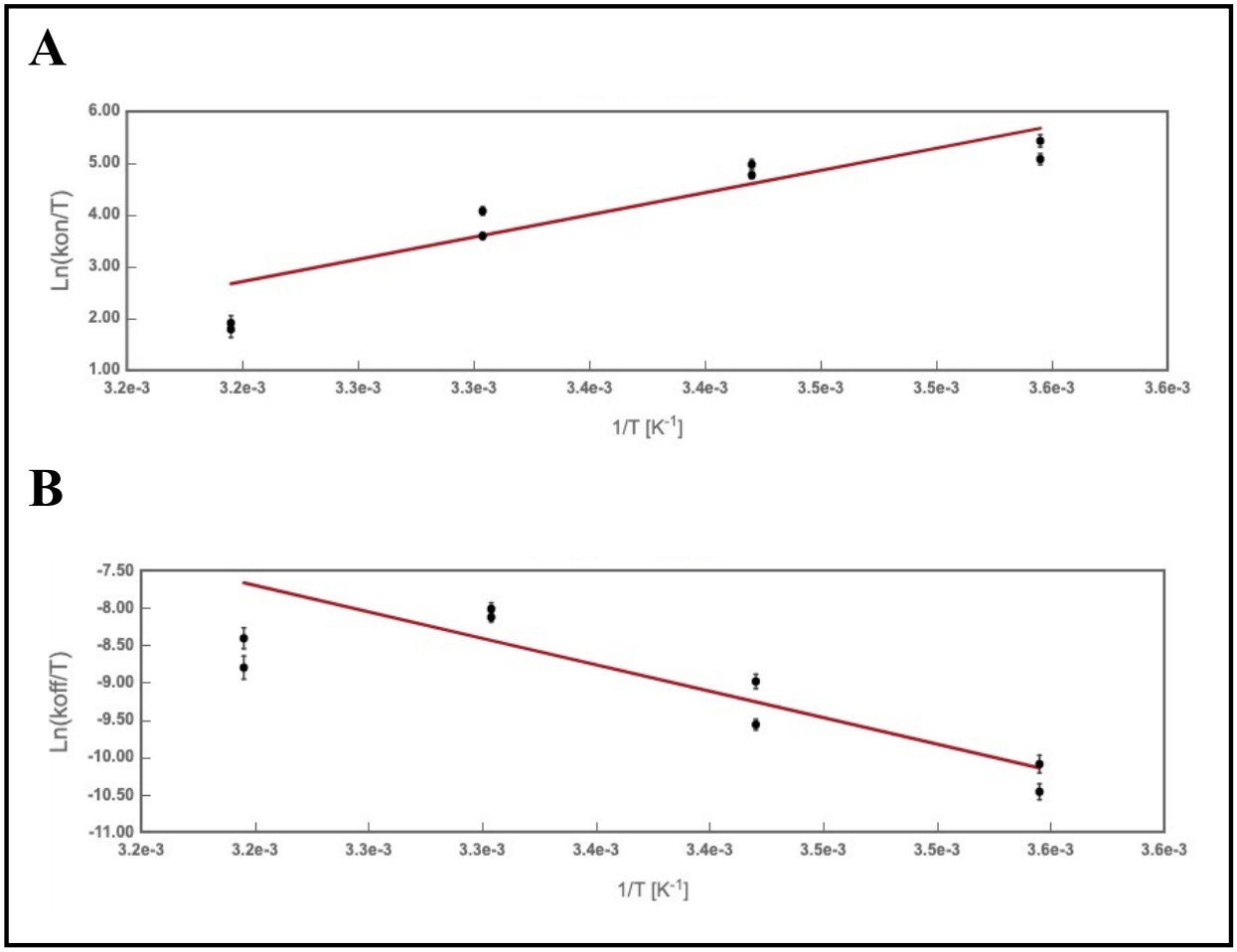


Figure 3.11: Eyring plots from the multitemperature series. The comparison of the **A)** k_{on} and **b)** k_{off} rates for the Original RNA aptamer with tBu (PEG) Hoechst dye at varying temperatures, generated by the kinITC software from the multitemperature ITC experiments.

Table 3.12: Thermodynamic properties of the activation energies determined from the Eyring plots.

$\Delta^{\ddagger}H_{on}$ (kcal mol^{-1})	$\Delta^{\ddagger}S_{on}$ (cal mol^{-1} K^{-1})	$\Delta^{\ddagger}H_{off}$ (kcal mol^{-1})	$\Delta^{\ddagger}S_{off}$ (cal mol^{-1} K^{-1})
-17.1 ± 0.6	-97 ± 2	14.1 ± 0.6	-17 ± 2

3.3 Conclusions

The experiments discussed in **Chapter 3** aimed to further characterize the variant RNA aptamers and tBu Hoechst dyes through more in-depth biophysical methods. The performed experiments allowed for a thorough analysis of the binding interactions present within each of the

aptamer systems through the acquisition of the thermodynamic and kinetic properties. The results were used to complement the fluorescence data discussed in **Chapter 2**.

From the native gel experiments, only the tBu-bound conformation of the Aptamer II RNA sequence was visualized on the unstained gel due to its tight nanomolar binding interactions. The other RNA aptamer variants dissociated from the tBu (PEG) Hoechst dye due to decreased binding interactions under electrophoresis conditions. The visualization of the unbound conformations of the RNA sequences revealed that each of the aptamers, except for the Aptamer II and Elongated Duplex sequences, form monomeric structures in solutions containing the desired experimental conditions. The Aptamer II sequence was found to form a dimeric structure and exhibits variations in folding, while the Elongated Duplex forms two major species, a monomer and a multimeric complex. The ITC-determined binding affinities agree with the fluorescence titration assays, except for the Duplex and Elongated Duplex RNA aptamers. The complete removal of the tetraloop sequence causes the aptamers to undergo conformational rearrangements upon interaction with the tBu Hoechst dye, which likely affected the fluorescence produced by the bound complex.

Overall, the conclusions that were drawn from the ITC experiments regarding the potential helical conformations and molecular interactions of the RNA aptamer variants were consistent with fluorescence methods. In agreement with the fluorescence data, the Original and Short Stem RNA aptamers were found to be the optimal systems for binding to the tBu (PEG) Hoechst dye. Both aptamer sequences are short in length, form monomeric structures in solution and have strong binding affinities for the tBu (PEG) Hoechst dye. They were also found to form the most favourable binding interactions between the hypothesized Helix 2 binding region and the tBu (PEG) Hoechst dye in comparison to all the other RNA aptamer variants studied within this

research project. Although the large size of the Aptamer II sequence promotes tight binding with the tBu (PEG) Hoechst dye, the variations in folding were found to reduce the favourable binding interactions and promote disorder within the bound system. Furthermore, the Duplex RNA aptamer was found to have strong binding interactions with the tBu (PEG) Hoechst dye, but its conformational rearrangements when bound to the tBu Hoechst dye also reduce the favourable binding interactions within the Helix 2 binding region. The conformational rigidity of the UUCG and GAAA Tetraloop RNA aptamers appear to hinder the aptamer's ability to adapt for ligand binding, which not only reduces their binding strengths but also the favourable binding interactions within the aptamer systems. Moreover, the addition of extra base pairs to Helix 1 and 2 of the Elongated Duplex resulted in the most significant changes to the aptamer system. The Elongated Duplex was found to contain two main species in solution with some additional variations in folding. Consequently, the large degree of variation within the aptamer system greatly reduces the favourable binding interactions and results in a higher degree of disorder. However, due to the poor fit of the ITC data further optimizations are required for a proper analysis of the Elongated Duplex's biochemical properties. Finally, in accordance with the fluorescence experiments, the addition of the biotin motif of the biotinylated tBu (PEG) Hoechst dye was once again observed to reduce the binding recognition mechanisms of the Original RNA aptamer. Therefore, the in-depth biochemical analysis of the RNA aptamer variants and tBu Hoechst dye derivatives allowed for a better understanding of the binding mechanisms and the potential helical conformations of the folded aptamer sequences. This information can be used in conjunction with NMR spectroscopy experiments to aid in the three-dimensional structure elucidation of the Aptamer II-mini3-4 RNA-tBu (PEG) Hoechst dye complex.

Chapter 4: Summary and Future Work

4.0 Summary and Future Work

Through the presented research project, an in-depth investigation of each RNA aptamer variant and tBu Hoechst dye derivative was conducted to obtain a complete biochemical profile, as summarized in **Table 4.1**. These biochemical investigations served to not only understand the molecular interactions that are present within the aptamer systems, but they were also conducted to help elucidate the three-dimensional structure of the tBu-bound aptamer by identifying the conditions and systems suitable for an NMR-based structure determination. The performed experiments also helped to reveal some optimizations that can be made to the aptamer system for its potential applications as a building block for the development of an aptamer-based biosensor.

From the fluorescence results, the Original and Short Stem RNA aptamers were deemed the best candidates for an aptamer-based biosensor. Not only are these sequences short in length, at 29 and 21-nt respectively, but the fluorescence experiments revealed that these two aptamers have the highest relative I_{on}/I_{off} ratios and binding affinities for the tBu (PEG) Hoechst dye. Similarly, through the native gel and ITC experiments, the Short Stem and Original RNA aptamers appeared to form optimal complexes with the tBu (PEG) Hoechst dye due to their monomeric structures and favourable binding interactions. The ITC experiments also showcased the potential of the Duplex aptamer for development as an aptamer-based biosensor through its ability to consistently bind to the tBu (PEG) Hoechst dye with strong binding interactions. The Duplex aptamer, however, was found to undergo conformational rearrangements upon interaction with the tBu dye which affects the overall fluorescence produced by the complex. This may not be ideal for biosensor applications as strong fluorescent signals are required to detect binding to the target molecule.

Table 4.1: Summary of the biochemical properties determined at 25 °C for each of the tBu Hoechst-RNA aptamer systems that were studied within this research project.

Aptamer System		Fluorescence		ITC				
RNA Aptamer Variant	**tBu Hoechst Dye Derivative**	**Relative I_{on}/I_{off}**	**K_d (μM)**	**K_d (μM)**	**ΔH_{25} (kcal mol^{-1})**	**$T\Delta S_{25}$ (K kcal mol^{-1})**	**k_{on} ($M^{-1}s^{-1}$)**	**k_{off} (s^{-1})**
Original	tBu (PEG) Hoechst	1.00	1.38	6.9 ± 0.4	-18.8 ± 0.5	-11.7 ± 0.5	(1.4 ± 0.1) × 10^4	(9.3 ± 0.7) × 10^{-2}
Aptamer II		0.285	0.0582	0.34 ± 0.03	-5.49 ± 0.06	3.35 ± 0.08	(1.4 ± 0.2) × 10^5	(4.9 ± 0.8) × 10^{-2}
Aptamer II-mini3-4		0.956	2.10	n/a	n/a	n/a	n/a	n/a
UUCG Tetraloop		0.788	1.42	9 ± 1	-14 ± 1	-7 ± 1	(1.8 ± 0.3) × 10^4	(1.7 ± 0.3) × 10^{-1}
GAAA Tetraloop		0.887	2.05	13 ± 1	-13.7 ± 0.6	-7.0 ± 0.6	(1.2 ± 0.2) × 10^4	(1.5 ± 0.2) × 10^{-1}
Duplex		0.775	8.51	3.8 ± 0.2	-11.5 ± 0.2	-4.1 ± 0.2	(2.4 ± 0.2) × 10^4	(8.7 ± 0.6) × 10^{-2}
Elongated Duplex		0.440	3.40	6 ± 1	-2.1 ± 0.1	5.2 ± 0.2	(1.2 ± 0.2) × 10^4	(3.9 ± 0.6) × 10^{-2}
Short Stem		1.09	0.895	1.35 ± 0.08	-16.2 ± 0.7	-8.2 ± 0.7	(2.9 ± 0.2) × 10^4	(3.4 ± 0.2) × 10^{-2}
Original	Biotinylated tBu (PEG) Hoechst	0.711	6.31	13.3 ± 0.6	-14.6 ± 0.3	-7.9 ± 0.3	(4.7 ± 0.5) × 10^3	(6.3 ± 0.7) × 10^{-2}

For future studies, further optimizations of the native gel experiments will be carried out to observe the derivative tBu Hoechst-bound conformations of all the RNA aptamer variants that were studied within this research project. For instance, the native gels will be run at lower voltages and in a cold room to reduce the heat produced during electrophoresis.[190,209,213] Moreover, optimizations will be made to the ITC experiments for the Elongated Duplex to obtain a reliable fit of the processed data. This would help to improve the accuracy of the biochemical properties determined for the aptamer system, including the dissociation constant as well as thermodynamic and kinetic parameters. Hence, this would enhance the comparisons that can be made between the Elongated Duplex and the other RNA aptamer variants that were studied within this research project. Furthermore, it may be interesting to perform an ITC multitemperature series of the optimized Short Stem RNA aptamer at 5, 15, 25 and 35 °C for comparison with the results obtained for the Original RNA aptamer.[199,202] SPR experiments will also be carried out between the RNA aptamer variants and the biotinylated version of the tBu Hoechst dye.[235] This will serve as an additional method to evaluate the dissociation constant, as well as the kinetic properties of the binding reaction. Comparisons can also be made regarding how the aptamer systems behave in solution versus when surface-bound.[236] Additionally, computational modelling, such as molecular docking and molecular dynamics experiments, will be carried out on each of the aptamer systems that were studied within this research project.[237,238] This will help to visualize and evaluate the conformational flexibility and rigidity of the RNA aptamer variants when interacting with the tBu Hoechst dye derivatives. The molecular simulations will also aid in observing the binding interactions between the tBu Hoechst dyes and the proposed binding regions of the folded aptamer sequence, such as the bulge and Helix 2 regions. The information gained from these modelling studies, in combination with the biochemical investigations reported within this thesis will be used

to support NMR spectroscopy data for the eventual structure elucidation of the Aptamer II-mini3-4-tBu Hoechst dye complex.[239,240] A series of NMR samples will be prepared for the various RNA aptamer variants, including the Original, Short Stem, Duplex, UUCG Tetraloop and GAAA Tetraloop RNA variants. These newly designed RNA sequences can be used to identify which NMR signals correspond to specific regions of the folded aptamer sequence. For instance, the UUCG and GAAA Tetraloops can be useful in identifying which signals correspond to the tetraloop portion of the sequence. In addition, the Short Stem RNA aptamer can unambiguously reveal the signals which arise from Helix 1 of the RNA aptamer. Finally, an investigation was previously conducted by Kyla Egerdeen to characterize the biochemical and structural properties of the tBu Hoechst-binding DNA aptamer that was also selected by the Sando et al. research group in the year 2007.[123,133] Further studies of the DNA aptamer are currently being carried out by present members of the Dieckmann Lab at the University of Waterloo. Therefore, it would be interesting to eventually compare the complete biochemical profiles and solved three-dimensional structures of both the RNA and DNA aptamer sequences when complexed with the tBu Hoechst dye derivative.

References

(1) Ziółkowski, R.; Jarczewska, M.; Górski, Ł.; Malinowska, E. From Small Molecules toward Whole Cells Detection: Application of Electrochemical Aptasensors in Modern Medical Diagnostics. *Sensors* **2021**, *21* (3), 724. DOI: 10.3390/s21030724

(2) Tombelli, S.; Minunni, M.; Mascini, M. Aptamers-Based Assays for Diagnostics, Environmental and Food Analysis. *Biomol. Eng.* **2007**, *24* (2), 191–200. DOI: 10.1016/j.bioeng.2007.03.003

(3) Hu, X.; Mu, L.; Zhou, Q.; Wen, J.; Pawliszyn, J. ssDNA Aptamer-Based Column for Simultaneous Removal of Nanogram Per Liter Level of Illicit and Analgesic Pharmaceuticals in Drinking Water. *Environ. Sci. Technol.* **2011**, *45* (11), 4890–4895. DOI: 10.1021/es104241z

(4) Zhang, W.; Liu, Q.; Guo, Z.; Lin, J. Practical Application of Aptamer-Based Biosensors in Detection of Low Molecular Weight Pollutants in Water Sources. *Molecules* **2018**, *23* (2), 344. DOI: 10.3390/molecules23020344

(5) Chen, K.; Zhou, J.; Shao, Z.; Liu, J.; Song, J.; Wang, R.; Li, J.; Tan, W. Aptamers as Versatile Molecular Tools for Antibody Production Monitoring and Quality Control. *J. Am. Chem. Soc.* **2020**, *142* (28), 12079–12086. DOI: 10.1021/jacs.9b13370

(6) Zhou, J.; Rossi, J. Aptamers as Targeted Therapeutics: Current Potential and Challenges. *Nat. Rev. Drug Discov.* **2017**, *16* (3), 181–202. DOI: 10.1038/nrd.2016.199

(7) Tombelli, S.; Minunni, M.; Mascini, M. Analytical Applications of Aptamers. *Biosens. Bioelectron.* **2005**, *20* (12), 2424–2434. DOI: 10.1016/j.bios.2004.11.006

(8) Williams, R.; Maher, E.; Sooter, L. In Vitro Selection of a Single-Stranded DNA Molecular Recognition Element for the Pesticide Malathion. *Comb. Chem. High Throughput Screen.* **2014**, *17* (8), 694–702. DOI: 10.2174/1386207317666140827123631

(9) Bilibana, M. P.; Citartan, M.; Yeoh, T. S.; Rozhdestvensky, T. S.; Tang, T.-H. Aptamers as the

Agent in Decontamination Assays (Apta-Decontamination Assays): From the Environment to the Potential Application In Vivo. *J. Nucleic Acids* **2017**, *2017*, 3712070. DOI: 10.1155/2017/3712070

(10) Nimjee, S. M.; White, R. R.; Becker, R. C.; Sullenger, B. A. Aptamers as Therapeutics. *Annu. Rev. Pharmacol. Toxicol.* **2017**, *57*, 61–79. DOI: 10.1146/annurev-pharmtox-010716-104558

(11) Breaker, R. R.; Joyce, G. F. The Expanding View of RNA and DNA Function. *Chem. Biol.* **2014**, *21* (9), 1059–1065. DOI: 10.1016/j.chembiol.2014.07.008

(12) Flinders, J.; DeFina, S. C.; Brackett, D. M.; Baugh, C.; Wilson, C.; Dieckmann, T. Recognition of Planar and Nonplanar Ligands in the Malachite Green-RNA Aptamer Complex. *ChemBioChem* **2004**, *5* (1), 62–72. DOI: 10.1002/cbic.200300701

(13) Kortmann, J.; Narberhaus, F. Bacterial RNA Thermometers: Molecular Zippers and Switches. *Nat. Rev. Microbiol.* **2012**, *10* (4), 255–265. DOI: 10.1038/nrmicro2730

(14) Kim, D. H.; Rossi, J. J. RNAi Mechanisms and Applications. *Biotechniques* **2008**, *44* (5), 613–616. DOI: 10.2144/000112792

(15) Kruger, K.; Grabowski, P. J.; Zaug, A. J.; Sands, J.; Gottschling, D. E.; Cech, T. R. Self-Splicing RNA: Autoexcision and Autocyclization of the Ribosomal RNA Intervening Sequence of Tetrahymena. *Cell* **1982**, *31* (1), 147–157. DOI: 10.1016/0092-8674(82)90414-7

(16) Chastain, M.; Tinoco, I. Structural Elements in RNA. *Prog. Nucleic Acid Res. Mol. Biol.* **1991**, *41*, 131–177. DOI: 10.1016/S0079-6603(08)60008-2

(17) Wang, D.; Farhana, A. *Biochemistry, RNA Structure*; StatPearls Publishing: Treasure Island (FL), 2023.

(18) Conn, G. L.; Draper, D. E. RNA Structure. *Curr. Opin. Struct. Biol.* **1998**, *8* (3), 278–285. DOI: 10.1016/S0959-440X(98)80059-6

(19) Lim, C. S.; Brown, C. M. Know Your Enemy: Successful Bioinformatic Approaches to Predict Functional RNA Structures in Viral RNAs. *Front. Microbiol.* **2018**, *8*, 2582. DOI:

10.3389/fmicb.2017.02582

(20) Chen, Y. G.; Hur, S. Cellular Origins of dsRNA, Their Recognition and Consequences. *Nat. Rev. Mol. Cell Biol.* **2022**, *23* (4), 286–301. DOI: 10.1038/s41580-021-00430-1

(21) Matsumoto, M.; Funami, K.; Oshiumi, H.; Seya, T. Toll-IL-1-Receptor-Containing Adaptor Molecule-1: A Signaling Adaptor Linking Innate Immunity to Adaptive Immunity. *Prog. Mol. Biol. Transl. Sci.* **2013**, *117*, 487–510. DOI: 10.1016/B978-0-12-386931-9.00018-0

(22) Dock-Bregeon, A. C.; Chevrier, B.; Podjarny, A.; Johnson, J.; de Bear, J. S.; Gough, G. R.; Gilham, P. T.; Moras, D. Crystallographic Structure of an RNA Helix: [U(UA)6A]2. *J. Mol. Biol.* **1989**, *209* (3), 459–474. DOI: 10.1016/0022-2836(89)90010-7

(23) Lipfert, J.; Skinner, G. M.; Keegstra, J. M.; Hensgens, T.; Jager, T.; Dulin, D.; Köber, M.; Yu, Z.; Donkers, S. P.; Chou, F.-C.; Das, R.; Dekker, N. H. Double-Stranded RNA under Force and Torque: Similarities to and Striking Differences from Double-Stranded DNA. *Proc. Natl. Acad. Sci.* **2014**, *111* (43), 15408–15413. DOI: 10.1073/pnas.1407197111

(24) Saenger, W. *Principles of Nucleic Acid Structure*; Cantor, C. R., Ed.; Springer: New York, 1984; p 220-252. DOI: 10.1007/978-1-4612-5190-3

(25) Tinoco, I.; Davis, P. W.; Hardin, C. C.; Puglisi, J. D.; Walker, G. T.; Wyatt, J. RNA Structure from A to Z. *Cold Spring Harb. Symp. Quant. Biol.* **1987**, *52*, 135–146. DOI: 10.1101/SQB.1987.052.01.018

(26) Tian, B.; Bevilacqua, P. C.; Diegelman-Parente, A.; Mathews, M. B. The Double-Stranded-RNA-Binding Motif: Interference and Much More. *Nat. Rev. Mol. Cell Biol.* **2004**, *5* (12), 1013–1023. DOI: 10.1038/nrm1528

(27) Corley, M.; Burns, M. C.; Yeo, G. W. How RNA-Binding Proteins Interact with RNA: Molecules and Mechanisms. *Mol. Cell* **2020**, *78* (1), 9–29. DOI: 10.1016/j.molcel.2020.03.011

(28) Ryter, J. M.; Schultz, S. C. Molecular Basis of Double-Stranded RNA-Protein Interactions: Structure of a dsRNA-Binding Domain Complexed with dsRNA. *EMBO J.* **1998**, *17* (24),

7505–7513. DOI: 10.1093/emboj/17.24.7505

(29) Bevilacqua, P. C.; Cech, T. R. Minor-Groove Recognition of Double-Stranded RNA by the Double-Stranded RNA-Binding Domain from the RNA-Activated Protein Kinase PKR. *Biochemistry* **1996**, *35* (31), 9983–9994. DOI: 10.1021/bi9607259

(30) Arias-Gonzalez, J. R. Single-Molecule Portrait of DNA and RNA Double Helices. *Integr. Biol.* **2014**, *6* (10), 904–925. DOI: 10.1039/C4IB00163J

(31) Goddard, T. D.; Huang, C. C.; Meng, E. C.; Pettersen, E. F.; Couch, G. S.; Morris, J. H.; Ferrin, T. E. UCSF ChimeraX: Meeting Modern Challenges in Visualization and Analysis. *Protein Sci.* **2018**, *27* (1), 14–25. DOI: 10.1002/pro.3235

(32) Pettersen, E. F.; Goddard, T. D.; Huang, C. C.; Meng, E. C.; Couch, G. S.; Croll, T. I.; Morris, J. H.; Ferrin, T. E. UCSF ChimeraX: Structure Visualization for Researchers, Educators, and Developers. *Protein Sci.* **2021**, *30* (1), 70–82. DOI: 10.1002/pro.3943

(33) Bock, L. C.; Griffin, L. C.; Latham, J. A.; Vermaas, E. H.; Toole, J. J. Selection of Single-Stranded DNA Molecules That Bind and Inhibit Human Thrombin. *Nature* **1992**, *355* (6360), 564–566. DOI: 10.1038/355564a0

(34) Kalra, P.; Dhiman, A.; Cho, W. C.; Bruno, J. G.; Sharma, T. K. Simple Methods and Rational Design for Enhancing Aptamer Sensitivity and Specificity. *Front. Mol. Biosci.* **2018**, *5*, 41. DOI: 10.3389/fmolb.2018.00041

(35) Ellington, A. D.; Szostak, J. W. In Vitro Selection of RNA Molecules That Bind Specific Ligands. *Nature* **1990**, *346* (6287), 818–822. DOI: 10.1038/346818a0

(36) Da Costa, J. B.; Andreiev, A. I.; Dieckmann, T. Thermodynamics and Kinetics of Adaptive Binding in the Malachite Green RNA Aptamer. *Biochemistry* **2013**, *52* (38), 6575–6583. DOI: 10.1021/bi400549s

(37) Hermann, T.; Patel, D. J. Adaptive Recognition by Nucleic Acid Aptamers. *Science* **2000**, *287* (5454), 820–825. DOI: 10.1126/science.287.5454.820

(38) Boussebayle, A.; Groher, F.; Suess, B. RNA-Based Capture-SELEX for the Selection of Small Molecule-Binding Aptamers. *Methods* **2019**, *161*, 10–15. DOI: 10.1016/j.ymeth.2019.04.004

(39) Elskens, J. P.; Elskens, J. M.; Madder, A. Chemical Modification of Aptamers for Increased Binding Affinity in Diagnostic Applications: Current Status and Future Prospects. *Int. J. Mol. Sci.* **2020**, *21* (12), 4522. DOI: 10.3390/ijms21124522

(40) Nimjee, S. M.; Rusconi, C. P.; Sullenger, B. A. Aptamers: An Emerging Class of Therapeutics. *Annu. Rev. Med.* **2005**, *56*, 555–583. DOI: 10.1146/annurev.med.56.062904.144915

(41) Cullen, B. R.; Greene, W. C. Regulatory Pathways Governing HIV-1 Replication. *Cell* **1989**, *58* (3), 423–426. DOI: 10.1016/0092-8674(89)90420-0

(42) Gold, L. SELEX: How It Happened and Where It Will Go. *J. Mol. Evol.* **2015**, *81* (5–6), 140–143. DOI:10.1007/s00239-015-9705-9

(43) Zhu, Z.; Yang, C.; Zhou, X.; Qin, J. Label-Free Aptamer-Based Sensors for l-Argininamide by Using Nucleic Acid Minor Groove Binding Dyes. *Chem. Commun.* **2011**, *47* (11), 3192. DOI: 10.1039/c0cc04844e

(44) Song, K.-M.; Lee, S.; Ban, C. Aptamers and Their Biological Applications. *Sensors* **2012**, *12* (1), 612–631. DOI: 10.3390/s120100612

(45) Yoon, S.; Rossi, J. J. Aptamers: Uptake Mechanisms and Intracellular Applications. *Adv. Drug Deliv. Rev.* **2018**, *134*, 22–35. DOI: 10.1016/j.addr.2018.07.003

(46) Sando, S.; Narita, A.; Hayami, M.; Aoyama, Y. Transcription Monitoring Using Fused RNA with a Dye-Binding Light-up Aptamer as a Tag: A Blue Fluorescent RNA. *Chem. Commun.* **2008**, (33), 3858-3860. DOI: 10.1039/b808449a

(47) Lakhin, A. V.; Tarantul, V. Z.; Gening, L. V. Aptamers: Problems, Solutions and Prospects. *Acta Naturae* **2013**, *5* (4), 34–43. DOI: 10.32607/20758251-2013-5-4-34-43

(48) Ponce, A. T.; Hong, K. L. A Mini-Review: Clinical Development and Potential of Aptamers for Thrombotic Events Treatment and Monitoring. *Biomedicines* **2019**, *7* (3), 55. DOI:

10.3390/biomedicines7030055

(49) Reif, R.; Haque, F.; Guo, P. Fluorogenic RNA Nanoparticles for Monitoring RNA Folding and Degradation in Real Time in Living Cells. *Nucleic Acid Ther.* **2012**, *22* (6), 428–437. DOI: 10.1089/nat.2012.0380

(50) Palmer, T.; Bonner, P. L. The Chemical Nature of Enzyme Catalysis. *Enzymes* **2011**, 189–221. DOI: 10.1533/9780857099921.2.189

(51) Heikrujam, J.; Kishor, R.; Behari Mazumder, P. The Chemistry Behind Plant DNA Isolation Protocols. *Biochem. Anal. Tools – Methods Bio-Mol. Stud.* **2020**, 1–12. DOI: 10.5772/intechopen.92206

(52) Raines, R. T. Ribonuclease A. *Chem. Rev.* **1998**, *98* (3), 1045–1066. DOI: 10.1021/cr960427h

(53) Findly, D.; Herries, D. G.; Mathias, A. P.; Rabin, B. R.; Ross, C. A. The Active Site and Mechanism of Action of Bovine Pancreatic Ribonuclease. *Nature* **1961**, *190*, 781–784. DOI: 10.1038/190781a0

(54) Hoffmann, S.; Hoos, J.; Klussmann, S.; Vonhoff, S. RNA Aptamers and Spiegelmers: Synthesis, Purification, and Post-Synthetic PEG Conjugation. *Curr. Protoc. Nucleic Acid Chem.* **2011**. DOI: 10.1002/0471142700.nc0446s46

(55) Vater, A.; Klussmann, S. Turning Mirror-Image Oligonucleotides into Drugs: The Evolution of Spiegelmer® Therapeutics. *Drug Discov. Today* **2015**, *20* (1), 147–155. DOI: 10.1016/j.drudis.2014.09.004

(56) Maasch, C.; Buchner, K.; Eulberg, D.; Vonhoff, S.; Klussmann, S. Physicochemical Stability of NOX-E36, a 40mer L-RNA (Spiegelmer) for Therapeutic Applications. *Nucleic Acids Symp. Ser.* **2008**, (52), 61–62. DOI: 10.1093/nass/nrn031

(57) Vater, A.; Sahlmann, J.; Kröger, N.; Zöllner, S.; Lioznov, M.; Maasch, C.; Buchner, K.; Vossmeyer, D.; Schwoebel, F.; Purschke, W. G.; Vonhoff, S.; Kruschinski, A.; Hübel, K.; Humphrey, M.; Klussmann, S.; Fliegert, F. Hematopoietic Stem and Progenitor Cell

Mobilization in Mice and Humans by a First-in-Class Mirror-Image Oligonucleotide Inhibitor of CXCL12. *Clin. Pharmacol. Ther.* **2013**, *94* (1), 150–157. DOI: 10.1038/clpt.2013.58

(58) Breaker, R. R. Riboswitches and the RNA World. *Cold Spring Harb. Perspect. Biol.* **2012**, *4* (2), a003566. DOI: 10.1101/cshperspect.a003566

(59) Kong, H. Y.; Byun, J. Nucleic Acid Aptamers: New Methods for Selection, Stabilization, and Application in Biomedical Science. *Biomol. Ther.* **2013**, *21* (6), 423–434. DOI: 10.4062/biomolther.2013.085

(60) Tuerk, C.; Gold, L. Systematic Evolution of Ligands by Exponential Enrichment: RNA Ligands to Bacteriophage T4 DNA Polymerase. *Science* **1990**, *249* (4968), 505–510. DOI: 10.1126/science.2200121

(61) Klug, S. J.; Famulok, M. All You Wanted to Know about SELEX. *Mol. Biol. Rep.* **1994**, *20* (2), 97–107. DOI: 10.1007/BF00996358

(62) Zhuo, Z.; Yu, Y.; Wang, M.; Li, J.; Zhang, Z.; Liu, J.; Wu, X.; Lu, A.; Zhang, G.; Zhang, B. Recent Advances in SELEX Technology and Aptamer Applications in Biomedicine. *Int. J. Mol. Sci.* **2017**, *18* (10), 2142. DOI: 10.3390/ijms18102142

(63) Hasegawa, H.; Savory, N.; Abe, K.; Ikebukuro, K. Methods for Improving Aptamer Binding Affinity. *Molecules* **2016**, *21* (4), 421. DOI: 10.3390/molecules21040421

(64) Cho, M.; Xiao, Y.; Nie, J.; Steward, R.; Csordas, A. T.; Oh, S. S.; Thomson, J. A.; Soh, H. T. Quantitative Selection of DNA Aptamers through Microfluidic Selection and High-Throughput Sequencing. *Proc. Natl. Acad. Sci.* **2010**, *107* (35), 15373–15378. DOI: 10.1073/pnas.1015181108

(65) Mi, J.; Liu, Y.; Rabbani, Z. N.; Yang, Z.; Urban, J. H.; Sullenger, B. A.; Clary, B. M. In Vivo Selection of Tumor-Targeting RNA Motifs. *Nat. Chem. Biol.* **2010**, *6* (1), 22–24. DOI: 10.1038/nchembio.277

(66) Naresh, V.; Lee, N. A Review on Biosensors and Recent Development of Nanostructured

Materials-Enabled Biosensors. *Sensors* **2021**, *21* (4), 1109. DOI: 10.3390/s21041109

(67) Mehrotra, P. Biosensors and Their Applications – A Review. *J. Oral Biol. Craniofacial Res.* **2016**, *6* (2), 153–159. DOI: 10.1016/j.jobcr.2015.12.002

(68) Guilbault, G. G. Biosensors. *Curr. Opin. Biotechnol.* **1991**, *2* (1), 3–8. DOI: 10.1016/0958-1669(91)90054-9

(69) German, N.; Ramanaviciene, A.; Voronovic, J.; Ramanavicius, A. Glucose Biosensor Based on Graphite Electrodes Modified with Glucose Oxidase and Colloidal Gold Nanoparticles. *Microchim. Acta* **2010**, *168* (3–4), 221–229. DOI: 10.1007/s00604-009-0270-z

(70) Arora, P.; Sindhu, A.; Dilbaghi, N.; Chaudhury, A. Biosensors as Innovative Tools for the Detection of Food Borne Pathogens. *Biosens. Bioelectron.* **2011**, *28* (1), 1–12. DOI: 10.1016/j.bios.2011.06.002

(71) Ercole, C.; Del Gallo, M.; Mosiello, L.; Baccella, S.; Lepidi, A. Escherichia Coli Detection in Vegetable Food by a Potentiometric Biosensor. *Sensors Actuators B Chem.* **2003**, *91* (1–3), 163–168. DOI: 10.1016/S0925-4005(03)00083-2

(72) Jhaveri, S. D.; Kirby, R.; Conrad, R.; Maglott, E. J.; Bowser, M.; Kennedy, R. T.; Glick, G.; Ellington, A. D. Designed Signaling Aptamers That Transduce Molecular Recognition to Changes in Fluorescence Intensity. *J. Am. Chem. Soc.* **2000**, *122* (11), 2469–2473. DOI: 10.1021/ja992393b

(73) Musumeci, D.; Platella, C.; Riccardi, C.; Moccia, F.; Montesarchio, D. Fluorescence Sensing Using DNA Aptamers in Cancer Research and Clinical Diagnostics. *Cancers.* **2017**, *9* (12), 174. DOI: 10.3390/cancers9120174

(74) Kato, T.; Shimada, I.; Kimura, R.; Hyuga, M. Light-up Fluorophore–DNA Aptamer Pair for Label-Free Turn-on Aptamer Sensors. *Chem. Commun.* **2016**, *52* (21), 4041–4044. DOI: 10.1039/C5CC08816J

(75) Sassanfar, M.; Szostak, J. W. An RNA Motif That Binds ATP. *Nature* **1993**, *364* (6437), 550–

553. DOI: 10.1038/364550a0

(76) Huizenga, D. E.; Szostak, J. W. A DNA Aptamer That Binds Adenosine and ATP. *Biochemistry* **1995**, *34* (2), 656–665. DOI: 10.1021/bi00002a033

(77) Xu, W.; Lu, Y. Label-Free Fluorescent Aptamer Sensor Based on Regulation of Malachite Green Fluorescence. *Anal. Chem.* **2010**, *82* (2), 574–578. DOI: 10.1021/ac9018473

(78) Grate, D.; Wilson, C. Laser-Mediated, Site-Specific Inactivation of RNA Transcripts. *Proc. Natl. Acad. Sci.* **1999**, *96* (11), 6131–6136. DOI: 10.1073/pnas.96.11.6131

(79) Huang, C.-C.; Chang, H.-T. Aptamer-Based Fluorescence Sensor for Rapid Detection of Potassium Ions in Urine. *Chem. Commun.* **2008**, (12), 1461-1463. DOI: 10.1039/b718752a

(80) Chang, A. L.; McKeague, M.; Liang, J. C.; Smolke, C. D. Kinetic and Equilibrium Binding Characterization of Aptamers to Small Molecules Using a Label-Free, Sensitive, and Scalable Platform. *Anal. Chem.* **2014**, *86* (7), 3273–3278. DOI: 10.1021/ac5001527

(81) Carothers, J. M.; Oestreich, S. C.; Szostak, J. W. Aptamers Selected for Higher-Affinity Binding Are Not More Specific for the Target Ligand. *J. Am. Chem. Soc.* **2006**, *128* (24), 7929–7937. DOI: 10.1021/ja060952q

(82) Cupello, A.; Hydén, H. Binding Experiment k d Values and Physiologically Active Gaba Concentrations: An Only Apparent Contradiction? *Int. J. Neurosci.* **1986**, *30* (4), 297–301. DOI: 10.3109/00207458608985681

(83) Lyford, L. K.; Lee, J. W.; Rosenberg, R. L. Low-Affinity Ca(2+) and Ba(2+) Binding Sites in the Pore of A7 Nicotinic Acetylcholine Receptors. *Biochim. Biophys. Acta* **2002**, *1559* (1), 69–78. DOI: 10.1016/S0005-2736(01)00437-0

(84) Du, X.; Li, Y.; Xia, Y.-L.; Ai, S.-M.; Liang, J.; Sang, P.; Ji, X.-L.; Liu, S.-Q. Insights into Protein–Ligand Interactions: Mechanisms, Models, and Methods. *Int. J. Mol. Sci.* **2016**, *17* (2), 144. DOI: 10.3390/ijms17020144

(85) Dumas, P.; Ennifar, E.; Da Veiga, C.; Bec, G.; Palau, W.; Di Primo, C.; Piñeiro, A.; Sabin, J.;

Muñoz, E.; Rial, J. Extending ITC to Kinetics with KinITC. *Methods Enzymol.* **2016**, *567*, 157–180. DOI: 10.1016/bs.mie.2015.08.026

(86) Lin, P.-H.; Yen, S.-L.; Lin, M.-S.; Chang, Y.; Louis, S. R.; Higuchi, A.; Chen, W.-Y. Microcalorimetrics Studies of the Thermodynamics and Binding Mechanism between L-Tyrosinamide and Aptamer. *J. Phys. Chem. B* **2008**, *112* (21), 6665–6673. DOI: 10.1021/jp8000866

(87) Jarmoskaite, I.; AlSadhan, I.; Vaidyanathan, P. P.; Herschlag, D. How to Measure and Evaluate Binding Affinities. *Elife* **2020**, *9*, e57264. DOI: 10.7554/eLife.57264

(88) Reynolds, C. H.; Holloway, M. K. Thermodynamics of Ligand Binding and Efficiency. *ACS Med. Chem. Lett.* **2011**, *2* (6), 433–437. DOI: 10.1021/ml200010k

(89) Dunitz, J. D. Win Some, Lose Some: Enthalpy-Entropy Compensation in Weak Intermolecular Interactions. *Chem. Biol.* **1995**, *2* (11), 709–712. DOI: 10.1016/1074-5521(95)90097-7

(90) Holdgate, G. A.; Ward, W. H. J. Measurements of Binding Thermodynamics in Drug Discovery. *Drug Discov. Today* **2005**, *10* (22), 1543–1550. DOI: 10.1016/S1359-6446(05)03610-X

(91) Searle, M. S.; Williams, D. H. On the Stability of Nucleic Acid Structures in Solution: Enthalpy - Entropy Compensations, Internal Rotations and Reversibility. *Nucleic Acids Res.* **1993**, *21* (9), 2051–2056. DOI: 10.1093/nar/21.9.2051

(92) Damian, L. Isothermal Titration Calorimetry for Studying Protein–Ligand Interactions. *Methods* **2013**, *1008*, 103–118. DOI: 10.1007/978-1-62703-398-5_4

(93) Neubacher, S.; Hennig, S. RNA Structure and Cellular Applications of Fluorescent Light-Up Aptamers. *Angew. Chemie Int. Ed.* **2019**, *58* (5), 1266–1279. DOI: 10.1002/anie.201806482

(94) Dolgosheina, E. V.; Unrau, P. J. Fluorophore-binding RNA Aptamers and Their Applications. *Wiley Interdiscip Rev. RNA* **2016**, *7* (6), 843–851. DOI: 10.1002/wrna.1383

(95) Paige, J. S.; Wu, K. Y.; Jaffrey, S. R. RNA Mimics of Green Fluorescent Protein. *Science* **2011**, *333* (6042), 642–646. DOI: 10.1126/science.1207339

(96) Filonov, G. S.; Moon, J. D.; Svensen, N.; Jaffrey, S. R. Broccoli: Rapid Selection of an RNA Mimic of Green Fluorescent Protein by Fluorescence-Based Selection and Directed Evolution. *J. Am. Chem. Soc.* **2014**, *136* (46), 16299–16308. DOI: 10.1021/ja508478x

(97) Dolgosheina, E. V.; Jeng, S. C. Y.; Panchapakesan, S. S. S.; Cojocaru, R.; Chen, P. S. K.; Wilson, P. D.; Hawkins, N.; Wiggins, P. A.; Unrau, P. J. RNA Mango Aptamer-Fluorophore: A Bright, High-Affinity Complex for RNA Labeling and Tracking. *ACS Chem. Biol.* **2014**, *9* (10), 2412–2420. DOI: 10.1021/cb500499x

(98) Song, W.; Filonov, G. S.; Kim, H.; Hirsch, M.; Li, X.; Moon, J. D.; Jaffrey, S. R. Imaging RNA Polymerase III Transcription Using a Photostable RNA–Fluorophore Complex. *Nat. Chem. Biol.* **2017**, *13* (11), 1187–1194. DOI: 10.1038/nchembio.2477

(99) Steinmetzger, C.; Palanisamy, N.; Gore, K. R.; Höbartner, C. A Multicolor Large Stokes Shift Fluorogen-Activating RNA Aptamer with Cationic Chromophores. *Chemistry* **2019**, *25* (8), 1931–1935. DOI: 10.1002/chem.201805882

(100) Chen, X.; Zhang, D.; Su, N.; Bao, B.; Xie, X.; Zuo, F.; Yang, L.; Wang, H.; Jiang, L.; Lin, Q.; Fang, M.; Li, N.; Hua, X.; Chen, Z.; Bao, C.; Xu, J.; Du, W.; Zhang, L.; Zhao, Y.; Zhu, L.; Loscalzo, J.; Yang, Y. Visualizing RNA Dynamics in Live Cells with Bright and Stable Fluorescent RNAs. *Nat. Biotechnol.* **2019**, *37* (11), 1287–1293. DOI: 10.1038/s41587-019-0249-1

(101) Al Mazid, M. F.; Shkel, O.; Kharkivska, Y.; Lee, J.-S. Application of Fluorescent Turn-on Aptamers in RNA Studies. *Mol. Omi.* **2021**, *17* (4), 483–491. DOI: 10.1039/D1MO00085C

(102) Pothoulakis, G.; Ceroni, F.; Reeve, B.; Ellis, T. The Spinach RNA Aptamer as a Characterization Tool for Synthetic Biology. *ACS Synth. Biol.* **2014**, *3* (3), 182–187. DOI: 10.1021/sb400089c

(103) Guet, D.; Burns, L. T.; Maji, S.; Boulanger, J.; Hersen, P.; Wente, S. R.; Salamero, J.; Dargemont, C. Combining Spinach-Tagged RNA and Gene Localization to Image Gene

Expression in Live Yeast. *Nat. Commun.* **2015**, *6*, 8882. DOI: 10.1038/ncomms9882

(104) Stojanovic, M. N.; Kolpashchikov, D. M. Modular Aptameric Sensors. *J. Am. Chem. Soc.* **2004**, *126* (30), 9266–9270. DOI: 10.1021/ja032013t

(105) Paige, J. S.; Nguyen-Duc, T.; Song, W.; Jaffrey, S. R. Fluorescence Imaging of Cellular Metabolites with RNA. *Science* **2012**, *335* (6073), 1194. DOI: 10.1126/science.1218298

(106) Baugh, C.; Grate, D.; Wilson, C. 2.8 Å Crystal Structure of the Malachite Green Aptamer. *J. Mol. Biol.* **2000**, *301* (1), 117–128. DOI: 10.1006/jmbi.2000.3951

(107) Babendure, J. R.; Adams, S. R.; Tsien, R. Y. Aptamers Switch on Fluorescence of Triphenylmethane Dyes. *J. Am. Chem. Soc.* **2003**, *125* (48), 14716–14717. DOI: 10.1021/ja037994o

(108) Srivastava, S.; Sinha, R.; Roy, D. Toxicological Effects of Malachite Green. *Aquat. Toxicol.* **2004**, *66* (3), 319–329. DOI: 10.1016/j.aquatox.2003.09.008

(109) Chudakov, D. M.; Matz, M. V.; Lukyanov, S.; Lukyanov, K. A. Fluorescent Proteins and Their Applications in Imaging Living Cells and Tissues. *Physiol. Rev.* **2010**, *90* (3), 1103–1163. DOI: 10.1152/physrev.00038.2009

(110) Warner, K. D.; Chen, M. C.; Song, W.; Strack, R. L.; Thorn, A.; Jaffrey, S. R.; Ferré-D'Amaré, A. R. Structural Basis for Activity of Highly Efficient RNA Mimics of Green Fluorescent Protein. *Nat. Struct. Mol. Biol.* **2014**, *21* (8), 658–663. DOI: 10.1038/nsmb.2865

(111) Strack, R. L.; Disney, M. D.; Jaffrey, S. R. A Superfolding Spinach2 Reveals the Dynamic Nature of Trinucleotide Repeat–Containing RNA. *Nat. Methods* **2013**, *10* (12), 1219–1224. DOI: 10.1038/nmeth.2701

(112) Autour, A.; Westhof, E.; Ryckelynck, M. iSpinach: A Fluorogenic RNA Aptamer Optimized for in Vitro Applications. *Nucleic Acids Res.* **2016**, *44* (6), 2491–2500. DOI: 10.1093/nar/gkw083

(113) Nygren, J.; Svanvik, N.; Kubista, M. The Interactions between the Fluorescent Dye Thiazole

Orange and DNA. *Biopolymers* **1998**, *46* (1), 39–51. DOI: 10.1002/(SICI)1097-0282(199807)46:1<39::AID-BIP4>3.0.CO;2-Z

(114) Autour, A.; C. Y. Jeng, S.; D. Cawte, A.; Abdolahzadeh, A.; Galli, A.; Panchapakesan, S. S. S.; Rueda, D.; Ryckelynck, M.; Unrau, P. J. Fluorogenic RNA Mango Aptamers for Imaging Small Non-Coding RNAs in Mammalian Cells. *Nat. Commun.* **2018**, *9* (1), 656. DOI: 10.1038/s41467-018-02993-8

(115) Lalande, M. E.; Ling, V.; Miller, R. G. Hoechst 33342 Dye Uptake as a Probe of Membrane Permeability Changes in Mammalian Cells. *Proc. Natl. Acad. Sci.* **1981**, *78* (1), 363–367. DOI: 10.1073/pnas.78.1.363

(116) Latt, S. A.; Stetten, G. Spectral Studies on 33258 Hoechst and Related Bisbenzimidazole Dyes Useful for Fluorescent Detection of Deoxyribonucleic Acid Synthesis. *J. Histochem. Cytochem.* **1976**, *24* (1), 24–33. DOI: 10.1177/24.1.943439

(117) Bucevičius, J.; Lukinavičius, G.; Gerasimaitė, R. The Use of Hoechst Dyes for DNA Staining and Beyond. *Chemosensors* **2018**, *6* (2), 18. DOI: 10.3390/chemosensors6020018

(118) Teng, M.; Usman, N.; Frederick, C. A.; Wang, A. H.-J. The Molecular Structure of the Complex of Hoechst 33258 and the DNA Dodecamer d(CGCGAATTCGCG). *Nucleic Acids Res.* **1988**, *16* (6), 2671–2690. DOI: 10.1093/nar/16.6.2671

(119) Ligasová, A.; Koberna, K. DNA Dyes—Highly Sensitive Reporters of Cell Quantification: Comparison with Other Cell Quantification Methods. *Molecules* **2021**, *26* (18), 5515. DOI: 10.3390/molecules26185515

(120) Durand, R. E.; Olive, P. L. Cytotoxicity, Mutagenicity and DNA Damage by Hoechst 33342. *J. Histochem. Cytochem.* **1982**, *30* (2), 111–116. DOI: 10.1177/30.2.7061816

(121) Sriram, M.; van der Marel, G. A.; Roelen, H. L.; van Boom, J. H.; Wang, A. H. Conformation of B-DNA Containing O6-Ethyl-G-C Base Pairs Stabilized by Minor Groove Binding Drugs: Molecular Structure of d(CGC[E6G]AATTCGCG Complexed with Hoechst 33258 or Hoechst

33342. *EMBO J.* **1992**, *11* (1), 225–232. DOI: 10.1002/j.1460-2075.1992.tb05045.x

(122) Han, F.; Taulier, N.; Chalikian, T. V. Association of the Minor Groove Binding Drug Hoechst 33258 with d(CGCGAATTCGCG) 2 : Volumetric, Calorimetric, and Spectroscopic Characterizations. *Biochemistry* **2005**, *44* (28), 9785–9794. DOI: 10.1021/bi047374f

(123) Sando, S.; Narita, A.; Aoyama, Y. Light-Up Hoechst–DNA Aptamer Pair: Generation of an Aptamer-Selective Fluorophore from a Conventional DNA-Staining Dye. *ChemBioChem* **2007**, *8* (15), 1795–1803. DOI: 10.1002/cbic.200700325

(124) Liu, B.; Li, S.; Hu, J. Technological Advances in High-Throughput Screening. *Am. J. PharmacoGenomics* **2004**, *4* (4), 263–276. DOI: 10.2165/00129785-200404040-00006

(125) Radotić, K.; Kalauzi, A.; Djikanović, D.; Jeremić, M.; Leblanc, R. M.; Cerović, Z. G. Component Analysis of the Fluorescence Spectra of a Lignin Model Compound. *J. Photochem. Photobiol. B Biol.* **2006**, *83* (1), 1–10. DOI: 10.1016/j.jphotobiol.2005.12.001

(126) Jovanović, K. K.; Savić, A. G.; Janković, R.; Radulović, S.; Spasić, S. Z.; Radotić, K. Detection of DNA Mutations Based on Analysis of Multiple Wavelength Excitation/Emission Fluorescence Kinetics Curves in Real-Time PCR. *Med. Hypotheses* **2013**, *80* (4), 376–379. DOI: 10.1016/j.mehy.2013.01.004

(127) Xu, B.; Tan, D.; Yang, X.; Hu, X.; Xie, Y.; Qin, J.; Chen, C.; He, C.; Li, Y.; Pu, J.; Liao, F. Fluorometric Titration Assay of Affinity of Tight-Binding Nonfluorescent Inhibitor of Glutathione S-Transferase. *J. Fluoresc.* **2015**, *25* (1), 1–8. DOI: 10.1007/s10895-014-1475-z

(128) Wang, H.; Peng, P.; Liu, S.; Li, T. Thioflavin T Behaves as an Efficient Fluorescent Ligand for Label-Free ATP Aptasensor. *Anal. Bioanal. Chem.* **2016**, *408* (28), 7927–7934. DOI: 10.1007/s00216-016-9926-9

(129) Hartmann, R. K., Bindereif, A., Schön, A., Westhof, E. *Handbook of RNA Biochemistry*, 2nd ed.; WILEY-VCH: Weinheim, 2014; p 3-20. DOI: 10.1002/9783527647064

(130) Conrad, T.; Plumbom, I.; Alcobendas, M.; Vidal, R.; Sauer, S. Maximizing Transcription of

Nucleic Acids with Efficient T7 Promoters. *Commun. Biol.* **2020**, *3* (1). DOI: 10.1038/s42003-020-01167-x

(131) Koplin, J.; Mu, Y.; Richter, C.; Schwalbe, H.; Stock, G. Structure and Dynamics of an RNA Tetraloop: A Joint Molecular Dynamics and NMR Study. *Structure* **2005**, *13* (9), 1255–1267. DOI: 10.1016/j.str.2005.05.015

(132) D'Ascenzo, L.; Vicens, Q.; Auffinger, P. Identification of Receptors for UNCG and GNRA Z-Turns and Their Occurrence in rRNA. *Nucleic Acids Res.* **2018**, *46* (15), 7989–7997. DOI: 10.1093/nar/gky578

(133) Egerdeen, K. Investigation of the Presence of a G-Quadruplex In the Hoechst Dye Binding DNA Aptamer. MSc. Thesis, University of Waterloo, Waterloo, ON, 2022. https://uwspace.uwaterloo.ca/handle/10012/18162 (accessed 2023-03-10).

(134) Nandi, I.; Bateson, M.; Bari, M.; Joshi, H. N. Synergistic Effect of PEG-400 and Cyclodextrin to Enhance Solubility of Progesterone. *AAPS PharmSciTech* **2003**, *4* (1), E1. DOI: 10.1208/pt040101

(135) Milligan, J. F.; Uhlenbeck, O. C. Synthesis of Small RNAs Using T7 RNA Polymerase. *Methods Enzymol.* **1989**, *180*, 51–62. DOI: 10.1016/0076-6879(89)80091-6

(136) Chen, Z.; Zhang, Y. Dimethyl Sulfoxide Targets Phage RNA Polymerases to Promote Transcription. *Biochem. Biophys. Res. Commun.* **2005**, *333* (3), 664–670. DOI: 10.1016/j.bbrc.2005.05.166

(137) Juang, J.-K.; Liu, H.-J. The Effect of DMSO on Natural DNA Conformation in Enhancing Transcription. *Biochem. Biophys. Res. Commun.* **1987**, *146* (3), 1458–1464. DOI: 10.1016/0006-291X(87)90813-8

(138) Kartje, Z. J.; Janis, H. I.; Mukhopadhyay, S.; Gagnon, K. T. Revisiting T7 RNA Polymerase Transcription in Vitro with the Broccoli RNA Aptamer as a Simplified Real-Time Fluorescent Reporter. *J. Biol. Chem.* **2021**, *296*, 100175. DOI: 10.1074/jbc.RA120.014553

(139) Milligan, J. F.; Groebe, D. R.; Witherell, G. W.; Uhlenbeck, O. C. Oligoribonucleotide Synthesis Using T7 RNA Polymerase and Synthetic DNA Templates. *Nucleic Acids Res.* **1987**, *15* (21), 8783–8798. DOI: 10.1093/nar/15.21.8783

(140) Chamberlin, M.; Ring, J. Characterization of T7-Specific Ribonucleic Acid Polymerase. *J. Biol. Chem.* **1973**, *248* (6), 2235–2244. DOI: 10.1016/S0021-9258(19)44211-7

(141) Sastry, S. S.; Ross, B. M. Nuclease Activity of T7 RNA Polymerase and the Heterogeneity of Transcription Elongation Complexes. *J. Biol. Chem.* **1997**, *272* (13), 8644–8652. DOI: 10.1074/jbc.272.13.8644

(142) Arnold, S.; Siemann, M.; Scharnweber, K.; Werner, M.; Baumann, S.; Reuss, M. Kinetic Modeling and Simulation of in Vitro Transcription by Phage T7 RNA Polymerase. *Biotechnol. Bioeng.* **2001**, *72* (5), 548–561.

(143) Das, M.; Dasgupta, D. Enhancement of Transcriptional Activity of T7 RNA Polymerase by Guanidine Hydrochloride. *FEBS Lett.* **1998**, *427* (3), 337–340. DOI: 10.1016/S0014-5793(98)00458-X

(144) Summer, H.; Grämer, R.; Dröge, P. Denaturing Urea Polyacrylamide Gel Electrophoresis (Urea PAGE). *J. Vis. Exp.* **2009**, (32). DOI: 10.3791/1485

(145) Slatko, B. E.; Albright, L. M. Denaturing Gel Electrophoresis for Sequencing. *Current Prot. Mol. Biol.* **2001**, *16* (1). DOI: 10.1002/0471142727.mb0706s16

(146) Gholamalipour, Y.; Karunanayake Mudiyanselage, A.; Martin, C. T. 3′ End Additions by T7 RNA Polymerase Are RNA Self-Templated, Distributive and Diverse in Character—RNA-Seq Analyses. *Nucleic Acids Res.* **2018**, *46* (18), 9253–9263. DOI: 10.1093/nar/gky796

(147) Green, M. R.; Sambrook, J. Polyacrylamide Gel Electrophoresis. *Cold Spring Harb. Protoc.* **2020**, *2020* (12), pdb.prot100412. DOI: 10.1101/pdb.prot100412

(148) Petrov, A.; Wu, T.; Puglisi, E. V.; Puglisi, J. D. RNA Purification by Preparative Polyacrylamide Gel Electrophoresis. *Methods Enzymol.* **2013**, *530*, 315–330. DOI:

10.1016/B978-0-12-420037-1.00017-8

(149) Green, M. R.; Sambrook, J. Precipitation of RNA with Ethanol. *Cold Spring Harb. Protoc.* **2020**, *2020* (3), 101717. DOI: 10.1101/pdb.prot101717

(150) Koubek, J.; Lin, K. F.; Chen, Y. R.; Cheng, R. P.; Huang, J. J. T. Strong Anion-Exchange Fast Performance Liquid Chromatography as a Versatile Tool for Preparation and Purification of RNA Produced by in Vitro Transcription. *RNA* **2013**, *19* (10), 1449–1459. DOI: 10.1261/rna.038117.113

(151) Easton, L. E.; Shibata, Y.; Lukavsky, P. J. Rapid, Nondenaturing RNA Purification Using Weak Anion-Exchange Fast Performance Liquid Chromatography. *RNA* **2010**, *16* (3), 647–653. DOI: 10.1261/rna.1862210

(152) Kim, H.-S.; Huber, K. C. Simple Purification (Desalting) Procedure To Facilitate Structural Analysis of an Alkali-Solubilized/Neutralized Starch Solution by Intermediate-Pressure Size-Exclusion Chromatography. *J. Agric. Food Chem.* **2007**, *55* (13), 4944–4948. DOI: 10.1021/jf063694p

(153) Desjardins, P.; Conklin, D. NanoDrop Microvolume Quantitation of Nucleic Acids. *J. Vis. Exp.* **2010**, (45), 2565. DOI: 10.3791/2565

(154) Streltsov, S. A.; Gromyko, A. V.; Oleinikov, V. A.; Zhuze, A. L. The Hoechst 33258 Covalent Dimer Covers a Total Turn of the Double-Stranded DNA. *J. Biomol. Struct. Dyn.* **2006**, *24* (3), 285–302. DOI: 10.1080/07391102.2006.10507121

(155) Albani, J. R. Fluorescence: Principles and Observables. *Struct. Dynam. Macromol. Absorp. Fluor. Stud.* **2004**, 55–98. DOI: 10.1016/B978-044451449-3/50002-2

(156) Rand, R. N. The Role of Spectrophotometric Standards in the Clinical Chemistry Laboratory. *J. Res. Natl. Bur. Stand. Sect. A Phys. Chem.* **1972**, *76A* (5), 499-508. DOI: 10.6028/jres.076A.044

(157) Cavaluzzi, M. J.; Borer, P. N. Revised UV Extinction Coefficients for Nucleoside-5′-

Monophosphates and Unpaired DNA and RNA. *Nucleic Acids Res.* **2004**, *32* (1), e13. DOI: 10.1093/nar/gnh015

(158) Chai, B.; Zheng, J.; Zhao, Q.; Pollack, G. H. Spectroscopic Studies of Solutes in Aqueous Solution. *J. Phys. Chem. A* **2008**, *112* (11), 2242–2247. DOI: 10.1021/jp710105n

(159) DaCosta, R. S.; Andersson, H.; Wilson, B. C. Molecular Fluorescence Excitation–Emission Matrices Relevant to Tissue Spectroscopy. *Photochem. Photobiol.* **2003**, *78* (4), 384-392. DOI: 10.1562/0031-8655(2003)078<0384:MFEMRT>2.0.CO;2

(160) Nozaki, Y. Determination of the Concentration of Protein by Dry Weight—A Comparison with Spectrophotometric Methods. *Arch. Biochem. Biophys.* **1986**, *249* (2), 437–446. DOI: 10.1016/0003-9861(86)90020-2

(161) Grimsley, G. R.; Pace, C. N. Spectrophotometric Determination of Protein Concentration. *Curr. Protoc. Protein Sci.* **2004**, *33* (1), 1–9. DOI: 10.1002/0471140864.ps0301s33

(162) Xu, D.; Shi, H. Composite RNA Aptamers as Functional Mimics of Proteins. *Nucleic Acids Res.* **2009**, *37* (9), e71. DOI: 10.1093/nar/gkp243

(163) Eydeler, K.; Magbanua, E.; Werner, A.; Ziegelmüller, P.; Hahn, U. Fluorophore Binding Aptamers as a Tool for RNA Visualization. *Biophys. J.* **2009**, *96* (9), 3703–3707. DOI: 10.1016/j.bpj.2009.01.041

(164) Jeon, J.; Lee, K. H.; Rao, J. A Strategy to Enhance the Binding Affinity of Fluorophore–Aptamer Pairs for RNA Tagging with Neomycin Conjugation. *Chem. Commun.* **2012**, *48* (80), 10034–10036. DOI: 10.1039/c2cc34498j

(165) Sawaya, M. R.; Verma, M.; Balendiran, V.; Rath, N. P.; Cascio, D.; Balendiran, G. K. Characterization of WY 14,643 and Its Complex with Aldose Reductase. *Sci. Rep.* **2016**, *6*, 34394. DOI: 10.1038/srep34394

(166) Periasamy, N.; Verkman, A. S. Subtraction of Background Fluorescence in Multiharmonic Frequency-Domain Fluorimetry. *Anal. Biochem.* **1992**, *201* (1), 107–113. DOI: 10.1016/0003-

2697(92)90181-6

(167) Cai, B.; Chen, X.; Liu, F.; Li, J.; Gu, L.; Liu, J. R.; Liu, J. A Cell-Based Functional Assay Using a Green Fluorescent Protein-Based Calcium Indicator DCys-GCaMP. *Assay Drug Dev. Technol.* **2014**, *12* (6), 342–351. DOI: 10.1089/adt.2014.584

(168) McNamara, G.; Difilippantonio, M.; Ried, T.; Bieber, F. R. Microscopy and Image Analysis. *Curr. Protoc. Hum. Genet.* **2017**, *94*, 4.4.1-4.4.89. DOI: 10.1002/cphg.42

(169) Paul, A.; Borrelli, R.; Bouyanfif, H.; Gottis, S.; Sauvage, F. Tunable Redox Potential, Optical Properties, and Enhanced Stability of Modified Ferrocene-Based Complexes. *ACS Omega* **2019**, *4* (12), 14780–14789. DOI: 10.1021/acsomega.9b01341

(170) Wheeler, O. H.; Levy, E. M. Adsorption of Sterically Hindered Phenols on Carbon. *Can. J. Chem.* **1959**, *37* (8), 1235–1240. DOI: 10.1139/v59-182

(171) Stepanenko, O.; Stepanenko, O.; Kuznetsova, I.; Uversky, V.; Turoverov, K. Peculiarities of the Super-Folder GFP Folding in a Crowded Milieu. *Int. J. Mol. Sci.* **2016**, *17* (11), 1805. DOI: 10.3390/ijms17111805

(172) Sillen, A.; Verheyden, S.; Delfosse, L.; Braem, T.; Robben, J.; Volckaert, G.; Engelborghs, Y. Mechanism of Fluorescence and Conformational Changes of the Sarcoplasmic Calcium Binding Protein of the Sand Worm Nereis Diversicolor upon Ca2+ or Mg2+ Binding. *Biophys. J.* **2003**, *85* (3), 1882–1893. DOI: 10.1016/S0006-3495(03)74616-5

(173) Schmidt, C.; Kammel, A.; Tanner, J. A.; Kinghorn, A. B.; Khan, M. M.; Lehmann, W.; Menger, M.; Schedler, U.; Schierack, P.; Rödiger, S. A Multiparametric Fluorescence Assay for Screening Aptamer–Protein Interactions Based on Microbeads. *Sci. Rep.* **2022**, *12* (1), 2961. DOI: 10.1038/s41598-022-06817-0

(174) Vo, T.-D.-H.; Le, V.-G.; Nguyen, Q.-H.; Pham, T.-T.; Bui, T.-V.; Dang, B.-T.; Hoang, T.-T.-N.; Son, N. T.; Lin, K.-Y. A.; Bui, X.-T. Effects of Storage Conditions, PH and Mg:P Ratio on the Precipitation Process for Phosphate Recovery. *Case Stud. Chem. Environ. Eng.* **2022**, *5*,

100188. DOI: 10.1016/j.cscee.2022.100188

(175) Misra, V. K.; Draper, D. E. On the Role of Magnesium Ions in RNA Stability. *Biopolymers* **1998**, *48* (2–3), 113–135. DOI: 10.1002/(SICI)1097-0282(1998)48:2<113::AID-BIP3>3.0.CO;2-Y

(176) Ji, D.; Lyu, K.; Zhao, H.; Kwok, C. K. Circular L-RNA Aptamer Promotes Target Recognition and Controls Gene Activity. *Nucleic Acids Res.* **2021**, *49* (13), 7280–7291. DOI: 10.1093/nar/gkab593

(177) Mayhew, S. G.; Wassink, J. H. Determination of FMN and FAD by Fluorescence Titration with Apoflavodoxin. *Methods Enzymol.* **1980**, *66*, 217–220. DOI: 10.1016/0076-6879(80)66461-1

(178) Rispens, T.; Lakemond, C. M. M.; Derksen, N. I. L.; Aalberse, R. C. Detection of Conformational Changes in Immunoglobulin G Using Isothermal Titration Calorimetry with Low-Molecular-Weight Probes. *Anal. Biochem.* **2008**, *380* (2), 303–309. DOI: 10.1016/j.ab.2008.06.001

(179) Chen, Y.; Müller, J. D.; Tetin, S. Y.; Tyner, J. D.; Gratton, E. Probing Ligand Protein Binding Equilibria with Fluorescence Fluctuation Spectroscopy. *Biophys. J.* **2000**, *79* (2), 1074–1084. DOI: 10.1016/S0006-3495(00)76361-2

(180) Zaer, S.; Lerner, E. Utilizing Time-Resolved Protein-Induced Fluorescence Enhancement to Identify Stable Local Conformations One α-Synuclein Monomer at a Time. *J. Vis. Exp.* **2021**, (171), 10.3791/62655. DOI: 10.3791/62655

(181) Pierce, M. M.; Raman, C. S.; Nall, B. T. Isothermal Titration Calorimetry of Protein–Protein Interactions. *Methods* **1999**, *19* (2), 213–221. DOI: 10.1006/meth.1999.0852

(182) Steinmetzger, C.; Bessi, I.; Lenz, A.-K.; Höbartner, C. Structure–Fluorescence Activation Relationships of a Large Stokes Shift Fluorogenic RNA Aptamer. *Nucleic Acids Res.* **2019**, *47* (22), 11538–11550. DOI: 10.1093/nar/gkz1084

(183) Wang, Y.; Mittermaier, A. K. Characterizing Bi-Substrate Enzyme Kinetics at High Resolution by 2D-ITC. *Anal. Chem.* **2021**, *93* (37), 12723–12732. DOI: 10.1021/acs.analchem.1c02705

(184) Gao, Y.-S.; Su, J.-T.; Yan, Y.-B. Sequential Events in the Irreversible Thermal Denaturation of Human Brain-Type Creatine Kinase by Spectroscopic Methods. *Int. J. Mol. Sci.* **2010**, *11* (7), 2584–2596. DOI: 10.3390/ijms11072584

(185) Eschbach, S. H.; Lafontaine, D. A. RNA Conformational Changes Analyzed by Comparative Gel Electrophoresis. *Methods Mol. Biol.* **2014**, *1086*, 255-264. DOI: 10.1007/978-1-62703-667-2_15.

(186) Riccardi, C.; Napolitano, E.; Musumeci, D.; Montesarchio, D. Dimeric and Multimeric DNA Aptamers for Highly Effective Protein Recognition. *Molecules* **2020**, *25* (22), 5227. DOI: 10.3390/molecules25225227

(187) Vorobyeva, M.; Vorobjev, P.; Venyaminova, A. Multivalent Aptamers: Versatile Tools for Diagnostic and Therapeutic Applications. *Molecules* **2016**, *21* (12), 1613. DOI: 10.3390/molecules21121613

(188) Zou, Z.; Younas, T.; Dumsday, G.; Haritos, V. S.; He, L. Rapid Production of Multimeric RNA Aptamers Stabilized by a Designed Pseudo-circular Structure in E. Coli. *Biotechnol. J.* **2023**, *18* (3), e2200390. DOI: 10.1002/biot.202200390

(189) Velázquez-Campoy, A.; Ohtaka, H.; Nezami, A.; Muzammil, S.; Freire, E. Isothermal Titration Calorimetry. *Curr. Protoc. Cell Biol.* **2004**, *23* (1), 17.8.1-17.8.24. DOI: 10.1002/0471143030.cb1708s23

(190) Arndt, C.; Koristka, S.; Bartsch, H.; Bachmann, M. Native Polyacrylamide Gels. *Methods Mol. Biol.* **2012**, *869*, 49–53. DOI: 10.1007/978-1-61779-821-4_5

(191) Woodson, S. A.; Koculi, E. Analysis of RNA Folding by Native Polyacrylamide Gel Electrophoresis. *Methods Enzymol.* **2009**, *469*, 189–208. DOI: 10.1016/S0076-6879(09)69009-1

(192) Nowakowski, A. B.; Wobig, W. J.; Petering, D. H. Native SDS-PAGE: High Resolution Electrophoretic Separation of Proteins with Retention of Native Properties Including Bound Metal Ions. *Metallomics* **2014**, *6* (5), 1068–1078. DOI: 10.1039/C4MT00033A

(193) Chew, F. N.; Tan, W. S.; Ling, T. C.; Tan, C. S.; Tey, B. T. Quantitation of Green Fluorescent Protein Using a Gel-Based Imaging Method. *Anal. Biochem.* **2009**, *384* (2), 353–355. DOI: 10.1016/j.ab.2008.10.010

(194) Motohashi, K. Development of Highly Sensitive and Low-Cost DNA Agarose Gel Electrophoresis Detection Systems, and Evaluation of Non-Mutagenic and Loading Dye-Type DNA-Staining Reagents. *PLoS One* **2019**, *14* (9), e0222209. DOI: 10.1371/journal.pone.0222209

(195) Burnouf, D.; Ennifar, E.; Guedich, S.; Puffer, B.; Hoffmann, G.; Bec, G.; Disdier, F.; Baltzinger, M.; Dumas, P. KinITC: A New Method for Obtaining Joint Thermodynamic and Kinetic Data by Isothermal Titration Calorimetry. *J. Am. Chem. Soc.* **2012**, *134* (1), 559–565. DOI: 10.1021/ja209057d

(196) Nguyen, V.-T.; Kwon, Y. S.; Kim, J. H.; Gu, M. B. Multiple GO-SELEX for Efficient Screening of Flexible Aptamers. *Chem. Commun.* **2014**, *50* (72), 10513–10516. DOI: 10.1039/C4CC03953J

(197) Gilbert, S. D.; Batey, R. T. Monitoring RNA–Ligand Interactions Using Isothermal Titration Calorimetry. *Methods Mol. Biol.* **2009**, *540*, 97–114. DOI: 10.1007/978-1-59745-558-9_8

(198) Pilch, D. S. Calorimetry of Nucleic Acids. *Curr. Protoc. Nucleic Acid Chem.* **2001**. DOI: 10.1002/0471142700.nc0704s00

(199) Sahu, D.; Bastidas, M.; Lawrence, C. W.; Noid, W. G.; Showalter, S. A. Assessing Coupled Protein Folding and Binding Through Temperature-Dependent Isothermal Titration Calorimetry. *Methods Enzymol.* **2016**, *567*, 23–45. DOI: 10.1016/bs.mie.2015.07.032

(200) Muñoz, E.; Sabín, J.; Rial, J.; Pérez, D.; Ennifar, E.; Dumas, P.; Piñeiro, Á. Thermodynamic

and Kinetic Analysis of Isothermal Titration Calorimetry Experiments by Using KinITC in AFFINImeter. *Methods Mol. Biol.* **2019**, *1964*, 225–239. DOI: 10.1007/978-1-4939-9179-2_16

(201) Mizoue, L. S.; Tellinghuisen, J. The Role of Backlash in the "First Injection Anomaly" in Isothermal Titration Calorimetry. *Anal. Biochem.* **2004**, *326* (1), 125–127. DOI: 10.1016/j.ab.2003.10.048

(202) Barceló, F.; Capó, D.; Portugal, J. Thermodynamic Characterization of the Multivalent Binding of Chartreusin to DNA. *Nucleic Acids Res.* **2002**, *30* (20), 4567–4573. DOI: 10.1093/nar/gkf558

(203) Sokoloski, J. E.; Dombrowski, S. E.; Bevilacqua, P. C. Thermodynamics of Ligand Binding to a Heterogeneous RNA Population in the Malachite Green Aptamer. *Biochemistry* **2012**, *51* (1), 565–572. DOI: 10.1021/bi201642p

(204) Vander Meulen, K. A.; Butcher, S. E. Characterization of the Kinetic and Thermodynamic Landscape of RNA Folding Using a Novel Application of Isothermal Titration Calorimetry. *Nucleic Acids Res.* **2012**, *40* (5), 2140–2151. DOI: 10.1093/nar/gkr894

(205) Horn, J. R.; Russell, D.; Lewis, E. A.; Murphy, K. P. Van't Hoff and Calorimetric Enthalpies from Isothermal Titration Calorimetry: Are There Significant Discrepancies? *Biochemistry* **2001**, *40* (6), 1774–1778. DOI: 10.1021/bi002408e

(206) Machado, T. F. G.; Gloster, T. M.; da Silva, R. G. Linear Eyring Plots Conceal a Change in the Rate-Limiting Step in an Enzyme Reaction. *Biochemistry* **2018**, *57* (49), 6757–6761. DOI: 10.1021/acs.biochem.8b01099

(207) Ryder, S. P.; Recht, M. I.; Williamson, J. R. Quantitative Analysis of Protein-RNA Interactions by Gel Mobility Shift. *Methods Mol. Biol.* **2008**, *488*, 99–115. DOI: 10.1007/978-1-60327-475-3_7

(208) Yakhnin, A. V.; Yakhnin, H.; Babitzke, P. Gel Mobility Shift Assays to Detect Protein–RNA Interactions. *Methods Mol. Biol.* **2012**, *905*, 201–211. DOI: 10.1007/978-1-61779-949-5_12.

(209) Sanderson, B. A.; Araki, N.; Lilley, J. L.; Guerrero, G.; Lewis, L. K. Modification of Gel

Architecture and TBE/TAE Buffer Composition to Minimize Heating during Agarose Gel Electrophoresis. *Anal. Biochem.* **2014**, *454*, 44–52. DOI: 10.1016/j.ab.2014.03.003

(210) Kodama, H.; Kodama, Y.; Itokazu, N.; Shinozawa, S.; Kanemaru, R.; Sugimoto, T. Effect of Temperature on Serum Protein Binding Characteristics of Phenytoin in Monotherapy Paediatric Patients with Epilepsy. *J. Clin. Pharm. Ther.* **2001**, *26* (3), 175–179. DOI: 10.1046/j.1365-2710.2001.00340.x

(211) Wagstaff, K. M.; Dias, M. M.; Alvisi, G.; Jans, D. A. Quantitative Analysis of Protein–Protein Interactions by Native Page/Fluorimaging. *J. Fluoresc.* **2005**, *15*, 469–473. DOI: 10.1007/s10895-005-2819-5

(212) Hellman, L. M.; Fried, M. G. Electrophoretic Mobility Shift Assay (EMSA) for Detecting Protein–Nucleic Acid Interactions. *Nat. Protoc.* **2007**, *2* (8), 1849–1861. DOI: 10.1038/nprot.2007.249

(213) Roelofs, J.; Suppahia, A.; Waite, K. A.; Park, S. Native Gel Approaches in Studying Proteasome Assembly and Chaperones. *Methods Mol. Biol.* **2018**, *1844*, 237–260. DOI: 10.1007/978-1-4939-8706-1_16

(214) Dai, S.; Tam, K. C. Isothermal Titration Calorimetry Studies of Binding Interactions between Polyethylene Glycol and Ionic Surfactants. *J. Phys. Chem. B* **2001**, *105* (44), 10759–10763. DOI: 10.1021/jp0110354

(215) Boudker, O.; Oh, S. Isothermal Titration Calorimetry of Ion-Coupled Membrane Transporters. *Methods* **2015**, *76*, 171–182. DOI: 10.1016/j.ymeth.2015.01.012

(216) Dos Santos Rodrigues, F. H.; Delgado, G. G.; Santana da Costa, T.; Tasic, L. Applications of Fluorescence Spectroscopy in Protein Conformational Changes and Intermolecular Contacts. *BBA Adv.* **2023**, *3*, 100091. DOI: 10.1016/j.bbadva.2023.100091

(217) Amano, R.; Takada, K.; Tanaka, Y.; Nakamura, Y.; Kawai, G.; Kozu, T.; Sakamoto, T. Kinetic and Thermodynamic Analyses of Interaction between a High-Affinity RNA Aptamer and Its

Target Protein. *Biochemistry* **2016**, *55* (45), 6221–6229. DOI: 10.1021/acs.biochem.6b00748

(218) Grau, F. C.; Jaeger, J.; Groher, F.; Suess, B.; Muller, Y. A. The Complex Formed between a Synthetic RNA Aptamer and the Transcription Repressor TetR Is a Structural and Functional Twin of the Operator DNA–TetR Regulator Complex. *Nucleic Acids Res.* **2020**, *48* (6), 3366–3378. DOI: 10.1093/nar/gkaa083

(219) Piñeiro, Á.; Muñoz, E.; Sabín, J.; Costas, M.; Bastos, M.; Velázquez-Campoy, A.; Garrido, P. F.; Dumas, P.; Ennifar, E.; García-Río, L.; Rial, J.; Pérez, D.; Fraga, P.; Rodríguez, A.; Cotelo, C. AFFINImeter: A Software to Analyze Molecular Recognition Processes from Experimental Data. *Anal. Biochem.* **2019**, *577*, 117–134. DOI: 10.1016/j.ab.2019.02.031

(220) Holdgate, G. A. Kinetics, Thermodynamics, and Ligand Efficiency Metrics in Drug Discovery. *Comp. Med. Chem. III* **2017**, 180–211. DOI: 10.1016/B978-0-12-409547-2.12318-2

(221) Cerundolo, V.; Elliott, T.; Elvin, J.; Bastin, J.; Rammensee, H.-G.; Townsend, A. The Binding Affinity and Dissociation Rates of Peptides for Class I Major Histocompatibility Complex Molecules. *Eur. J. Immunol.* **1991**, *21* (9), 2069–2075. DOI: 10.1002/eji.1830210915

(222) Olesiak-Banska, J.; Matczyszyn, K.; Zaleśny, R.; Murugan, N. A.; Kongsted, J.; Ågren, H.; Bartkowiak, W.; Samoc, M. Revealing Spectral Features in Two-Photon Absorption Spectrum of Hoechst 33342: A Combined Experimental and Quantum-Chemical Study. *J. Phys. Chem. B* **2013**, *117* (40), 12013–12019. DOI: 10.1021/jp407144k

(223) Freiburger, L.; Auclair, K.; Mittermaier, A. Global ITC Fitting Methods in Studies of Protein Allostery. *Methods* **2015**, *76*, 149–161. DOI: 10.1016/j.ymeth.2014.12.018

(224) Wang, C.; Liu, L.; Zhao, Q. Low Temperature Greatly Enhancing Responses of Aptamer Electrochemical Sensor for Aflatoxin B1 Using Aptamer with Short Stem. *ACS Sensors* **2020**, *5* (10), 3246–3253. DOI: 10.1021/acssensors.0c01572

(225) Hlastala, M. P.; Woodson, R. D.; Wranne, B. Influence of Temperature on Hemoglobin-Ligand Interaction in Whole Blood. *J. Appl. Physiol. Respir. Environ. Exerc. Physiol.* **1977**, *43* (3),

545–550. DOI: 10.1152/jappl.1977.43.3.545

(226) Singh, O.; Venugopal, P. P.; Mathur, A.; Chakraborty, D. Temperature-Dependent Conformational Evolution of SARS CoV-2 RNA Genome Using Network Analysis. *J. Phys. Chem. B* **2021**, *125* (38), 10672–10681. DOI: 10.1021/acs.jpcb.1c05795

(227) Dragan, A.; Privalov, P.; Crane-Robinson, C. Thermodynamics of DNA: Heat Capacity Changes on Duplex Unfolding. *Eur. Biophys. J.* **2019**, *48* (8), 773–779. DOI: 10.1007/s00249-019-01403-1

(228) Prabhu, N. V.; Sharp, K. A. Heat Capacity in Proteins. *Annu. Rev. Phys. Chem.* **2005**, *56*, 521–548. DOI: 10.1146/annurev.physchem.56.092503.141202

(229) Williams, M. C.; Wenner, J. R.; Rouzina, I.; Bloomfield, V. A. Entropy and Heat Capacity of DNA Melting from Temperature Dependence of Single Molecule Stretching. *Biophys. J.* **2001**, *80* (4), 1932–1939. DOI: 10.1016/S0006-3495(01)76163-2

(230) Takase, K.; Niki, R.; Arima, S. A Sedimentation Equilibrium Study of the Temperature-Dependent Association of Bovine β-Casein. *Biochim. Biophys. Acta - Protein Struct.* **1980**, *622* (1), 1–8. DOI: 10.1016/0005-2795(80)90152-X

(231) Piletic, I. R.; Edney, E. O.; Bartolotti, L. J. Barrierless Reactions with Loose Transition States Govern the Yields and Lifetimes of Organic Nitrates Derived from Isoprene. *J. Phys. Chem. A* **2017**, *121* (43), 8306–8321. DOI: 10.1021/acs.jpca.7b08229

(232) Kamerlin, S. C. L.; Florián, J.; Warshel, A. Associative Versus Dissociative Mechanisms of Phosphate Monoester Hydrolysis: On the Interpretation of Activation Entropies. *ChemPhysChem* **2008**, *9* (12), 1767–1773. DOI: 10.1002/cphc.200800356

(233) Åqvist, J.; Kolmodin, K.; Florian, J.; Warshel, A. Mechanistic Alternatives in Phosphate Monoester Hydrolysis: What Conclusions Can Be Drawn from Available Experimental Data? *Chem. Biol.* **1999**, *6* (3), R71–R80. DOI: 10.1016/S1074-5521(99)89003-6

(234) Åqvist, J.; Kazemi, M.; Isaksen, G. V.; Brandsdal, B. O. Entropy and Enzyme Catalysis. *Acc.*

Chem. Res. **2017**, *50* (2), 199–207. DOI: 10.1021/acs.accounts.6b00321

(235) Lahiri, J.; Isaacs, L.; Tien, J.; Whitesides, G. M. A Strategy for the Generation of Surfaces Presenting Ligands for Studies of Binding Based on an Active Ester as a Common Reactive Intermediate: A Surface Plasmon Resonance Study. *Anal. Chem.* **1999**, *71* (4), 777–790. DOI: 10.1021/ac980959t

(236) Duan, X.; Li, Y.; Rajan, N. K.; Routenberg, D. A.; Modis, Y.; Reed, M. A. Quantification of the Affinities and Kinetics of Protein Interactions Using Silicon Nanowire Biosensors. *Nat. Nanotechnol.* **2012**, *7* (6), 401–407. DOI: 10.1038/nnano.2012.82

(237) Buglak, A. A.; Samokhvalov, A. V.; Zherdev, A. V.; Dzantiev, B. B. Methods and Applications of In Silico Aptamer Design and Modeling. *Int. J. Mol. Sci.* **2020**, *21* (22), 8420. DOI: 10.3390/ijms21228420

(238) Yan, S.; Ilgu, M.; Nilsen-Hamilton, M.; Lamm, M. H. Computational Modeling of RNA Aptamers: Structure Prediction of the Apo State. *J. Phys. Chem. B* **2022**, *126* (37), 7114–7125. DOI: 10.1021/acs.jpcb.2c04649

(239) Flinders, J.; Dieckmann, T. NMR Spectroscopy of Ribonucleic Acids. *Prog. Nucl. Magn. Reson. Spectrosc.* **2006**, *48* (2–3), 137–159. DOI: 10.1016/j.pnmrs.2006.03.001

(240) Dieckmann, T.; Piazza, M.; Bonneau, E.; Legault, P. Biomolecular NMR Spectroscopy of Ribonucleic Acids. *eLS* **2014**, 1–11. DOI: 10.1002/9780470015902.a0021033.pub2

Appendix A: Supplementary Figures

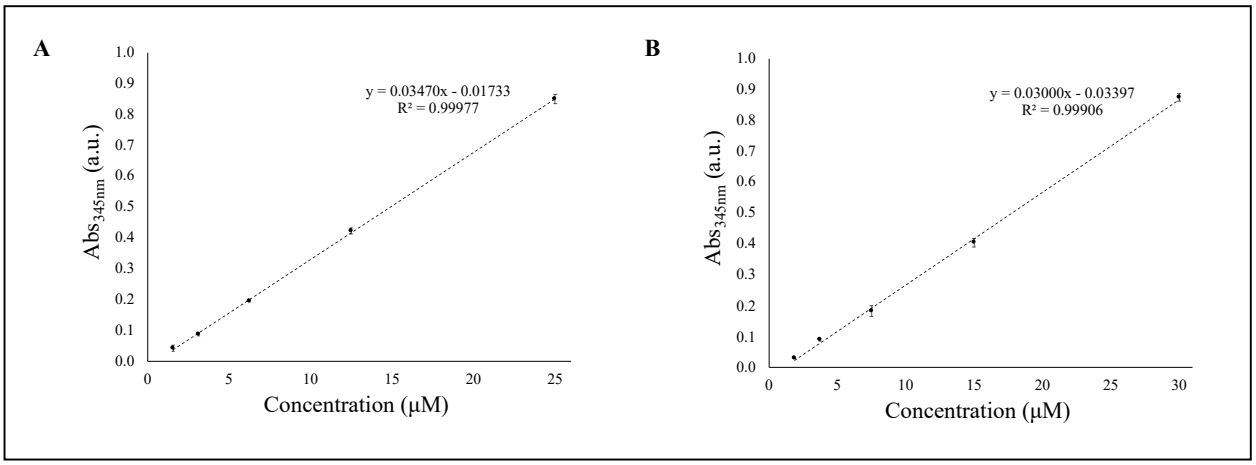


Figure 5.1: Dilution series to determine the molar extinction coefficient of the tBu Hoechst dye derivatives in MQW. A) tBu (PEG) Hoechst dye and **B)** biotinylated tBu (PEG) Hoechst dye.

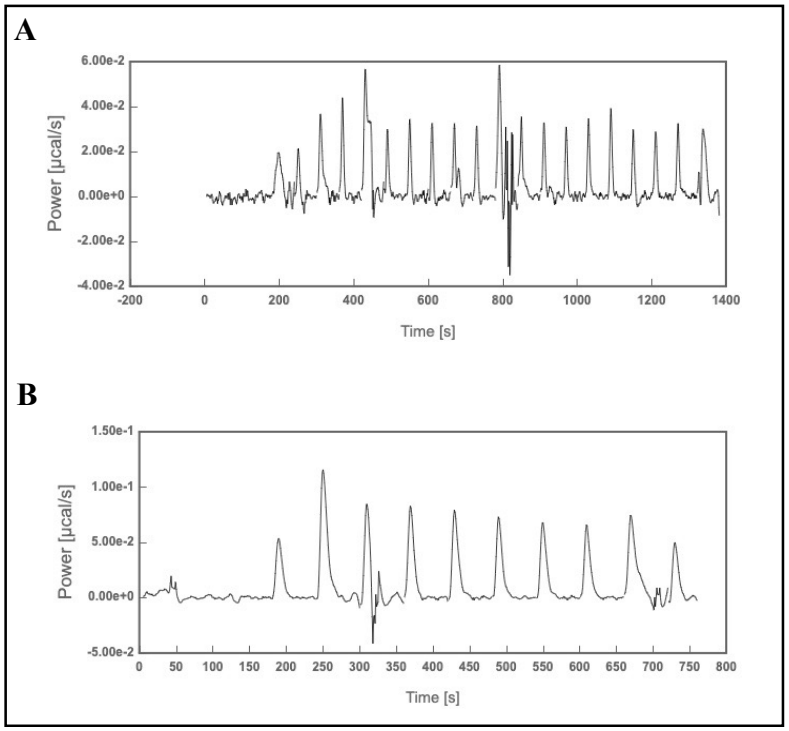


Figure 5.2: Control ITC experiments for the Original RNA aptamer and tBu (PEG) Hoechst dye. A) 1× PBS titrated into 50 μM Original RNA and **B)** 670 μM tBu (PEG) Hoechst dye titrated into 1× PBS.

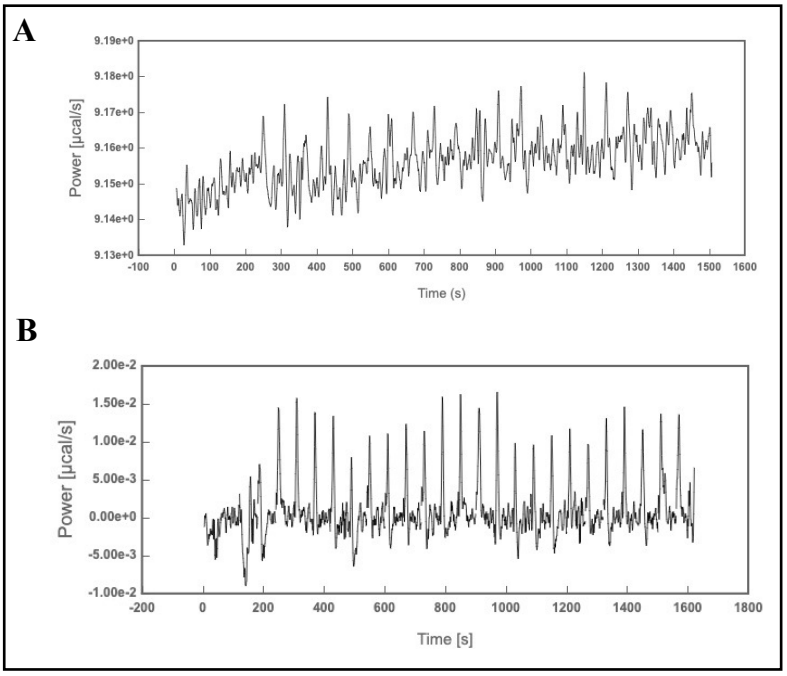


Figure 5.3: Control ITC experiments for the biotinylated tBu (PEG) Hoechst dye. **A)** 840 µM biotinylated tBu (PEG) Hoechst dye titrated into 1× PBS and **B)** 1× PBS titrated into 80 µM biotinylated tBu (PEG) Hoechst dye.

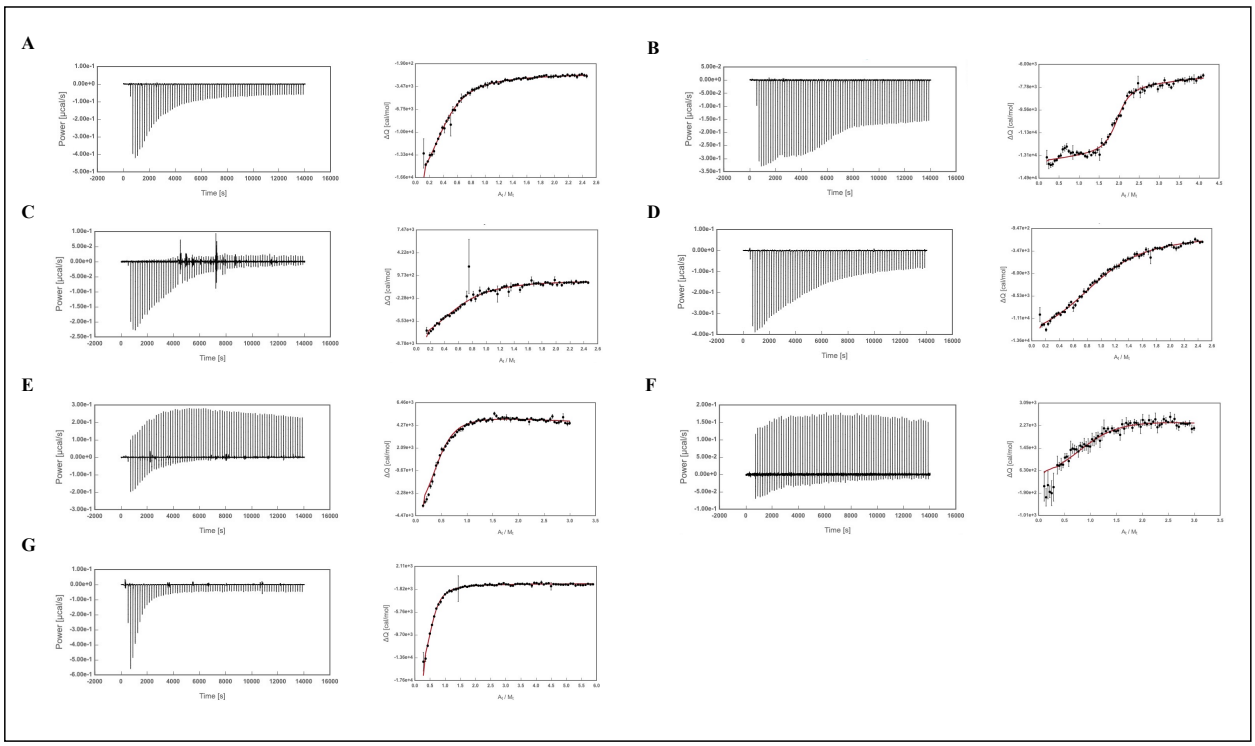


Figure 5.4: Duplicate data for the processed ITC and equilibrium isotherm data for the RNA aptamer variants. The titration of the tBu (PEG) Hoechst dye into the **A)** Original, **B)** Aptamer II, **C)** UUCG Tetraloop, **D)** GAAA Tetraloop**, E)** Duplex, **F)** Elongated Duplex, and **G)** Short Stem RNA aptamers at 25 °C.

Table 5.1: Raw data for the binding affinities and thermodynamic properties of the variant RNA aptamer with the tBu (PEG) Hoechst dye at 25 °C.

Variant RNA Aptamer	Replicate	K_A (μM^{-1})	K_D (μM)	ΔH_{25} ($kcal\ mol^{-1}$)	$T\Delta S_{25}$ ($K\ kcal\ mol^{-1}$)
Original RNA	1	0.18 ± 0.01	5.6 ± 0.4	-19.0 ± 0.6	-11.8 ± 0.6
	2	0.123 ± 0.006	8.1 ± 0.4	-18.6 ± 0.4	-11.6 ± 0.4
Aptamer II	1	3.7 ± 0.3	0.27 ± 0.02	-5.12 ± 0.05	3.84 ± 0.07
	2	2.5 ± 0.2	0.41 ± 0.04	-5.86 ± 0.07	2.86 ± 0.09
UUCG Tetraloop	1	0.10 ± 0.01	10 ± 1	-18 ± 2	-11 ± 2
	2	0.11 ± 0.01	9.0 ± 0.9	-10.7 ± 0.5	-3.8 ± 0.5
GAAA Tetraloop	1	0.109 ± 0.008	9.2 ± 0.7	-12.0 ± 0.3	-5.1 ± 0.3
	2	0.060 ± 0.005	17 ± 1	-15.4 ± 0.8	-8.9 ± 0.8
Duplex	1	0.36 ± 0.02	2.8 ± 0.1	-11.5 ± 0.2	-3.9 ± 0.2
	2	0.21 ± 0.01	4.8 ± 0.2	-11.5 ± 0.2	-4.2 ± 0.2
Elongated Duplex	1	0.10 ± 0.02	10 ± 2	-2.9 ± 0.2	3.9 ± 0.2
	4	0.54 ± 0.09	1.8 ± 0.3	-1.25 ± 0.04	6.6 ± 0.1
Short stem	1	0.51 ± 0.03	2.0 ± 0.1	-17.9 ± 0.8	-10.2 ± 0.8
	2	1.41 ± 0.09	0.71 ± 0.05	-14.6 ± 0.6	-6.2 ± 0.7

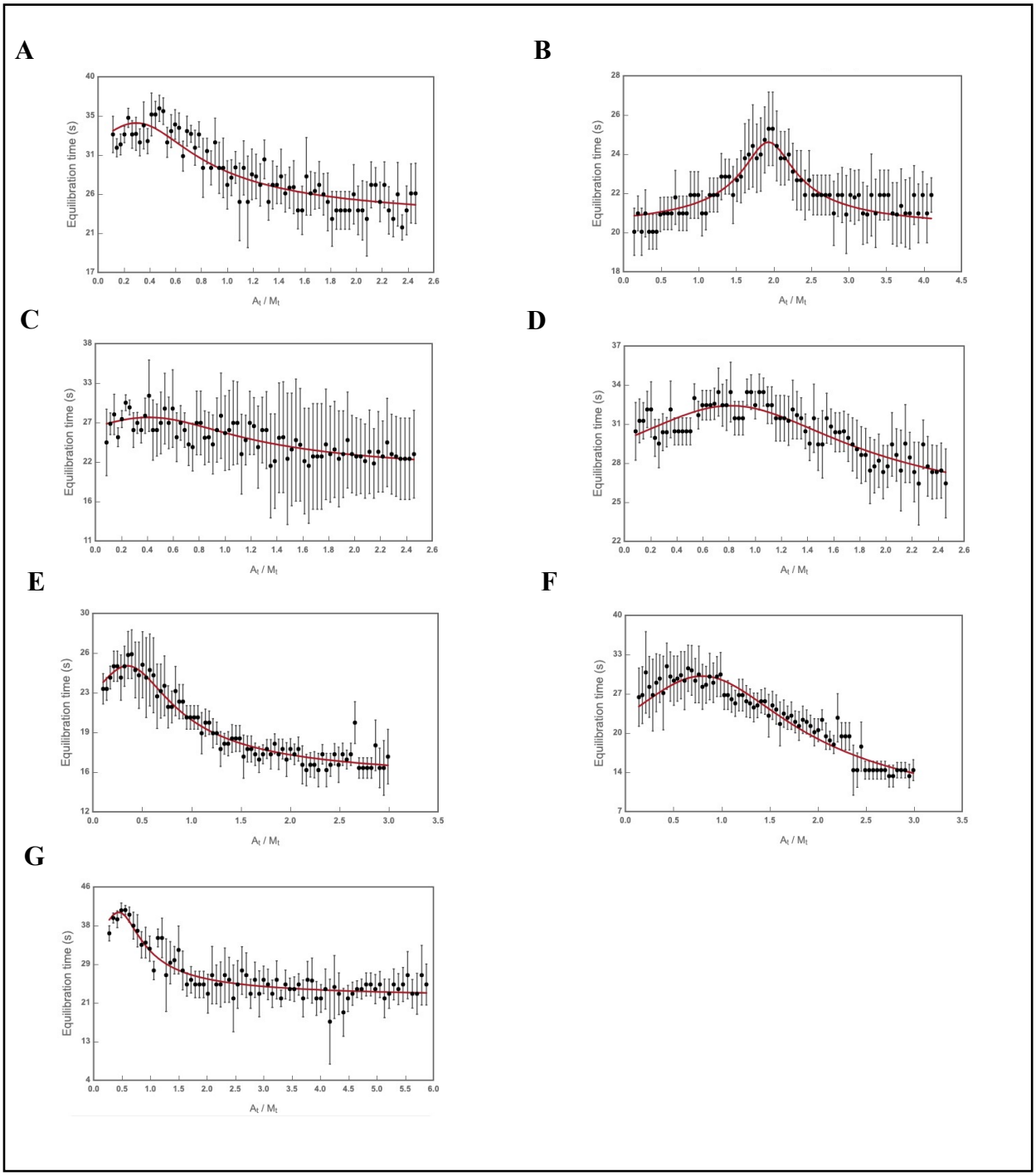


Figure 5.5: Duplicate data for the processed ETC for the RNA aptamer variants. The titration of tBu (PEG) Hoechst dye into the **A)** Original, **B)** Aptamer II, **C)** Aptamer II-mini3-4, **D)** UUCG Tetraloop, **E)** GAAA Tetraloop**, F)** Duplex, **G)** Elongated Duplex, and **H)** Short Stem RNA aptamers at 25 °C.

Table 5.2: Raw data for the kinetic properties of the RNA aptamer variants with the tBu (PEG) Hoechst dye at 25 °C.

Variant RNA Aptamer	Replicate	$k_{on}(\mathbf{M^{-1}s^{-1}})$	$k_{off}(\mathbf{s^{-1}})$
Original RNA	1	$(1.8 \pm 0.1) \times 10^4$	$(9.9 \pm 0.8) \times 10^{-2}$
	2	$(1.08 \pm 0.07) \times 10^4$	$(8.8 \pm 0.6) \times 10^{-2}$
Aptamer II	1	$(1.4 \pm 0.2) \times 10^5$	$(3.9 \pm 0.6) \times 10^{-2}$
	2	$(1.5 \pm 0.2) \times 10^5$	$(6 \pm 1) \times 10^{-2}$
UUCG Tetraloop	1	$(1.9 \pm 0.2) \times 10^4$	$(2 \pm 0.2) \times 10^{-1}$
	2	$(1.6 \pm 0.4) \times 10^4$	$(1.5 \pm 0.3) \times 10^{-1}$
GAAA Tetraloop	1	$(1.1 \pm 0.2) \times 10^4$	$(1.0 \pm 0.1) \times 10^{-1}$
	2	$(1.2 \pm 0.2) \times 10^4$	$(2.0 \pm 0.3) \times 10^{-1}$
Duplex	1	$(2.6 \pm 0.2) \times 10^4$	$(7.4 \pm 0.5) \times 10^{-2}$
	2	$(2.1 \pm 0.1) \times 10^4$	$(1.00 \pm 0.07) \times 10^{-1}$
Elongated Duplex	1	$(3.8 \pm 0.5) \times 10^3$	$(3.8 \pm 0.5) \times 10^{-2}$
	4	$(2.1 \pm 0.4) \times 10^4$	$(3.9 \pm 0.7) \times 10^{-2}$
Short Stem	1	$(2.2 \pm 0.1) \times 10^4$	$(4.3 \pm 0.3) \times 10^{-2}$
	2	$(3.5 \pm 0.2) \times 10^4$	$(2.5 \pm 0.2) \times 10^{-2}$

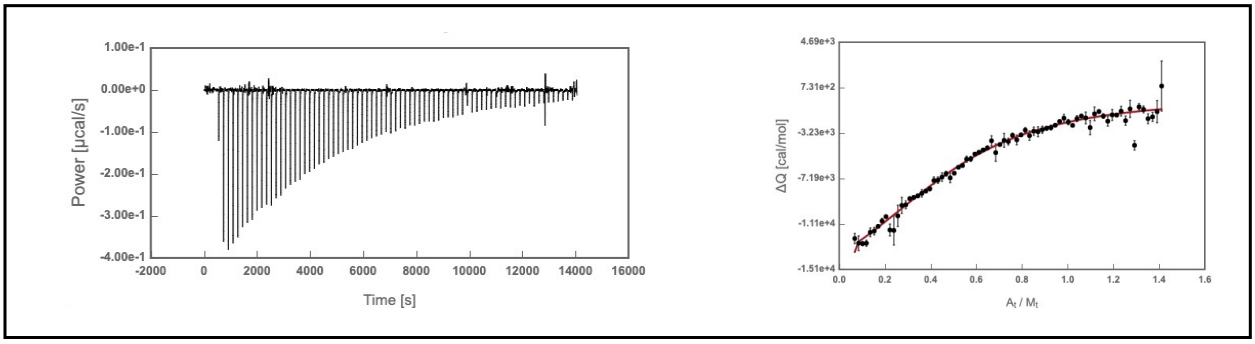


Figure 5.6: Duplicate data for the processed ITC and equilibrium isotherm data for the tBu Hoechst dye derivatives. the titration of the Original RNA aptamer into the biotinylated tBu (PEG) Hoechst dye at 25 °C.

Table 5.3: Raw data for the binding affinities and thermodynamic properties of the Original RNA aptamer with biotinylated versus non-biotinylated tBu Hoechst dye at 25 °C.

Hoechst Dye Derivative	Replicate	K_A (μM^{-1})	K_D (μM)	ΔH_{25} (kcal mol^{-1})	$T\Delta S_{25}$ (K kcal mol^{-1})
tBu (PEG) Hoechst	1	0.18 ± 0.01	5.6 ± 0.4	-19.0 ± 0.6	-11.8 ± 0.6
	2	0.123 ± 0.006	8.1 ± 0.4	-18.6 ± 0.4	-11.6 ± 0.4
Biotinylated tBu (PEG) Hoechst	1	0.090 ± 0.003	11.1 ± 0.4	-10.1 ± 0.1	-3.4 ± 0.1
	2	0.065 ± 0.003	15.5 ± 0.7	-19.1 ± 0.5	-12.5 ± 0.5

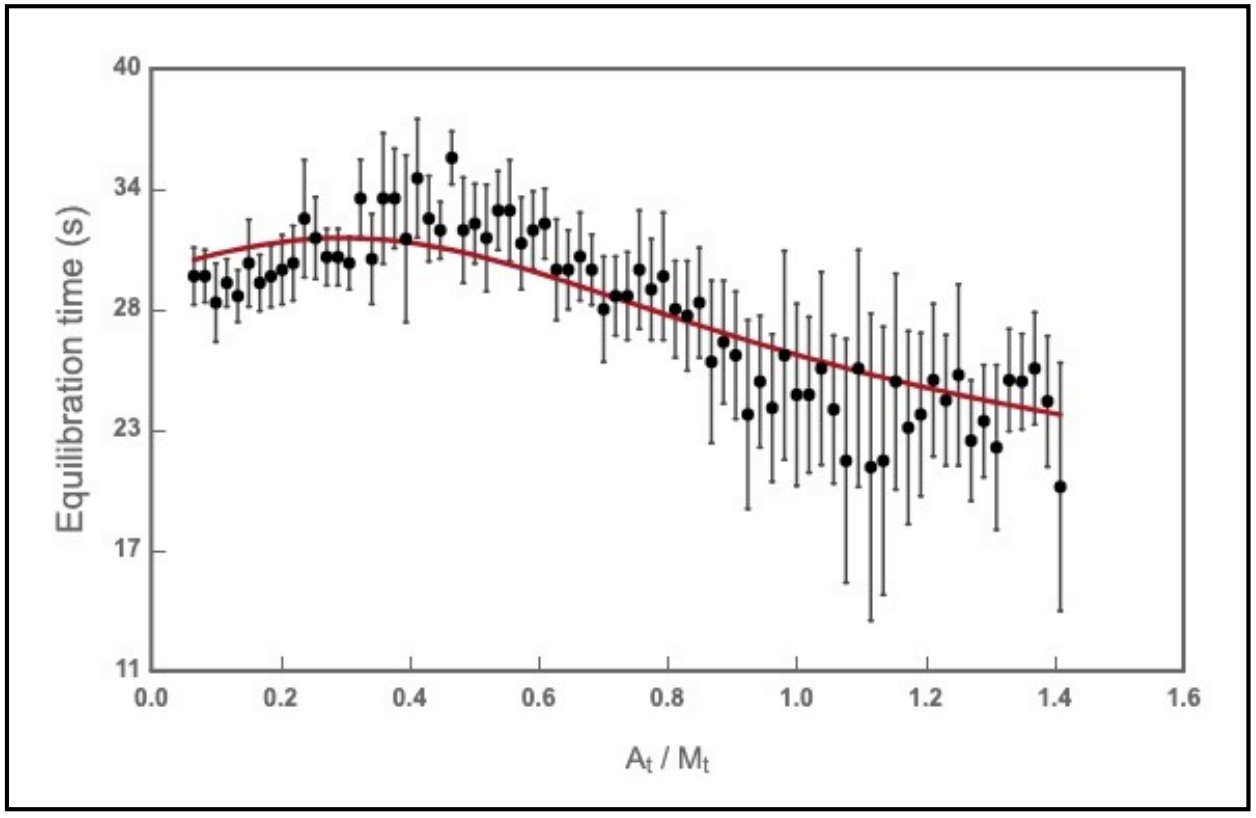


Figure 5.7: Duplicate data for the processed ETC for the tBu Hoechst dye derivatives. Processed ETC for the titration of the Original RNA aptamer into the biotinylated tBu (PEG) Hoechst dye at 25 °C.

Table 5.4: Raw data for kinetic properties of the Original RNA aptamer with biotinylated versus non-biotinylated tBu Hoechst dye at 25 °C.

Hoechst Dye Derivative	Replicate	k_{on} ($M^{-1}s^{-1}$)	k_{off} (s^{-1})
tBu (PEG) Hoechst	1	$(1.8 \pm 0.1) \times 10^4$	$(9.9 \pm 0.8) \times 10^{-2}$
	2	$(1.08 \pm 0.07) \times 10^4$	$(8.8 \pm 0.6) \times 10^{-2}$
Biotinylated tBu (PEG) Hoechst	1	$(3.9 \pm 0.3) \times 10^3$	$(4.4 \pm 0.4) \times 10^{-2}$
	2	$(5.4 \pm 0.6) \times 10^3$	$(8 \pm 1) \times 10^{-2}$

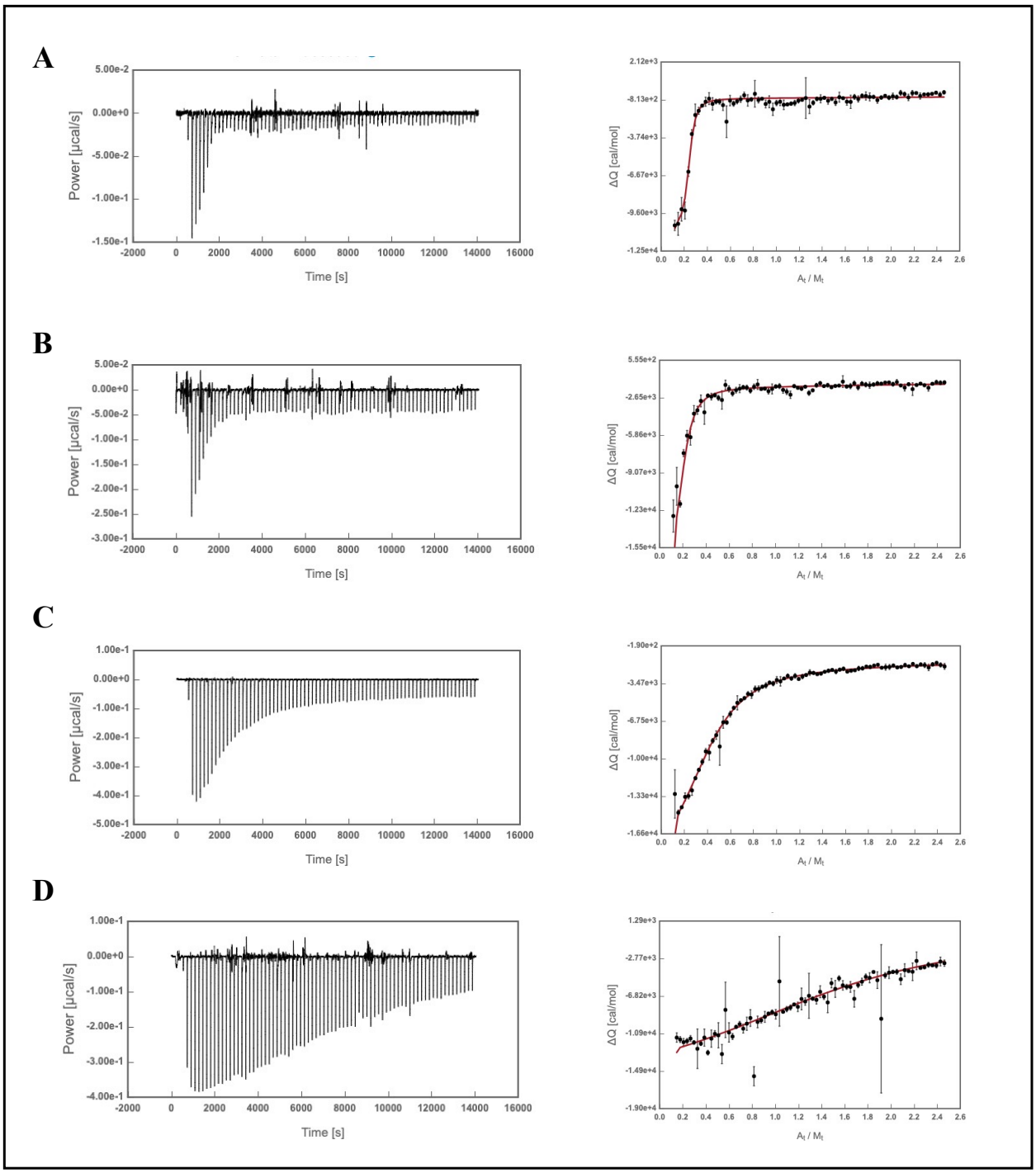


Figure 5.8: Duplicate data for the processed ITC and equilibrium isotherm data for the temperature series. Titration of the tBu (PEG) Hoechst dye into the Original RNA aptamer at **A)** 5 °C, **B)** 15 °C **C)** 25 °C and **D)** 35 °C.

Table 5.5: Raw data for the binding affinity and thermodynamic properties obtained for the titration of 600 µM tBu (PEG) Hoechst into 50 µM Original RNA at different temperatures.

Temperature (°C)	Replicate	K_A (M^{-1})	K_D (µM)	ΔH_{25} (kcal mol^{-1})	$T\Delta S_{25}$ (K kcal mol^{-1})
5	1	6 ± 1	0.18 ± 0.03	-12.5 ± 0.2	-3.9 ± 0.2
	2	5.6 ± 0.8	0.18 ± 0.03	-10.3 ± 0.4	-1.7 ± 0.4
15	1	1.7 ± 0.2	0.60 ± 0.05	-14.0 ± 0.7	-5.8 ± 0.7
	2	1.2 ± 0.2	0.9 ± 0.1	-17 ± 2	-9 ± 1
25	1	0.18 ± 0.01	5.6 ± 0.4	-19.0 ± 0.6	-11.8 ± 0.6
	2	0.123 ± 0.006	8.1 ± 0.4	-18.6 ± 0.4	-11.6 ± 0.4
35	1	0.030 ± 0.001	33 ± 1	-20.0 ± 0.4	-13.7 ± 0.4
	2	0.040 ± 0.003	25 ± 2	-17.0 ± 0.5	-10.6 ± 0.5

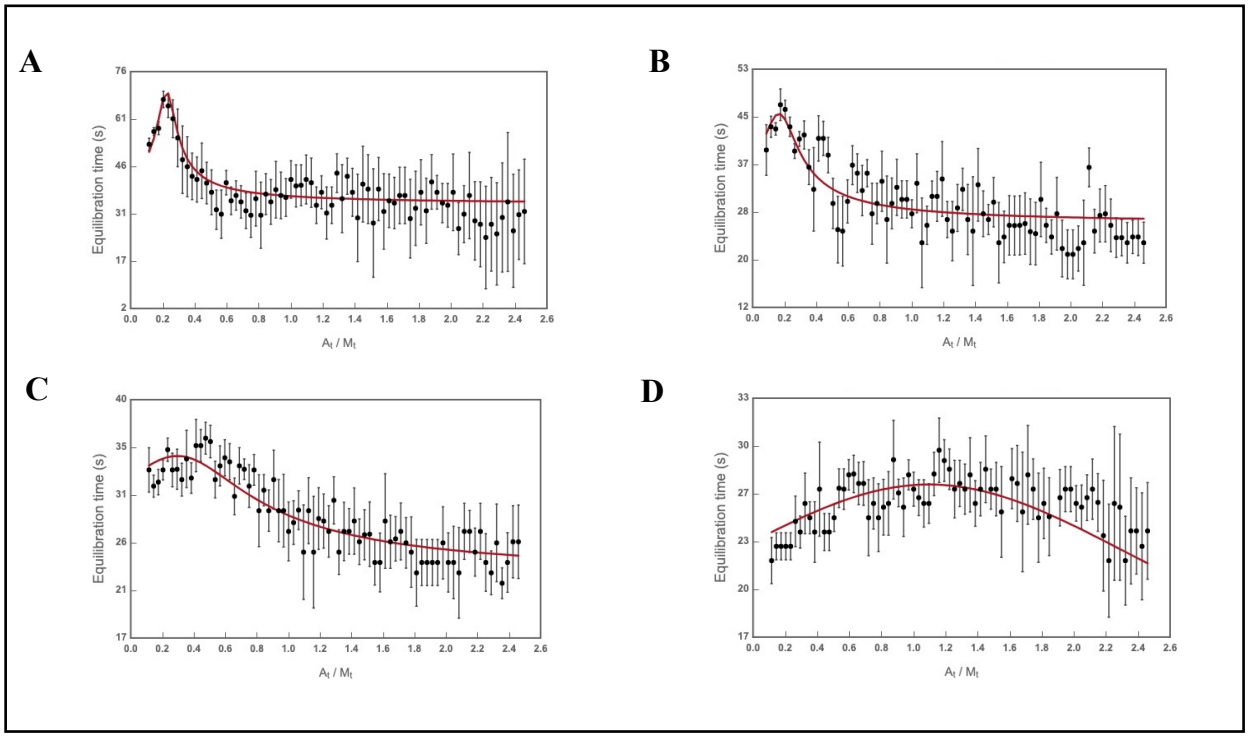


Figure 5.9: Duplicate data for the processed ETC for the temperature series. The Original RNA aptamer titrated with tBu (PEG) Hoechst dye at **A)** 5 °C, **B)** 15 °C **C)** 25 °C and **D)** 35 °C.

Table 5.6: Raw data for the kinetic parameters obtained from the titration of 600 μM tBu (PEG) Hoechst into 50 μM Original RNA at different temperatures.

Temperature (°C)	Replicate	k_{on} ($M^{-1}s^{-1}$)	k_{off} (s^{-1})
5	1	$(6.4 \pm 0.8) \times 10^4$	$(1.2 \pm 0.1) \times 10^{-2}$
	2	$(4.5 \pm 0.5) \times 10^4$	$(7.9 \pm 0.9) \times 10^{-3}$
15	1	$(3.4 \pm 0.2) \times 10^4$	$(2.0 \pm 0.1) \times 10^{-2}$
	2	$(4.2 \pm 0.4) \times 10^4$	$(3.6 \pm 0.4) \times 10^{-2}$
25	1	$(1.8 \pm 0.1) \times 10^4$	$(9.9 \pm 0.8) \times 10^{-2}$
	2	$(1.08 \pm 0.07) \times 10^4$	$(8.8 \pm 0.6) \times 10^{-2}$
35	1	$(2.1 \pm 0.3) \times 10^3$	$(7 \pm 1) \times 10^{-2}$
	2	$(1.8 \pm 0.3) \times 10^3$	$(4.6 \pm 0.7) \times 10^{-2}$